

CONFINEMENT AND CHIRAL PHASE TRANSITIONS IN SU(2) GAUGE
THEORY VIA TOPOLOGICAL OBJECTS

Miguel Ángel López Ruiz

Submitted to the faculty of the University Graduate School
in partial fulfillment of the requirements
for the degree
Doctor of Philosophy
in the Department of Physics,
Indiana University
May 2019

Accepted by the Graduate Faculty, Indiana University, in partial fulfillment of the requirements
for the degree of Doctor of Philosophy.

Doctoral Committee

Jinfeng Liao, Ph.D.

Gerardo Ortiz, Ph.D.

Adam Szczepaniak, Ph.D.

W. Michael Snow, Ph.D.

April 24, 2019

ACKNOWLEDGEMENTS

First and foremost, I would like to express my sincere gratitude to my advisor Jinfeng Liao, whose expertise, patience, mentorship, constant support, and motivation inspired me to never stop seeking knowledge and become the best researcher I can be.

I would also like to thank my Committee members: Gerardo Ortiz, Mike Snow, and Adam Szczepaniak for their insightful questions, comments, and suggestions to further extend this work into different directions.

Gratitude is also due to the Physics Department faculty which I had the pleasure to had as teachers, and to all the graduate students and postdocs from whom I learned quite a bit. In particular, Shuzhe Shi, Vincent Mathieu, Tochtli Yépez-Martínez, and Yin Jiang for the long discussions and conversations about physics, mathematics and life.

This work was partially financially supported by Mexico's National Council of Science and Technology (CONACYT), under Doctoral support Grant No. 669645.

I certainly would like to mention the amazing friendships I made along this journey, especially Nathan, Sam, Pepe, Mely, and The *Γαμάτο* Mesa: Alex, Ellie, and Lilian.

I am thankful to my parents which have always encouraged me at every stage in my career and despite the distance, I always felt their constant support.

Finally and most importantly, my eternal gratitude goes to my wife, Lilian. Your continuous support, endless patience, and love were the sole reason this thesis was finished.

Miguel Ángel López Ruiz

CONFINEMENT AND CHIRAL PHASE TRANSITIONS IN $SU(2)$ GAUGE THEORY VIA
TOPOLOGICAL OBJECTS

Confinement and chiral phase transitions are remarkable non-perturbative phenomena emerging from Quantum Chromodynamics, that is, the underlying theory of the strong interaction between subatomic particles. A theoretical understanding of these transitions and their interrelations is of fundamental importance. While it is widely perceived that their dynamics arises from non-trivial topological configurations in Yang-Mills theories, a concrete and sophisticated realization of such idea is an outstanding challenge. In this work, significant progress is presented along this direction by the construction of a new framework based on a statistical ensemble of topological objects called instanton-dyons, namely, the constituents of the finite-temperature instantons with non-trivial holonomy. I present a comprehensive numerical study of the confining properties in $SU(2)$ Yang-Mills theory at finite temperature, obtaining important observables which are then compared with available data from state of the art simulations of lattice gauge theory and are found to be in substantial agreement. Furthermore, with the inclusion of dynamical quarks in the system, I explore the non-trivial interplay between the confinement/deconfinement and chiral symmetry breaking/restoration phase transitions.

Jinfeng Liao, Ph.D.

Gerardo Ortiz, Ph.D.

Adam Szczepaniak, Ph.D.

W. Michael Snow, Ph.D.

TABLE OF CONTENTS

Acknowledgements	iii
Abstract	iv
Chapter 1: Introduction	1
Chapter 2: Non-Abelian Gauge Theories at Finite Temperature	5
2.1 Euclidean Quantum Chromodynamics	5
2.2 The Polyakov Loop and the Confinement Phase Transition	9
2.2.1 Center Symmetry Breaking	11
2.3 Chiral Symmetry	13
Chapter 3: Classical Gauge Field Configurations	16
3.1 Topology of Yang-Mills theory	16
3.2 The BPST Instanton	19
3.2.1 Moduli Space of the Instanton	25
3.2.2 Multi-instantons and 't Hooft Ansatz	27
3.3 The Harrington-Shepard Caloron	30
3.4 Monopoles and Dyons	33
3.5 The KvBLL Caloron with Non-Trivial Holonomy	39
3.5.1 The ADHM Construction	39
3.5.2 The KvBLL Caloron Solution	40

Chapter 4: The Instanton-Dyon ensemble in SU(2) Yang-Mills Theory	45
4.1 Construction of the Correlated Instanton-Dyon Ensemble	45
4.1.1 The Quantum Weight of the KvBLL Caloron	45
4.1.2 The Partition Function	48
4.1.3 The Monte-Carlo Simulations	51
4.2 Confinement-Deconfinement Transition	54
4.2.1 The Holonomy Potential	54
4.2.2 The Dyon and Antidyon Spatial Correlations	59
4.2.3 The Polyakov Loop Correlator	60
4.2.4 The Spatial Wilson Loop	66
4.3 Discussions	69
4.3.1 Finite Volume Effects	69
4.3.2 The Influence of Dyon-antidyon Short-Range Correlation	71
4.3.3 The Debye Screening Mass	74
4.4 Next-to-Leading Order Corrections and Other Improvements	74
4.4.1 Temperature Dependence of the Order Parameter	78
4.4.2 Instanton-Dyon Density and Correlations	86
Chapter 5: Fermions in the Instanton-Dyon Ensemble	89
5.1 The Fermion Determinant	89
5.2 Construction of the Instanton-dyon Ensemble	95
5.3 Numerical Simulations	96
5.3.1 Holonomy and Dyon Densities	98
5.3.2 The Chiral Phase Transition	101
5.4 Summary and Discussion	103

Chapter 6: Conclusions	104
Appendix A: Topological Charge	106
Appendix B: Properties of 't Hooft symbols.	111
Appendix C: Fermion Zero Modes	112
C.1 Right-handed solution	114
C.2 Left-handed solution	119
References	122
Curriculum Vitae	

CHAPTER 1

INTRODUCTION

After decades since its first iterations, Quantum Field Theory is still regarded as the proper theoretical framework to describe elementary particles and their interactions; with Quantum Electrodynamics and subsequently Electroweak theory, having remarkable success at elucidating the features of the electromagnetic and weak nuclear forces. In similar fashion, Quantum Chromodynamics (QCD) has been established as the fundamental theory of the strong nuclear force, with quarks and gluons its main degrees of freedom carrying color charges. Asymptotic freedom, the feature where the coupling strength decreases at asymptotically short distances [1, 2], enables the use of perturbative expansions at high energy scales, proving to be outstandingly effective in its phenomenological predictions. Despite this success, in the low energy regime, the validity of the perturbative approach fails and different techniques ought to be used for the understanding of phenomena such as the vacuum structure, the spontaneous breaking of chiral symmetry or the “confinement” of color charges, namely, the absence of free quarks and gluons in the physical spectrum, which always appear to be bound in color-singlet states. A very suitable approach to tackle non-perturbative phenomena has been the lattice formulation of gauge theories, a framework which allows the computation of physical observables from first principles via large-scale numerical simulations. Nevertheless, it does not provide the physical insight necessary to understand the mechanisms behind such phenomena, thus it is sensible to develop other methods which complement such calculations.

The discovery of the Yang-Mills instanton [3], marked a cornerstone in the development of models of the QCD vacuum [4–9]. They successfully provided an explanation for the spontaneous breaking of chiral symmetry [10–12] and were finally able to describe some other non-perturbative features of the strong interaction such as the anomalous breaking of the $U_A(1)$ symmetry due to the non-trivial topology of the instanton, which consequently solved the well known η' -puzzle

[13]. Models such as the Instanton Liquid Model (ILM) [14–20], based on a statistical ensemble of interacting instantons, also had phenomenological success in determining hadronic quantities via numerical and analytical methods¹.

The understanding of the QCD phase diagram and generally its thermodynamic properties, have shown to be essential in the description of natural phenomena; from the early universe to high energy physics in particle colliders. Since the early stages of QCD, later on verified in relativistic collisions of heavy ions, it has been argued that at sufficiently high temperatures and densities, the color degrees of freedom are deconfined into a so called “Quark-Gluon Plasma”. This change in state suggests a possible phase transition from confinement to deconfinement. Since it is believed that confinement originates from the gauge dynamics of the gluonic sector, examining the theory without dynamical quarks, i.e., pure Yang-Mills, provides a good description of a deconfinement phase transition where the expectation value of the Polyakov loop at spatial infinity (*holonomy*) is well defined as the order parameter. Moreover, this quantity happens to be a topological characteristic of gauge configurations, e.g., the finite temperature generalization of the instanton field, the *caloron*, is said to have trivial holonomy, which is in sharp contrast to the confining vacuum where the holonomy is maximally non-trivial; therefore, instanton configurations do not lead to confinement, a well known issue of ILM noticed since its inception.

The KvBLL *caloron* solution [23–25], which by construction acquires the necessary non-trivial holonomy for confinement, provided a promising new approach for the understanding of confinement dynamics and its phase transition. Moreover, the particular property that the KvBLL caloron is “made of” N_c (for $SU(N_c)$ theory) constituent dyon-like fields, namely with chromo-electric and -magnetic charges, is reminiscent of the idea that confinement may arise from chromo-magnetically charged and topologically non-trivial gauge configurations, with the vacuum being a “dual superconductor” of such magnetic objects².

The early success of instanton models and the emergence of such gauge configurations, led to the development of the ensemble framework of instanton-dyons/antidions³, arising from the constituents of the KvBLL calorons. First attempts to uncorrelated ensembles of these objects,

¹The instanton literature is quite extensive and we have only referenced a few of the works which seemed relevant to this thesis; however, Schäfer and Shuryak [21] and Diakonov [22] have compiled very complete reviews on instanton physics.

²See reviews in [26, 27] for more details.

³Also called in the literature instanton-quarks or instanton-monopoles.

already indicated that their contributions (alone) to the holonomy potential tends to push the system toward confining holonomy [28–31]. Nevertheless, it was later found that such contributions would not be enough to overcome the one-loop perturbative contributions to the holonomy potential (which favors the trivial holonomy). Shuryak and collaborators [31–33] have argued that an effective dyon-antidyon interaction with a short-range repulsive core is a necessary condition to enforce a confining holonomy at low temperatures. Moreover, via an effective mean field model for a Coulomb plasma of such instanton-dyons, a reasonable qualitative description of the low temperature properties of Yang-Mills theories was presented in [34, 35]⁴.

Similarly to the ILM, with the introduction of dynamical quarks into the Yang-Mills theory, one can investigate chiral properties and see if the instanton-dyon ensemble indeed reproduces the spontaneously broken chiral symmetry below some critical temperature and the expected restoration of symmetry above it. In other words, the chiral phase transition should be reproducible in this framework as well. This was also explored by Shuryak and collaborators via numerical simulations [40–42] and mean field models [43–46].

In this thesis, in the framework of a statistical ensemble of correlated instanton-dyons, we first present a systematic investigation of the confinement dynamics in $SU(2)$ Yang-Mills theory, based on extensive numerical simulations. We have obtained high precision results for quantities which characterize confinement and the critical properties of the deconfinement phase transition, such as the temperature dependence of the holonomy potential, the order parameter for deconfinement transition, static quark-antiquark potentials, as well as spatial Wilson loops. In particular, we study the influence of finite volume effects, the dyon-antidyon correlations as well as the screening mass on the confinement dynamics. The results presented in this thesis, which are based on the works published in [47, 48], are considerably improved compared with previous studies and we provide many results which have not been previously reported. In addition, we present a precise quantitative comparison with lattice data, showing a remarkable agreement between both results. The second part of this study consists in the modification of the ensemble to include dynamical quarks and investigate the fermionic effects in the deconfinement phase transition and observe the chiral phase transition.

⁴There are a variety of interesting alternative ideas about possible mechanisms and possible topological objects that may drive the confinement dynamics, such as [36–39].

The structure of this work is thus organized as follows. In Chapter 2 we give some preliminaries on field theories at finite temperature and the basic thermal properties of confinement and chiral symmetry. In Chapter 3, we review the derivation of several classical gauge configurations leading to the KvBLL caloron solution. Chapter 4 comprises the construction of the instanton-dyon ensemble in $SU(2)$ Yang-Mills, afterwards, details of the numerical simulations are explained thoroughly, ending with the presentation and discussion of all the results relevant to confining dynamics. In Chapter 5 we introduce one-flavor quarks into the ensemble, the main generalities of the fermionic contributions are discussed with an explicit calculation of the matrix elements which approximate the fermion determinant. We then analyze the influence of fermions to the deconfinement transition and the chiral properties of the system. A summary and final conclusions are discussed in Chapter 6. Finally, Appendices A, B and C contain detailed derivations of the topological charge in terms of gauge fields and the fermion zero modes in the background of instanton-dyons.

CHAPTER 2

NON-ABELIAN GAUGE THEORIES AT FINITE TEMPERATURE

In this chapter we review the fundamental properties of finite temperature field theory needed for the comprehension of the core material of this thesis. In addition, we present the general characteristics of confinement and chiral symmetry, with their associated phase transitions.

2.1 EUCLIDEAN QUANTUM CHROMODYNAMICS

Quantum Chromodynamics or QCD for short, the underlying quantum field theory of the strong interactions, is constructed as a non-Abelian gauge theory with $SU(3)$ the corresponding gauge group. Its Lorentz and gauge invariant Lagrangian¹ in Minkowski spacetime reads as

$$\mathcal{L}_{\text{QCD}} = -\frac{1}{4}F_{\mu\nu}^a F^{\mu\nu,a} + \sum_{k=1}^{N_f} \bar{\psi}_k (i\gamma^\mu D_\mu - m_k) \psi_k. \quad (2.1)$$

One may refer to QCD-like theories as quantum field theories with different gauge groups coupled with fermions, in particular the special $SU(N_c)$ group, where N_c defines the number of color degrees of freedom. The study of such theories are not only of mathematical interest, but can produce a great amount of physical insight and, in some instances, simplify the calculations significantly. For that reason, in this work we will focus on $SU(2)$ gauge theory, where the results can in principle be generalized to the more physical theory of $SU(3)$ by some embedding scheme.

The structure of the Lagrangian Eq. (2.1), clearly does not change with N_c , so let us examine

¹Technically, \mathcal{L} is a Lagrange density with the actual Lagrangian defined as $\int d^3x \mathcal{L}$; however, for the sake of simplicity and tradition, \mathcal{L} will be referred to as Lagrangian.

each component in detail. The first term, identified as the Yang-Mills Lagrangian

$$\mathcal{L}_{\text{YM}} = -\frac{1}{4}F_{\mu\nu}^a F^{\mu\nu,a}, \quad (2.2)$$

contains the ‘‘color’’ dynamics of the gauge fields $A_\mu \equiv A_\mu^a t^a$, with t^a the gauge group generators in the fundamental representation, normalized to $\text{Tr} [t^a t^b] = \delta^{ab}/2$ and satisfying the Lie algebra

$$[t^a, t^b] = if^{abc}t^c, \quad (2.3)$$

which, in the $SU(2)$ case, $t^a = \tau^a/2$ where τ are the well-known Pauli matrices and the structure constants of the Lie algebra are ε^{abc} , namely, the Levi-Civita tensor.

Analogous to Electrodynamics, $F_{\mu\nu} \equiv F_{\mu\nu}^a t^a$ is the non-Abelian gauge field strength tensor

$$F_{\mu\nu} = \partial_\mu A_\nu - \partial_\nu A_\mu - ig[A_\mu, A_\nu], \quad (2.4)$$

where g is the bare coupling of the theory.

The second term in Eq. (2.1) corresponds to the matter contribution, in particular, that of the fermion/quark fields ψ , which are spinors in the fundamental representation with mass m_k and total number of flavors N_f . The covariant derivative D_μ , induced by local gauge invariance, has the form

$$D_\mu = \partial_\mu - igA_\mu^a t^a, \quad (2.5)$$

which is multiplied by the Dirac matrices γ^μ .

As mentioned earlier, fascinating phenomena take place in the non-zero temperature domain of QCD. Hence, it is of the utmost interest to develop a method to study it. As it is known from statistical mechanics, the thermodynamics of a system characterized by a Hamiltonian H at temperature T , is best described through the canonical partition function

$$\mathcal{Z} \equiv \text{Tr} e^{-\beta H}, \quad \beta = \frac{1}{T} \quad (2.6)$$

When dealing with field theories, a subject that has evolved into a complete area of study [49–51]; it has been found that an Euclidean quantum field theory in $\mathbb{R}^D \times S^1$ spacetime is equivalent to quantum statistical mechanics in D -dimensional space (see [52] and references therein). The connection is easier to appreciate through the path integral representation of the partition function. Without exploring it in detail, let us see this by recalling that the generating functional of a free scalar field theory in $D + 1$ Minkowskian space-time is given by

$$Z[0] = \int \mathcal{D}\varphi e^{i \int d^{D+1}x \mathcal{L}(\varphi)}, \quad (2.7)$$

where $\mathcal{D}\varphi$ is the functional integration measure. On the other hand, the integral representation of the partition function of a system with Hamiltonian $H(q, p)$ is²

$$\mathcal{Z} = \int_{q(0)=q(\beta)} \mathcal{D}q e^{-\int_0^\beta d\tau L(q)}, \quad (2.8)$$

where the trace enforces periodic boundary conditions along the “*Euclidean time*” τ and $L(q)$ is the Euclidean Lagrangian. The similarities between Eqs. (2.7) and (2.8) lead to the conclusion that the partition function for a field theory is analogous to the generating functional $Z[0]$, but in Euclidean space-time and with the appropriate boundary conditions.

Consequently, the recipe to write the partition function of any field theory, say in $3 + 1$ dimensions, consists of analytically continuing time as $x_0 \rightarrow -ix_4$, also known as a Wick rotation, thus mapping Minkowskian spacetime into Euclidean space, with x_4 being the Euclidean time; and then writing the corresponding Lagrangian in the path integral, accounting for the correct boundary conditions: periodic for bosonic fields and antiperiodic for fermionic fields. Therefore, the general $SU(N_c)$ QCD partition function, ignoring ghost and gauge fixing terms, will look like

$$\mathcal{Z}_{\text{QCD}} = \int \mathcal{D}A_\mu^E \mathcal{D}\psi^E \mathcal{D}\psi^{\dagger E} \exp \left[- \int_0^\beta dx_4 \int d^3x \mathcal{L}_{\text{QCD}}^E \right], \quad (2.9)$$

where the label E stands for Euclidean and $A_\mu^E(\vec{x}, 0) = A_\mu^E(\vec{x}, \beta)$ and $\psi^E(\vec{x}, 0) = -\psi^E(\vec{x}, \beta)$. The explicit form of the Euclidean QCD Lagrangian is obtained by first noticing that the Euclidean

²Multiplied by some constant resulting from the integration $\int \mathcal{D}p$.

gauge fields are defined in terms of their Minkowskian counterparts as

$$A_i^E = -A_i^M, \quad A_4^E = -iA_0^M, \quad (2.10)$$

leading to an Euclidean covariant derivative and field strength tensor

$$D_\mu^E = \partial_\mu - igA_\mu^E, \quad F_{\mu\nu}^E = \partial_\mu A_\nu^E - \partial_\nu A_\mu^E - ig[A_\mu^E, A_\nu^E], \quad (2.11)$$

which are related to their Minkowskian counterparts as

$$\begin{aligned} D_i^E &= -D_i^M, & D_4^E &= -iD_0^M, \\ F_{ij}^E &= F_{ij}^M, & F_{4j}^E &= -iF_{0j}^M. \end{aligned} \quad (2.12)$$

For the fermionic part, the Euclidean γ -matrices, satisfying the Clifford algebra $\{\gamma_\mu, \gamma_\nu\} = 2\delta_{\mu\nu}$, are defined (in the chiral representation) as

$$\gamma_4 = \begin{pmatrix} 0 & \mathbf{1} \\ \mathbf{1} & 0 \end{pmatrix}, \quad \gamma_i = \begin{pmatrix} 0 & -i\sigma_i \\ i\sigma_i & 0 \end{pmatrix}, \quad (2.13)$$

with σ_i the well known Pauli matrices. To preserve Lorentz covariance, the Euclidean spinors are written as

$$\psi^E = \psi^M, \quad \psi^{\dagger E} = i\bar{\psi}^M, \quad (2.14)$$

such that under $SO(4)$ rotations, $\psi^{\dagger E}\psi^E$ transforms as a scalar and $\psi^{\dagger E}\gamma_\mu^E\psi^E$ as a vector [53, 54].

Finally, the Euclidean QCD Lagrangian is written as³

$$\mathcal{L}_{\text{QCD}}^E = \frac{1}{2g^2} \text{Tr} [F_{\mu\nu}^E F_{\mu\nu}^E] + \sum_{k=1}^{N_f} \psi_k^{\dagger E} (-i\gamma_\mu^E D_\mu^E - im_k) \psi_k^E. \quad (2.15)$$

From this point forward, we will drop the E label and it should be understood that we are working in Euclidean spacetime, unless otherwise specified.

³From the normalization $\text{Tr} [t^a t^b] = \delta^{ab}/2$, it follows that $\text{Tr} [F_{\mu\nu} F_{\mu\nu}] = \frac{1}{2} F_{\mu\nu}^a F_{\mu\nu}^a$. In addition, to simplify the notation in the following sections, we have absorbed the coupling g into the gauge field as $gA_\mu \rightarrow A_\mu$.

To conclude this section, let us make the simple topological remark that the periodic boundary conditions imposed by the trace is actually equivalent to the compactification of the temporal line into a circle of circumference β , in other words, the manifold in which D -dimensional finite temperature field theories are defined is $\mathbb{R}^D \times S^1$.

2.2 THE POLYAKOV LOOP AND THE CONFINEMENT PHASE TRANSITION

For a while, it has been known that at low temperatures, quarks and gluons are confined to form bound states, namely, hadrons. To unravel the nature of this phenomenon is quite challenging since it requires a deep understanding of the non-perturbative dynamics of the quark and gluon fields.

In the absence of dynamical fermions, that is, pure gauge theory or Yang-Mills theory, one can extract important information about confinement which can be further extended to the physical picture of QCD. At finite temperature, there is a crucial quantity which helps define the meaning of confinement in such a theory: the Polyakov loop [55, 56]

$$L(\vec{x}) = \mathcal{P} \exp \left[i \int_0^\beta dx_4 A_4(\vec{x}, x_4) \right], \quad (2.16)$$

where \mathcal{P} stands for path-ordered product since A_4 is an element of the Lie Algebra $\mathfrak{su}(N_c)$. Its physical meaning is related to the excess free energy of a static quark in a Yang-Mills vacuum.⁴ To make sense of this, let us begin by first defining the operators $\Psi^{\dagger a}(\vec{x}, x_4)$ and $\Psi^a(\vec{x}, x_4)$ which satisfy the equal-time anticommutation relation

$$\left\{ \Psi^a(\vec{x}_i, x_4), \Psi^{\dagger b}(\vec{x}_j, x_4) \right\} = \delta_{ij} \delta^{ab}. \quad (2.17)$$

Respectively, they create and annihilate a static quark, which transforms under the fundamental representation of the gauge group, at position \vec{x} , time x_4 and color component a . Let us consider a system with a single static test quark coupled to Yang-Mills fields. The free energy F_q of the test quark is clearly defined by the difference in free energy between the system with the quark and

⁴See [57–59] for more details.

that of pure Yang-Mills. Therefore,

$$\begin{aligned}
e^{-\beta F_q} &= \frac{1}{\mathcal{Z}} \sum_s \langle s | e^{-\beta H} | s \rangle \\
&= \frac{1}{\mathcal{Z}} \frac{1}{N_c} \sum_{s'} \sum_{a=1}^{N_c} \langle s' | \Psi^a(\vec{x}, 0) e^{-\beta H} \Psi^{\dagger a}(\vec{x}, 0) | s' \rangle,
\end{aligned} \tag{2.18}$$

with \mathcal{Z} the partition function of the pure gauge system. One should notice that the $|s'\rangle$ states correspond to those without the static quark, namely, the Yang-Mills vacuum states.

In the imaginary time formalism, the time evolution operator $e^{-x_4 H}$, generates time translations on an arbitrary operator $\hat{\mathcal{O}}(x_4)$ as

$$e^{\beta H} \hat{\mathcal{O}}(x_4) e^{-\beta H} = \hat{\mathcal{O}}(x_4 + \beta). \tag{2.19}$$

Moreover, in the static limit, where the quark mass is infinitely large, the ‘‘heavy’’ quark fields (in the appropriate gauge) satisfy the equation of motion

$$\left[\frac{\partial}{\partial x_4} - i A_4(\vec{x}, x_4) \right] \Psi(\vec{x}, x_4) = 0, \tag{2.20}$$

whose solution takes the form

$$\Psi(\vec{x}, x_4) = \mathcal{P} \exp \left[i \int_0^{x_4} dx'_4 A_4(\vec{x}, x'_4) \right] \Psi(\vec{x}, 0). \tag{2.21}$$

Therefore, making use of Eqs. (2.19) and (2.21), the anticommutation relations and inserting the Polyakov Loop definition of Eq. (2.16), we obtain the free energy of the single quark as follows

$$\begin{aligned}
e^{-\beta F_q} &= \frac{1}{\mathcal{Z}} \frac{1}{N_c} \sum_{s'} \sum_{a=1}^{N_c} \langle s' | e^{-\beta H} \Psi^a(\vec{x}, \beta) \Psi^{\dagger a}(\vec{x}, 0) | s' \rangle \\
&= \frac{1}{\mathcal{Z}} \frac{1}{N_c} \sum_{s'} \sum_{a=1}^{N_c} \langle s' | e^{-\beta H} L^{ab}(\vec{x}) \Psi^b(\vec{x}, 0) \Psi^{\dagger a}(\vec{x}, 0) | s' \rangle \\
&= \frac{1}{\mathcal{Z}} \frac{1}{N_c} \sum_{s'} \langle s' | e^{-\beta H} \text{Tr} L(\vec{x}) | s' \rangle \\
&= \left\langle \frac{1}{N_c} \text{Tr} L(\vec{x}) \right\rangle.
\end{aligned} \tag{2.22}$$

In a similar fashion, one could find the free energy of a quark-antiquark pair, $F_{q\bar{q}}$, simply by adding the corresponding charge conjugate creation and annihilation operators and use the right equations of motion. The result is

$$e^{-\beta F_{q\bar{q}}} = \frac{1}{N_c^2} \left\langle \text{Tr}L(\vec{x})\text{Tr}L^\dagger(\vec{y}) \right\rangle, \quad (2.23)$$

where \vec{x} and \vec{y} are the locations of the heavy quark and antiquark, respectively.

By examining Eq. (2.22), one can see that a vanishing thermal expectation value of the traced Polyakov loop yields infinite free energy, excluding the possibility of having isolated color charges in the system, i.e., the theory is in a *confined phase*. In contrast, a non-zero value results in finite free energy, free color charges are allowed, meaning the system is in the *deconfined phase*.

Regarding the correlator of traced Polyakov loops (Eq. (2.23)), the clustering property determines that at large separations

$$\left\langle \text{Tr}L(\vec{x})\text{Tr}L^\dagger(\vec{y}) \right\rangle \xrightarrow{|\vec{x}-\vec{y}|\rightarrow\infty} \langle \text{Tr}L(\vec{x}) \rangle \langle \text{Tr}L^\dagger(\vec{y}) \rangle = |\langle \text{Tr}L(\vec{x}) \rangle|^2. \quad (2.24)$$

If $\langle \text{Tr}L(\vec{x}) \rangle = 0$, the static quark-antiquark potential $F_{q\bar{q}}$ will grow to infinity with the separation of the quarks as $F_{q\bar{q}} \propto |\vec{x} - \vec{y}|$. The emergence of such rising linear potential is thus another key feature that a *confining* theory must satisfy.

2.2.1 Center Symmetry Breaking

The Euclidean Yang-Mills action, by construction, is invariant under gauge transformations of the form

$$A_\mu \rightarrow UA_\mu U^\dagger + iU\partial_\mu U^\dagger, \quad U(\vec{x}, x_4) \in SU(N_c), \quad (2.25)$$

where the Polyakov loop transforms as

$$L(\vec{x}) \rightarrow U(\vec{x}, 0)L(\vec{x})U^\dagger(\vec{x}, \beta). \quad (2.26)$$

Evidently, the trace of the transformed Polyakov loop is invariant when U is periodic; however,

for a certain type of non-periodic gauge transformations of the form

$$U(\vec{x}, x_4 + \beta) = zU(\vec{x}, x_4), \quad z = e^{2\pi i n/N_c} \mathbf{1}, \quad n \in [0, N_c - 1], \quad (2.27)$$

with z an element of the center⁵ of the gauge group (in particular $z \in Z(N_c)$ for $SU(N_c)$); the traced Polyakov loop will transform as

$$\text{Tr}L(\vec{x}) \rightarrow z\text{Tr}L(\vec{x}). \quad (2.28)$$

At low temperatures [60], a vanishing expectation value of $\langle \text{Tr}L(\vec{x}) \rangle = 0$, where we have already defined the theory in a confined phase, points to the realization of the *center symmetry*. Increasing the temperature above some critical value T_c , will lead to a non-zero expectation value $\langle \text{Tr}L(\vec{x}) \rangle \neq 0$, requiring the spontaneous breakdown of the symmetry. This defines the traced Polyakov loop as the order parameter of the deconfinement phase transition, characterized by the breaking of the $Z(N_c)$ center symmetry.

A very compelling feature conjectured by Svetitsky and Yaffe [61, 62] establishes that the confinement/deconfinement phase transition in pure gauge theories, shares critical behavior with other spins models. For instance, the $SU(2)$ Yang-Mills theory in (3+1) dimensions will belong to the same universality class as that of the $Z(2)$ 3-dimensional Ising model, indicating that the deconfinement phase transition should be second order. Several numerical studies, such as [63–68], strongly support this reasoning. Similarly, $SU(3)$ gauge theory would then be expected to have a first order deconfinement phase transition such as that of the $Z(3)$ Potts model, which has also been observed on lattice simulations [69, 70].

The introduction of dynamical quarks of finite mass, such as in QCD-like theories, makes the description of confinement much more intricate. The antiperiodic boundary conditions of the fermion fields break explicitly the center symmetry $Z(N_c)$ and the trace of the Polyakov loop is no longer an order parameter. Deconfinement changes from a non-analytic phase transition into a smooth crossover. Despite these difficulties, the Polyakov loop can still be considered as an indicator of confinement and thus a relevant observable to study.

⁵The center of a group G is defined as the subgroup whose elements commute with all other elements of G .

2.3 CHIRAL SYMMETRY

In the *chiral limit*, where the masses of the N_f fermions are zero, the QCD Lagrangian possess and additional symmetry under global transformations of the group

$$U_V(1) \times U_A(1) \times SU_L(N_f) \times SU_R(N_f). \quad (2.29)$$

Roughly speaking, the $U_V(1)$ symmetry results in the conservation of fermion number. The axial $U_A(1)$ symmetry, despite being satisfied by the classical Lagrangian, is not conserved at the quantum level, a phenomenon known as the *axial anomaly*. The *chiral* symmetry $SU_L(N_f) \times SU_R(N_f)$ is satisfied by the theory; however, this is not manifested in the mass spectrum of hadrons. The large mass difference between states with opposite parities and same quantum numbers cannot be attributed to the current quark mass which already breaks the symmetry explicitly. Consequently, the invariance of the vacuum state under chiral transformations suggests that the symmetry is spontaneously broken, following the pattern

$$SU_L(N_f) \times SU_R(N_f) \rightarrow SU_f(N_f), \quad (2.30)$$

with $SU_f(N_f)$ often called the *flavor group*.

Contrary to the center symmetry breaking explored previously, the broken symmetry in this case is continuous and, according to Goldstone's theorem [71–73], $N_f^2 - 1$ massless excitations should appear in the spectrum, the so called Nambu-Goldstone bosons. In QCD, these particles are the pseudoscalar mesons whose masses, although relatively small but non-zero nonetheless, is a consequence of the current quark masses.

The spontaneous breaking of the chiral symmetry should then have an order parameter that characterizes the chiral phase transition, namely, that it vanishes in the symmetric phase and is non-zero when the symmetry is broken. Such quantity is the *quark* or *chiral condensate* $\langle \psi^\dagger \psi \rangle$ (in Euclidean space). A very useful way to express the condensate is in terms of the density of eigenvalues of the Dirac operator. For this, let us notice that the fermion propagator $S(x, y)$ can

be written in the spectral representation as

$$S(x, y) = - \left\langle (i\mathcal{D} + im)^{-1} \right\rangle = - \sum_n \frac{\phi_n(x)\phi_n^\dagger(y)}{\lambda_n + im}, \quad (2.31)$$

where ϕ_n are the normalized eigenfunctions satisfying the eigenvalue equation $i\mathcal{D}\phi_n = \lambda_n\phi_n$. Since the spectrum is chirally symmetric, i.e., for every ϕ_n with eigenvalue λ_n , there is a “companion” state $\gamma^5\phi_n$ with eigenvalue $-\lambda_n$, the quark condensate is thus given by

$$\langle \psi^\dagger\psi \rangle = - \langle \text{Tr} S(x, x) \rangle = - \frac{1}{V} \left\langle \sum_{\lambda_n > 0} \frac{2m}{\lambda_n^2 + m^2} \right\rangle, \quad (2.32)$$

where V is the spacetime volume. In the infinite volume limit, the sum over states can be replaced by an integration, defining the density of eigenvalues per unit volume $\rho_\lambda(\lambda)$ as

$$\rho_\lambda(\lambda) = \left\langle \sum_n \delta(\lambda - \lambda_n) \right\rangle, \quad (2.33)$$

which is averaged over the total partition function of the system, leading to

$$\langle \psi^\dagger\psi \rangle = -2m \int d\lambda \frac{\rho_\lambda(\lambda)}{\lambda^2 + m^2}. \quad (2.34)$$

Finally, in the chiral limit where $m \rightarrow 0$, one obtains the famous Banks-Casher formula [74]

$$\langle \psi^\dagger\psi \rangle = -\pi\rho_\lambda(0). \quad (2.35)$$

At high enough temperatures, there is evidence that the chiral symmetry is restored, with a vanishing chiral condensate $\langle \psi^\dagger\psi \rangle = 0$. The order of the phase transition is arguably dependent on N_f , rather than on N_c [75], and based on universality arguments, it has been shown [76] that for $N_f = 2$ the transition should be of second order and of first order for $N_f = 3$.

Since the Dirac operator $i\mathcal{D}$ is defined in terms of a background gauge configuration A_μ , the Banks-Casher relation hints that the physics of chiral symmetry breaking are encoded in A_μ . Therefore, it would be convenient that fields responsible of confinement can be linked to the mechanism of

chiral symmetry breaking⁶. In the next chapter we will deal with the construction of classical gauge fields which will be used for the study of confinement and chiral symmetry at finite temperature.

⁶See discussion in [59].

CHAPTER 3

CLASSICAL GAUGE FIELD CONFIGURATIONS

In the first section of this chapter we introduce and discuss some topological properties of Euclidean Yang-Mills theory. The following sections, contain an in-depth construction of some classical $SU(2)$ gauge configurations, starting with the BPST instanton in \mathbb{R}^4 , followed by its finite temperature generalization, the Harrington-Shepard caloron. Monopole solutions are reviewed later on and finally, an essential ingredient for the construction of the instanton-dyon ensemble, the KvBLL caloron with non-trivial holonomy solution is introduced.

3.1 TOPOLOGY OF YANG-MILLS THEORY

The gauge fields or vector potentials $A_\mu(x)$ are the dynamical variables of Yang-Mills Theory, with a gauge invariant action defined in Euclidean space \mathbb{R}^4 by

$$S_{\text{YM}} \equiv \int d^4x \mathcal{L}_{\text{YM}} = \frac{1}{2g^2} \int d^4x \text{Tr} [F_{\mu\nu} F_{\mu\nu}]. \quad (3.1)$$

Variations with respect to the gauge fields A_μ , lead to the classical equations of motion

$$\frac{\delta S_{\text{YM}}}{\delta A_\mu} = 0 \quad \Rightarrow \quad D_\mu F_{\mu\nu} = 0. \quad (3.2)$$

Solutions to these equations are required to have finite action. As a result, the field strength $F_{\mu\nu}$ must decrease fast enough for the integral to converge, in fact, it should fall off faster than $1/|x|^2$ as $|x| \equiv \sqrt{x_\mu x_\mu} \rightarrow \infty$. This means, that $F_{\mu\nu}$ should vanish on the boundary of \mathbb{R}^4 ; in other words, it should vanish all over the 3-sphere of infinite radius S_E^3 , where E stands for Euclidean space. Clearly, if $A_\mu \rightarrow 0$ then $F_{\mu\nu} \rightarrow 0$ as well; however, we can see that for *pure gauge* configurations,

i.e. $A_\mu = iU\partial_\mu U^\dagger$, with $U \in SU(N_c)$, then

$$F_{\mu\nu} \left(A_\mu = iU\partial_\mu U^\dagger \right) = i\partial_\mu U \partial_\nu U^\dagger - i\partial_\nu U \partial_\mu U^\dagger - i\partial_\mu U \partial_\nu U^\dagger + i\partial_\nu U \partial_\mu U^\dagger = 0,$$

where we have used the identity $\partial_\mu (UU^\dagger) = (\partial_\mu U)U^\dagger + U\partial_\mu U^\dagger = 0$.

Therefore, to have finite action configurations, the necessary boundary condition is that the field approaches a pure gauge, i.e.

$$A_\mu(x) \xrightarrow[|x| \rightarrow \infty]{} iU\partial_\mu U^\dagger. \quad (3.3)$$

Lie groups have the interesting topological property that they can be viewed as manifolds. For instance, $SU(2)$ is the group of 2×2 unitary matrices with unit determinant whose elements are defined as

$$SU(2) = \{a_4 \mathbf{1} + i\vec{a} \cdot \vec{\tau} \mid a_\mu \in \mathbb{R}, a_\mu a_\mu = 1\}, \quad (3.4)$$

where $\vec{\tau} \equiv (\tau^1, \tau^2, \tau^3)$ is the Pauli vector. The space of parameters which characterizes $SU(2)$ is topologically equivalent to that of a unit 3D sphere which we shall call $S_{SU(2)}^3$. Formally, it is said that $SU(2)$ is homeomorphic to S^3 .

The boundary condition Eq. (3.3), requires that U is defined on S_E^3 , i.e., it describes the mapping $U : S_E^3 \rightarrow S_{SU(2)}^3$. Homotopy theory tells us that this mapping is characterized by the homotopy group $\pi_3(S^3)$, which is in a one to one correspondence (isomorphic) to the additive group of integers \mathbb{Z} . In other words, these integers classify the “winding number” of U , meaning how many times one of the spheres is wrapped around the other via the U -mapping. Therefore, we could say that there is a discrete infinity of homotopy classes or sectors, each defined by an integer, often called the *Pontryagin index* or *topological charge* Q_T , that uniquely characterizes the gauge transformations.

It is important to mention that elements belonging to a given sector Q_T , can be continuously deformed into another one of the same sector; however, they cannot be deformed into another one of a different sector, namely, they are not homotopic to each other.

Since we demand that the vector potential A_μ approaches a pure gauge at infinity, it follows that it must be classified into topological sectors with the same charge Q_T as that of U .

The definition of the topological charge Q_T , in terms of the gauge fields A_μ , is given by¹

$$Q_T = \frac{1}{16\pi^2} \int d^4x \operatorname{Tr} F_{\mu\nu} \tilde{F}_{\mu\nu} = \frac{1}{32\pi^2} \int d^4x F_{\mu\nu}^a \tilde{F}_{\mu\nu}^a, \quad (3.5)$$

where $\tilde{F}_{\mu\nu} = \frac{1}{2}\varepsilon_{\mu\nu\alpha\beta}F_{\alpha\beta}$ is the dual field strength tensor.

At finite temperature, where the temporal direction is compactified into S^1 , the gauge fields should still approach vacuum configurations at spatial infinity. In addition to the topological charge, there is an additional parameter which labels the vacuum states [23, 24, 77]: the *holonomy*, defined as the traced Polyakov loop at spatial infinity

$$L_\infty \equiv \lim_{|\vec{x}| \rightarrow \infty} \frac{1}{N_c} \operatorname{Tr} L(\vec{x}). \quad (3.6)$$

Gauge invariance of its eigenvalues allows it to be conveniently parametrized as

$$L(|\vec{x}| \rightarrow \infty) = \operatorname{diag} (e^{2\pi i \mu_1}, \dots, e^{2\pi i \mu_{N_c}}), \quad \sum_{i=1}^{N_c} \mu_i = 0. \quad (3.7)$$

The holonomy is said to be trivial if L is in the center group $Z(N_c)$. Because $Z(N_c)$ only has N_c one-dimensional complex irreducible representations, there are N_c choices for the trivial holonomy:

$$\mu_m = \begin{cases} k/N - 1 & \text{when } m \leq k \\ k/N & \text{when } m > k \end{cases}, \quad \text{where } k = 1, \dots, N_c.$$

For $L \notin Z(N_c)$, the holonomy is non-trivial, the most relevant of this kind being the so-called “*maximally non-trivial*” where all μ 's are equidistant [29]

$$\mu_m = -\frac{1}{2} - \frac{1}{2N} + \frac{m}{N}, \quad (3.8)$$

It is straightforward to see that the latter holonomy leads to $L_\infty = 0$, which recalling from the previous chapter, is a signature of confinement. The thermal expectation value of the holonomy $\langle L_\infty \rangle$ is then equivalently used as the order parameter for the confinement/deconfinement phase transition. Gauge configurations with this feature are then of utmost interest since they suggest to

¹See Appendix A for a detailed derivation.

be relevant for the description of the confinement dynamics.

In the following sections we will discuss the construction of different gauge field solutions which are historically and conceptually important, starting with the \mathbb{R}^4 -instanton up to the caloron with non-trivial holonomy.

3.2 THE BPST INSTANTON

The BPST instanton², discovered in 1975 by Belavin, Polyakov, Schwartz and Tyupkin [3], is a topologically non-trivial classical solution to the $SU(2)$ Yang-Mills equations of motion in Euclidean space Eq. (3.2). Despite the conveniently compact form of these equations, they constitute a highly non-linear system of second order differential equations. In principle, obtaining solutions is a highly non-trivial task; however, a clever way to do it was formulated by Bogomol'nyi [82], by first examining the inequality (now known as Bogomol'nyi bound)

$$0 \leq \int d^4x \left(F_{\mu\nu}^a \mp \tilde{F}_{\mu\nu}^a \right)^2 = \int d^4x \left(2F^2 \mp 2F_{\mu\nu}^a \tilde{F}_{\mu\nu}^a \right) = 8g^2 S_{\text{YM}} \mp 64\pi^2 Q_{\text{T}}, \quad (3.9)$$

which assigns a lower bound on the action given by $S_{\text{YM}} \geq \pm \frac{8\pi^2}{g^2} Q_{\text{T}}$. This inequality is saturated if and only if the (anti)self-duality condition $F_{\mu\nu}^a = \pm \tilde{F}_{\mu\nu}^a$ is satisfied; therefore, to find the instanton solution let us recall that the $SU(2)$ generators of the Lie algebra are $t^a = \tau^a/2$, where τ^a are the Pauli matrices satisfying $\tau^a \tau^b = \delta^{ab} + i\varepsilon^{abc} \tau^c$. It will be convenient to define the matrix 4-vector $\tau_{\mu}^{\pm} \equiv (\vec{\tau}, \mp i)$, which satisfies

$$\tau_{\mu}^{+} \tau_{\nu}^{-} = \delta_{\mu\nu} + i\eta_{\mu\nu}^a \tau^a, \quad \tau_{\mu}^{-} \tau_{\nu}^{+} = \delta_{\mu\nu} + i\bar{\eta}_{\mu\nu}^a \tau^a \quad (3.10)$$

where $\eta_{\mu\nu}^a$ are the so called 't Hooft symbols defined as³

$$\eta_{\mu\nu}^a = \varepsilon_{\mu\nu}^a + \delta_{\mu}^a \delta_{\nu 4} - \delta_{\nu}^a \delta_{\mu 4}, \quad \bar{\eta}_{\mu\nu}^a = \varepsilon_{\mu\nu}^a - \delta_{\mu}^a \delta_{\nu 4} + \delta_{\nu}^a \delta_{\mu 4} \quad (3.11)$$

²There is a plethora of scientific literature about instanton properties. Refer to [53, 78–81] for a good pedagogical approach.

³See Appendix B for some formulas and properties of 't Hooft symbols.

which are antisymmetric and (anti)self-dual in the vector indices

$$\eta_{\mu\nu}^a = \frac{1}{2}\varepsilon_{\mu\nu\alpha\beta}\eta_{\alpha\beta}^a, \quad \bar{\eta}_{\mu\nu}^a = -\frac{1}{2}\varepsilon_{\mu\nu\alpha\beta}\bar{\eta}_{\alpha\beta}^a, \quad \eta_{\mu\nu}^a = -\eta_{\nu\mu}^a. \quad (3.12)$$

The goal is to construct a solution which not only satisfies the boundary condition Eq. (3.3), namely, that it approaches a pure gauge configuration at infinity, but that it also possesses a non-trivial topological charge, $Q_T \neq 0$. To achieve this, we must find a suitable group element U which meets the latter condition. Let us choose

$$U_1^\pm(x) = \frac{i\tau_\mu^\pm x_\mu}{|x|}, \quad (3.13)$$

and use the surface integral expression of Q_T from Eq. (A.9), which we rewrite here for convenience:

$$Q_T = \frac{1}{24\pi^2} \oint_{S_E^3} ds_\mu \varepsilon_{\mu\nu\alpha\beta} \text{Tr} \left\{ \left(U_1^+ \partial_\nu (U_1^+)^\dagger \right) \left(U_1^+ \partial_\alpha (U_1^+)^\dagger \right) \left(U_1^+ \partial_\beta (U_1^+)^\dagger \right) \right\}. \quad (3.14)$$

By substituting the explicit form of U_1^+ , we see that each factor in the trace is of the form

$$\begin{aligned} U_1^+ \partial_\mu (U_1^+)^\dagger &= \left(\frac{\tau_\nu^+ x_\nu}{|x|} \right) \partial_\mu \left(\frac{\tau_\alpha^- x_\alpha}{|x|} \right) \\ &= \left(\frac{\tau_\nu^+ x_\nu}{|x|} \right) \tau_\alpha^- \left(\frac{\delta_{\mu\alpha}}{|x|} - \frac{x_\alpha x_\mu}{|x|^3} \right) \\ &= \frac{x_\nu}{x^2} \left(\tau_\nu^+ \tau_\mu^- - \frac{\tau_\nu^+ \tau_\alpha^- x_\alpha x_\mu}{x^2} \right) \\ &= \frac{x_\nu}{x^2} \left(i\eta_{\nu\mu}^a \tau^a + \delta_{\nu\mu} - \frac{(i\eta_{\nu\alpha}^a \tau^a + \delta_{\nu\alpha}) x_\alpha x_\mu}{x^2} \right) \\ &= \frac{i\eta_{\nu\mu}^a \tau^a x_\nu}{x^2} + \frac{x_\mu}{x^2} - \frac{i\eta_{\nu\alpha}^a \tau^a x_\nu x_\alpha x_\mu}{x^2} - \frac{x_\nu x_\mu x_\mu}{x^4} \\ &= -2i\eta_{\mu\nu}^a \frac{x_\nu}{x^2} t^a, \end{aligned} \quad (3.15)$$

with $x^2 \equiv |x|^2$. Therefore, the full trace in Eq. (3.14) can be reduced to

$$\begin{aligned} \text{Tr} \left\{ \left(U_1^+ \partial_\nu (U_1^+)^\dagger \right) \left(U_1^+ \partial_\alpha (U_1^+)^\dagger \right) \left(U_1^+ \partial_\beta (U_1^+)^\dagger \right) \right\} &= 8i\eta_{\nu\rho}^a \eta_{\alpha\tau}^b \eta_{\beta\gamma}^c \frac{x_\rho x_\tau x_\gamma}{x^6} \text{Tr} t^a t^b t^c \\ &= -2\varepsilon^{abc} \eta_{\nu\rho}^a \eta_{\alpha\tau}^b \eta_{\beta\gamma}^c \frac{x_\rho x_\tau x_\gamma}{x^6} \end{aligned} \quad (3.16)$$

Using identity Eq. (B.8) followed by Eq. (B.5), we expand the last term

$$\begin{aligned}
-2\varepsilon^{abc}\eta_{\nu\rho}^a\eta_{\alpha\tau}^b\eta_{\beta\gamma}^c\frac{x_\rho x_\tau x_\gamma}{x^6} &= -2\frac{x_\rho x_\tau x_\gamma}{x^6}\eta_{\nu\rho}^a(\delta_{\alpha\beta}\eta_{\tau\gamma}^a - \delta_{\alpha\gamma}\eta_{\tau\beta}^a - \delta_{\tau\beta}\eta_{\alpha\gamma}^a + \delta_{\tau\gamma}\eta_{\alpha\beta}^a) \\
&= -2\frac{x_\rho x_\tau x_\gamma}{x^6}[\delta_{\alpha\beta}(\delta_{\nu\tau}\delta_{\rho\gamma} - \delta_{\nu\gamma}\delta_{\rho\tau} + \varepsilon_{\nu\rho\tau\gamma}) \\
&\quad - \delta_{\alpha\gamma}(\delta_{\nu\tau}\delta_{\rho\beta} - \delta_{\nu\beta}\delta_{\rho\tau} + \varepsilon_{\nu\rho\tau\beta}) \\
&\quad - \delta_{\tau\beta}(\delta_{\nu\alpha}\delta_{\rho\gamma} - \delta_{\nu\gamma}\delta_{\rho\alpha} - \varepsilon_{\nu\rho\alpha\gamma}) \\
&\quad + \delta_{\tau\gamma}(\delta_{\nu\alpha}\delta_{\rho\beta} - \delta_{\nu\beta}\delta_{\rho\alpha} + \varepsilon_{\nu\rho\alpha\beta})]. \tag{3.17}
\end{aligned}$$

Finally, we multiply the last result by $\varepsilon_{\mu\nu\alpha\beta}$, which due to its antisymmetric nature, it is straightforward to see that most terms will vanish, remaining only

$$\begin{aligned}
-2\frac{x_\rho x_\tau x_\gamma}{x^6}\varepsilon_{\mu\nu\alpha\beta}(-\delta_{\alpha\gamma}\delta_{\nu\tau}\delta_{\rho\beta} + \delta_{\tau\beta}\delta_{\nu\gamma}\delta_{\rho\alpha} + \delta_{\tau\gamma}\varepsilon_{\nu\rho\alpha\beta}) &= -2\frac{\varepsilon_{\mu\nu\alpha\beta}}{x^6}(x^2x_\rho\varepsilon_{\nu\rho\alpha\beta}) \\
&= 12\frac{x_\mu}{x^4}, \tag{3.18}
\end{aligned}$$

where we have used the identity $\varepsilon_{\mu\nu\alpha\beta}\varepsilon_{\nu\rho\alpha\beta} = -6\delta_{\mu\rho}$ in the last equality.

The integral Eq. (3.14) can now be easily computed by plugging-in the integrand, rewrite the surface element as $d\vec{s}_\mu = \hat{x}_\mu x^3 d\Omega = x_\mu x^2 d\Omega$ and make use of the definition of the solid angle in d -dimensions $\Omega^d = 2\pi^{d/2}/\Gamma(\frac{d}{2})$, leading to

$$Q_T = \frac{1}{24\pi^2} \oint_{S_E^3} d\vec{s}_\mu \left(12\frac{x_\mu}{x^4}\right) = \frac{1}{2\pi^2} \int d\Omega = 1. \tag{3.19}$$

Therefore, a gauge field A_μ which satisfies the boundary condition

$$\lim_{|x|\rightarrow\infty} A_\mu(x) = iU_1^+ \partial_\mu (U_1^+)^\dagger = 2\eta_{\mu\nu}^a \frac{x_\nu}{x^2} t^a, \tag{3.20}$$

will have unit topological charge $Q_T = 1$. Analogously, for U_1^- , one obtains $Q_T = -1$ and

$$\lim_{|x|\rightarrow\infty} \bar{A}_\mu(x) = iU_1^- \partial_\mu (U_1^-)^\dagger = 2\bar{\eta}_{\mu\nu}^a \frac{x_\nu}{x^2} t^a. \tag{3.21}$$

The next in the construction of the full instanton field is to look for solutions of the self-dual

equations $F_{\mu\nu}^a = \tilde{F}_{\mu\nu}^a$. Our previous results, suggest taking the ansatz [78]

$$A_\mu^a(x) = 2\eta_{\mu\nu}^a \frac{x_\nu}{x^2} f(x^2) \quad (3.22)$$

where f must satisfy the boundary conditions

$$\lim_{x^2 \rightarrow \infty} f(x^2) = 1 \quad \text{and} \quad \lim_{x^2 \rightarrow 0} f(x^2) \propto x^2 \quad (3.23)$$

The last condition ensures there are no singularities at the origin. Substituting the ansatz into the field strength tensor one gets

$$\begin{aligned} F_{\mu\nu}^a &= \partial_\mu A_\nu^a - \partial_\nu A_\mu^a + \varepsilon^{abc} A_\mu^b A_\nu^c \\ &= 2\eta_{\nu\alpha}^a \partial_\mu \left(\frac{x_\alpha f}{x^2} \right) - 2\eta_{\mu\alpha}^a \partial_\nu \left(\frac{x_\alpha f}{x^2} \right) + \frac{4x_\alpha x_\beta f}{x^4} \varepsilon^{abc} \eta_{\mu\alpha}^b \eta_{\nu\beta}^c \end{aligned} \quad (3.24)$$

The last term can be expanded using identity Eq. (B.8), such that

$$\frac{4x_\alpha x_\beta f}{x^4} \varepsilon^{abc} \eta_{\mu\alpha}^b \eta_{\nu\beta}^c = \frac{4f^2}{x^4} (\delta_{\mu\nu} x_\alpha x_\beta \eta_{\alpha\beta}^a - x_\alpha x_\mu \eta_{\alpha\nu}^a + x^2 \eta_{\mu\nu}^a - x_\nu x_\beta \eta_{\mu\beta}^a). \quad (3.25)$$

Therefore, since $\partial_\mu f = 2x_\mu f'$ with $f' \equiv \partial f / \partial(x^2)$,

$$\begin{aligned} F_{\mu\nu}^a &= \frac{2\eta_{\nu\mu}^a}{x^2} f + \frac{4\eta_{\nu\alpha}^a x_\mu x_\alpha}{x^2} f' - \frac{4\eta_{\nu\alpha}^a x_\mu x_\alpha}{x^4} f - \frac{2\eta_{\mu\nu}^a}{x^2} f - \frac{4\eta_{\mu\alpha}^a x_\nu x_\alpha}{x^2} f' + \frac{4\eta_{\mu\alpha}^a x_\nu x_\alpha}{x^4} f \\ &+ \frac{4\eta_{\mu\nu}^a}{x^2} f^2 - \frac{4\eta_{\alpha\nu}^a x_\alpha x_\mu}{x^4} f^2 - \frac{4\eta_{\mu\alpha}^a x_\alpha x_\nu}{x^4} f^2 \\ &= -\frac{4\eta_{\mu\nu}^a}{x^2} f(1-f) - 4x^2 f' \left(\frac{\eta_{\mu\alpha}^a x_\nu x_\alpha - \eta_{\nu\alpha}^a x_\mu x_\alpha}{x^4} \right) \\ &+ 4f \left(\frac{\eta_{\mu\alpha}^a x_\nu x_\alpha - \eta_{\nu\alpha}^a x_\mu x_\alpha}{x^4} \right) - 4f^2 \left(\frac{\eta_{\mu\alpha}^a x_\nu x_\alpha - \eta_{\nu\alpha}^a x_\mu x_\alpha}{x^4} \right) \\ &= -4 \left\{ \frac{\eta_{\mu\nu}^a}{x^2} f(1-f) - \left(\frac{\eta_{\mu\alpha}^a x_\nu x_\alpha - \eta_{\nu\alpha}^a x_\mu x_\alpha}{x^4} \right) [f(1-f) - x^2 f'] \right\}. \end{aligned} \quad (3.26)$$

Similarly, the dual strength tensor takes the form

$$\begin{aligned}\tilde{F}_{\mu\nu}^a &= \frac{1}{2}\varepsilon_{\mu\nu\beta\gamma}F_{\beta\gamma}^a \\ &= -4\left\{\eta_{\mu\nu}^a f' + \left(\frac{\eta_{\mu\alpha}^a x_\nu x_\alpha - \eta_{\nu\alpha}^a x_\mu x_\alpha}{x^4}\right)[f(1-f) - x^2 f']\right\}.\end{aligned}\quad (3.27)$$

The self-duality condition $F_{\mu\nu}^a = \tilde{F}_{\mu\nu}^a$ leads to

$$F_{\mu\nu}^a - \tilde{F}_{\mu\nu}^a = -4\left\{\frac{\eta_{\mu\nu}^a}{x^2} - 2\left(\frac{\eta_{\mu\alpha}^a x_\nu x_\alpha - \eta_{\nu\alpha}^a x_\mu x_\alpha}{x^4}\right)\right\}[f(1-f) - x^2 f'] = 0, \quad (3.28)$$

which is only realized when $f(1-f) - x^2 f' = 0$. The solution to this differential equation is easily obtainable and found to be

$$f(x^2) = \frac{x^2}{x^2 + \rho^2}. \quad (3.29)$$

Here, ρ^2 is a constant of integration and ρ is usually called the *instanton size* or *instanton radius*. The construction of the solution is now complete, so plugging the last result into the ansatz Eq. (3.22), we obtain that the BPST instanton in the so called regular gauge is

$$A_\mu^a(x) = 2\eta_{\mu\nu}^a \frac{x_\nu}{x^2 + \rho^2}. \quad (3.30)$$

The field strength tensor of the instanton (in regular gauge) is straightforward to compute by noticing that since the second term in Eq. (3.26) vanishes, it is reduced to

$$F_{\mu\nu}^a = -4\eta_{\mu\nu}^a \frac{\rho^2}{(x^2 + \rho^2)^2}. \quad (3.31)$$

Direct calculation of the instanton action yields

$$S = \frac{1}{4g^2} \int d^4x F_{\mu\nu}^a F_{\mu\nu}^a = \frac{1}{4g^2} \int d^4x \left[\frac{192\rho^4}{(x^2 + \rho^2)^4} \right] = \frac{8\pi^2}{g^2}, \quad (3.32)$$

as expected for an object with topological charge $Q_T = 1$ and minimal action.

On Fig. 3.1, the action density $\text{Tr}F_{\mu\nu}F_{\mu\nu}$ is plotted as a function of z and x_4 . The observed lump in the x_4 -direction shows that the field is not only localized in space, but also in Euclidean

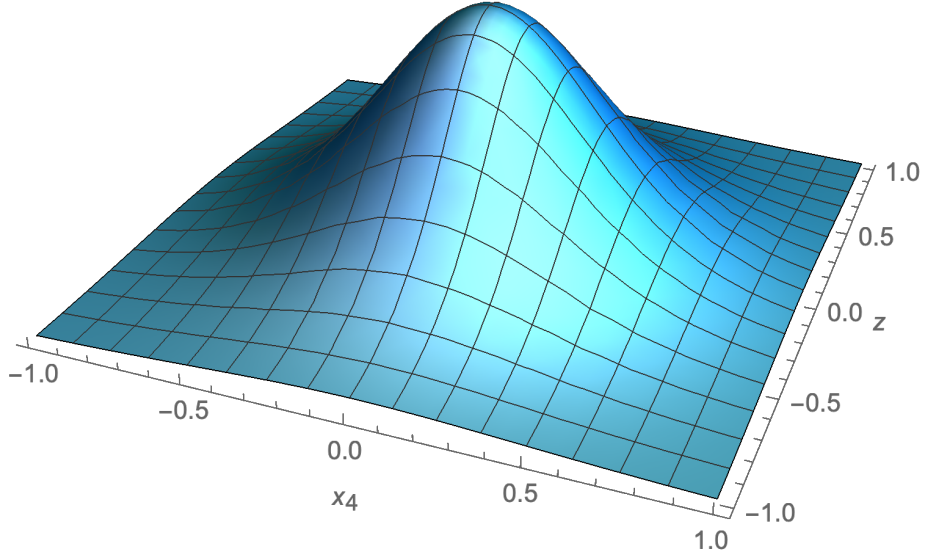


Figure 3.1: Action density of the BPST instanton field for $y = z = 0$ and $\rho = 1$.

time; this feature and its similarities with solitons were the motivation for the term “instanton”, coined by ’t Hooft [78].

The anti-instanton solution $\bar{A}_\mu(x)$ is obtained from Eq. (3.21) and requiring an anti-self-dual condition for its correspondent field strength tensor.

For the sake of completeness, we write the instanton field in the *singular gauge* by means of the gauge transformation U_1^- (see Eq. (3.13))

$$A_\mu \rightarrow A_\mu^S = U_1^- A_\mu (U_1^-)^\dagger + iU_1^- \partial_\mu (U_1^-)^\dagger \quad (3.33)$$

taking the form

$$\begin{aligned} A_\mu^S(x) &= -2\bar{\eta}_{\mu\nu}^a \frac{x_\nu}{x^2 + \rho^2} t^a + 2\bar{\eta}_{\mu\nu}^a \frac{x_\nu}{x^2} t^a \\ &= 2\bar{\eta}_{\mu\nu}^a \frac{x_\nu \rho^2}{x^2 (x^2 + \rho^2)} t^a. \end{aligned} \quad (3.34)$$

The anti-instanton \bar{A}_μ^S is simply obtained via the substitution $\bar{\eta}_{\mu\nu}^a \rightarrow \eta_{\mu\nu}^a$, i.e., the gauge trans-

formation needed would be U_1^+ . The field strength tensor in this gauge is given by

$$F_{\mu\nu}^a = \frac{4\rho^2}{x^2(x^2 + \rho^2)^2} (2\bar{\eta}_{\mu\alpha}^a x_\nu x_\alpha - 2\bar{\eta}_{\nu\alpha}^a x_\mu x_\alpha - \bar{\eta}_{\mu\nu}^a x^2). \quad (3.35)$$

Despite the presence of a singularity at the origin (hence the name “singular gauge”) in A_μ^S and $F_{\mu\nu}$, the action density $F_{\mu\nu}^a F_{\mu\nu}^a$ remains unchanged and smooth due to gauge invariance; therefore, such singularity is unphysical and simply a gauge effect. Nevertheless, the interesting topological properties are now located at the origin, rather than infinity [21].

3.2.1 Moduli Space of the Instanton

The *moduli space* or the set of *collective coordinates* is defined as the space of all solutions to the self-dual equations, modulo gauge transformations, in a given topological sector Q_T and gauge group. Collective coordinates are essentially the degrees of freedom of the instanton field, and are of interest since they give rise to zero modes which are crucial for the calculation of the instanton measure.

The Yang-Mills action has no dimensional parameters and is conformally invariant at the classical level [53]. This ensures that the instanton collective coordinates are determined by the conformal group. One may say that each symmetry transformation belonging to the conformal group which does not leave the instanton solution intact, gives rise to a separate collective coordinate.

The conformal algebra in 4-D has 15 generators: 4 translations, 1 dilatation, 4 special conformal transformations and 6 Lorentz rotations (or $SO(4)$ rotations in Euclidean space). Furthermore, Yang-Mills theory is gauge invariant; however, as we have seen so far, local gauge transformations transform the solution into a different gauge, thus global gauge transformations or color rotations will have to be considered as 3 additional degrees of freedom (for $SU(2)$) leaving a total of 18 possible collective coordinates.

First of all, *translational* invariance is represented by shifting the instanton solutions Eq. (3.30) or Eq. (3.34) to an arbitrary center x_0 , thus the new family of solutions is obtained through the substitution $x_\mu \rightarrow (x - x_0)_\mu$.

Under *dilatations*, space coordinates transform as $x \rightarrow \lambda x$ with $\lambda \in \mathbb{R}$. To find how A_μ transforms we notice that at classical level, Yang-Mills theory is scale invariant, i.e., is invariant

under dilatations; therefore, it is required that the equations of motion remain invariant under the transformations

$$x \rightarrow x' = \lambda x \quad \text{and} \quad A_\mu \rightarrow A'_\mu(x') = \lambda^\Delta A_\mu(x). \quad (3.36)$$

By direct substitution of these transformations into the equations of motion $D_\mu F_{\mu\nu} = 0$, one easily finds that $\Delta = -1$. For example, the BPST instanton in regular gauge⁴ transforms under dilatations as

$$A_\mu^a(x) \rightarrow A_\mu^a(x') = 2\eta_{\mu\nu}^a \frac{1}{\lambda} \frac{x_\nu}{x^2 + \rho^2} = 2\eta_{\mu\nu}^a \frac{x'_\nu}{x'^2 + (\lambda\rho)^2}. \quad (3.37)$$

The new family of solutions is characterized by the parameter $\lambda\rho$. Accordingly, the collective coordinate associated to dilatations is ρ .

Special conformal transformations can be represented as combination of translations and inversion. We already counted translations as the collective coordinate x_0 ; however, under inversions defined as

$$x_\mu \rightarrow x'_\mu = \frac{x_\mu}{x^2} \quad \text{and} \quad A_\mu(x) \rightarrow x'^2 A_\mu(x'), \quad (3.38)$$

the instanton in regular gauge transforms into the anti-instanton in singular gauge, meaning that no new family of solutions is generated by special conformal transformations [83].

We now have to consider the 6 $SO(4)$ rotations and the 3 $SU_c(2)$ global gauge transformations⁵. For this, we notice that since $SO(4) \cong SU(2) \times SU(2)$, it can be proven [53] that transformations from one of the $SU(2)$ subgroups leave the instanton solution intact while the other ones are equivalent to those of color rotations from $SU_c(2)$. Thus, from the remaining 9 possible collective coordinates, we are left with only three which are chosen to be the orientation in color space defined by the transformation

$$A_\mu \rightarrow M A_\mu M^\dagger, \quad (3.39)$$

⁴The same result is obtained with the singular gauge solution.

⁵The index c is introduced to distinguish the color gauge group from the $SO(4)$ subgroups.

with M a global gauge transformation matrix. In terms of color coordinates, it can be parametrized in terms of a rotation matrix as

$$A'_\mu t^a = \frac{A_\mu^a}{2} M \tau^a M^\dagger \Rightarrow A'^a t^a t^b = \frac{A_\mu^a}{4} M \tau^a M^\dagger \tau^b \Rightarrow A'^a = \frac{A_\mu^a}{2} \text{Tr} \left(M \tau^a M^\dagger \tau^b \right) = R^{ab} A_\mu^b \quad (3.40)$$

In summary, the moduli space of the $SU(2)$ instanton consists of 8 collective coordinates: 4 translations, 1 dilatation and 3 color orientations. The field A_μ in the regular and singular gauge are thus generalized as

$$A_\mu^a = 2R^{ab} \eta_{\mu\nu}^b \frac{(x-x_0)_\nu}{(x-x_0)^2 + \rho^2} \quad \text{and} \quad A_\mu^a = 2R^{ab} \bar{\eta}_{\mu\nu}^b \frac{(x-x_0)_\nu \rho^2}{(x-x_0)^2 [(x-x_0)^2 + \rho^2]}. \quad (3.41)$$

3.2.2 Multi-instantons and 't Hooft Ansatz

It is possible to construct configurations with higher topological charge Q_T by “superimposing” those with $Q_T = \pm 1$. This was proposed by 't Hooft [13, 84] when noticing that the singular gauge configuration from Eq. (3.41) (taking $R^{ab} = \delta^{ab}$ for simplicity) can be expressed as

$$A_\mu^a(x) = -\bar{\eta}_{\mu\nu}^a \partial_\nu \log \left[1 + \frac{\rho^2}{(x-x_0)^2} \right], \quad (3.42)$$

which suggests the general ansatz⁶

$$A_\mu^a(x) = -\bar{\eta}_{\mu\nu}^a \partial_\nu \log W(x), \quad (3.43)$$

where the function $W(x)$ is found by imposing the self-dual condition $F_{\mu\nu}^a = \tilde{F}_{\mu\nu}^a$. Direct substitution of the ansatz Eq. (3.43) into the definition of $F_{\mu\nu}$ and $\tilde{F}_{\mu\nu}$ leads to

$$F_{\mu\nu}^a - \tilde{F}_{\mu\nu}^a = \bar{\eta}_{\mu\nu}^a \left[(\partial_\alpha \log W)^2 + \partial_\alpha \partial_\alpha \log W \right] = \bar{\eta}_{\mu\nu}^a \frac{\partial_\alpha \partial_\alpha W}{W}. \quad (3.44)$$

⁶Notice we wrote A_μ instead of A_μ^S just for the sake of simplicity, nevertheless it is understood that the instanton is expressed in the singular gauge.

Hence, for self-dual fields, the function $W(x)$ must satisfy

$$\frac{\partial_\alpha \partial_\alpha W}{W} = 0. \quad (3.45)$$

A solution to this equation associated with finite action was proposed by 't Hooft and takes the form

$$W(x) = 1 + \sum_{l=1}^n \frac{\rho_l^2}{(x - x_l)^2}. \quad (3.46)$$

In [83] it is shown that a more general solution is given by

$$W(x) = \sum_{l=1}^{n+1} \frac{\rho_l^2}{(x - x_l)^2} \quad (3.47)$$

which is conformally covariant and from which one recovers Eq. (3.46) in the limit when $\rho_{n+1} \rightarrow \infty$, $x_{n+1} \rightarrow \infty$ with $\rho_{n+1}^2/x_{n+1}^2 = 1$.

This gauge field is known as a *multi-instanton* configuration, its topology is quite interesting and can be appreciated by computing its topological charge Q_T . First, let us recall from Eq. (3.21) that

$$iU_1^- \partial_\mu (U_1^-)^\dagger = 2\bar{\eta}_{\mu\nu}^a \frac{(x - x_l)_\nu}{(x - x_l)^2} t^a, \quad (3.48)$$

will allow to rewrite Eq. (3.43) with 't Hooft's solution for $W(x)$ as

$$\begin{aligned} A_\mu &= -\bar{\eta}_{\mu\nu} \partial_\nu \log W(x) \\ &= \sum_{l=1}^n \frac{2\bar{\eta}_{\mu\nu} \rho_l^2 (x - x_l)_\nu}{(x - x_l)^4} \left[1 + \sum_{m=1}^n \frac{\rho_m^2}{(x - x_m)^2} \right]^{-1} \\ &= \sum_{l=1}^n iU_1^- \partial_\mu (U_1^-)^\dagger \phi_l(x), \end{aligned} \quad (3.49)$$

with $\phi_l(x) = \frac{\rho_l^2}{(x - x_l)^2} \left[1 + \sum_{m=1}^n \frac{\rho_m^2}{(x - x_m)^2} \right]^{-1}$ and $\bar{\eta}_{\mu\nu} \equiv \bar{\eta}_{\mu\nu}^a t^a$.

It is easy to see that $\phi_l(x)$ takes the limiting values

$$\phi_l(x) = \begin{cases} 1 & \text{when } x \rightarrow x_l \\ 0 & \text{when } x \rightarrow x_j, \text{ for } j \neq l \end{cases} \Rightarrow \lim_{x \rightarrow x_j} \phi_l(x) = \delta_{jl}. \quad (3.50)$$

Therefore, in the neighborhood of any of the singularities x_j , the gauge potential behaves as a pure gauge configuration

$$\lim_{x \rightarrow x_j} A_\mu = iU_1^-(x - x_j)\partial_\mu [U_1^-(x - x_j)]^\dagger. \quad (3.51)$$

At first glance, it may seem that the n singularities can cause issues in the integration for the topological charge. However, as it was mentioned previously for the single instanton in singular gauge, the singularities are a consequence of the choice of gauge and can be removed by a suitable gauge transformation. This means that the action density (or topological density), being a gauge invariant quantity, is non-singular everywhere and thus we are able to use Gauss theorem to calculate Q_T . First, we define the volume of integration in Eq. (3.5), denoted by V , as the volume of a four dimensional sphere of infinite radius with n spherical ‘‘holes’’ each centered at x_j and radius ε , where $\varepsilon \rightarrow 0$. Therefore⁷

$$\begin{aligned} Q_T &= \lim_{\varepsilon \rightarrow 0} \frac{1}{16\pi^2} \int_V d^4x \operatorname{Tr} F_{\mu\nu} \tilde{F}_{\mu\nu} \\ &= \lim_{\varepsilon \rightarrow 0} \oint_{\partial V} ds_\mu K_\mu \\ &= \lim_{\varepsilon \rightarrow 0} \left[\oint_{S_E^3} ds_\mu K_\mu - \oint_{s_1} ds_\mu K_\mu - \dots - \oint_{s_n} ds_\mu K_\mu \right], \end{aligned} \quad (3.52)$$

where each s_i is the boundary of the four dimensional spherical hole and the minus signs appear when taking all surface elements pointing outwards the surface.

The integral over the surface S_E^3 is computed by noticing from Eq. (3.49) that in the limit where $|x| \rightarrow \infty$, $A_\mu \rightarrow 1/x^3$. Since the integrand is proportional to $\operatorname{Tr} \{A_\nu A_\beta A_\alpha\}$, it will fall as $\sim 1/x^6$ and the integral will vanish when $|x| \rightarrow \infty$.

As already mentioned, A_μ is pure gauge in the neighborhood of the singularities x_i , thus each

⁷See Appendix A for the definition of the Chern-Simmons current K_μ .

of the integrals over the surfaces s_i can be written as Eq. (A.9). Analogously to the calculation done for U_1^+ , we can obtain that for each s_i

$$\begin{aligned} \oint_{s_i} ds_\mu K_\mu &= \frac{1}{24\pi^2} \oint_{s_i} ds_\mu \varepsilon_{\mu\nu\alpha\beta} \text{Tr} \left\{ \left(U_1^- \partial_\nu (U_1^-)^\dagger \right) \left(U_1^- \partial_\alpha (U_1^-)^\dagger \right) \left(U_1^- \partial_\beta (U_1^-)^\dagger \right) \right\} \\ &= -1. \end{aligned} \tag{3.53}$$

Substituting all these results into Eq. (3.52), we found that the topological charge of the multi-instanton configuration is given by

$$Q_T = \lim_{\varepsilon \rightarrow 0} [0 - (-1) - \dots - (-1)] = n. \tag{3.54}$$

To conclude this section on the BPST instanton, we want to address the fact that even though we have seen that using 't Hooft ansatz, a configuration with arbitrary topological charge is easily constructed, this is not the most general solution. A generalization can be obtained through the ADHM formalism which will be discussed later on to obtain the KvBLL caloron. However, the immediate step for a generalized solution is to obtain a field with arbitrary temperature; this will be done in the following section.

3.3 THE HARRINGTON-SHEPARD CALORON

The study of the thermodynamics of Yang-Mills theory, evidently requires temperature-dependent fields. On that account, it was natural to look for a generalization of the instanton field at non-zero temperature. It was Harrington and Shepard [85, 86] who first found an analytic expression of the periodic $SU(2)$ gauge field, proposing the name “caloron”; eventually known in the literature as the *Harrington-Shepard caloron* or *H-S caloron* for short.

In this section we will aim to derive such expression in detail and discuss some basic properties. To begin, let us recall that in a finite-temperature field theory, bosonic fields are constrained to be periodic in (Euclidean) time, such that

$$A_\mu(\vec{x}, x_4) = A_\mu(\vec{x}, x_4 + \beta) \tag{3.55}$$

where the period is the inverse temperature $\beta \equiv 1/T$. Recalling 't Hooft's general ansatz for multi-instanton configurations (see Eqs. (3.43) and (3.46))

$$A_\mu = -\bar{\eta}_{\mu\nu}\partial_\nu \log W, \quad W(x) = 1 + \sum_{l=1}^n \frac{\rho_l^2}{(x - x_l)^2},$$

the periodicity of the field is achieved by constructing a prepotential $\Pi(x)$ similar to $W(x)$, where the spatial locations and the instanton sizes are fixed to \vec{y} and ρ respectively, resulting in

$$\Pi(x) \equiv 1 + \sum_{l=-\infty}^{\infty} \frac{\rho^2}{(x - x_l)^2} = 1 + \sum_{l=-\infty}^{\infty} \frac{\rho^2}{\mathcal{Z}^2 + (\tau - l\beta)^2}, \quad (3.56)$$

with $\mathcal{Z} = |\vec{x} - \vec{y}|$, $\tau = x_4 - y_4$ and $0 \leq y_4 \leq \beta$. This can be interpreted as an infinite chain of instantons along the temporal direction, all having the same orientation in color space [87].

The sum is usually evaluated with a similar approach to that of the Matsubara frequency sums commonly found in thermal field theory texts. Therefore, it is useful to rewrite it as

$$\begin{aligned} \sum_{l=-\infty}^{\infty} \frac{\rho^2}{\mathcal{Z}^2 + (\tau - l\beta)^2} &= \frac{1}{2\mathcal{Z}} \sum_{l=-\infty}^{\infty} \left[\frac{\rho^2}{\mathcal{Z} + i(\tau - l\beta)} + \frac{\rho^2}{\mathcal{Z} - i(\tau - l\beta)} \right] \\ &= \frac{\rho^2}{2\mathcal{Z}\beta} \left[\sum_{l=-\infty}^{\infty} \frac{1}{(\mathcal{Z} + i\tau)/\beta - il} + \sum_{l=-\infty}^{\infty} \frac{1}{(\mathcal{Z} - i\tau)/\beta + il} \right] \\ &= \frac{\rho^2}{2\mathcal{Z}\beta} \left[\sum_{l=-\infty}^{\infty} \frac{2\pi}{\varsigma - i\omega_l} + \sum_{l=-\infty}^{\infty} \frac{2\pi}{\varsigma^* + i\omega_l} \right], \end{aligned} \quad (3.57)$$

where we have defined $\varsigma = 2\pi(\mathcal{Z} + i\tau)/\beta$ and $\omega_l = 2\pi l$. Each sum, although tedious, is rather simple to compute using standard complex analysis techniques such as the Residue Theorem. We will not attempt to derive it and will only show the final result which is⁸

$$\Pi(x) = 1 + \frac{\pi\rho^2}{\mathcal{Z}\beta} \left[\coth \frac{\varsigma}{2} + \coth \frac{\varsigma^*}{2} \right]. \quad (3.58)$$

Finally, after substituting ς , \mathcal{Z} and some algebra manipulation, the superpotential $\Pi(x)$ takes

⁸The convergence value of the initial sum Eq. (3.56) can also be found in [88] (Series No. 858).

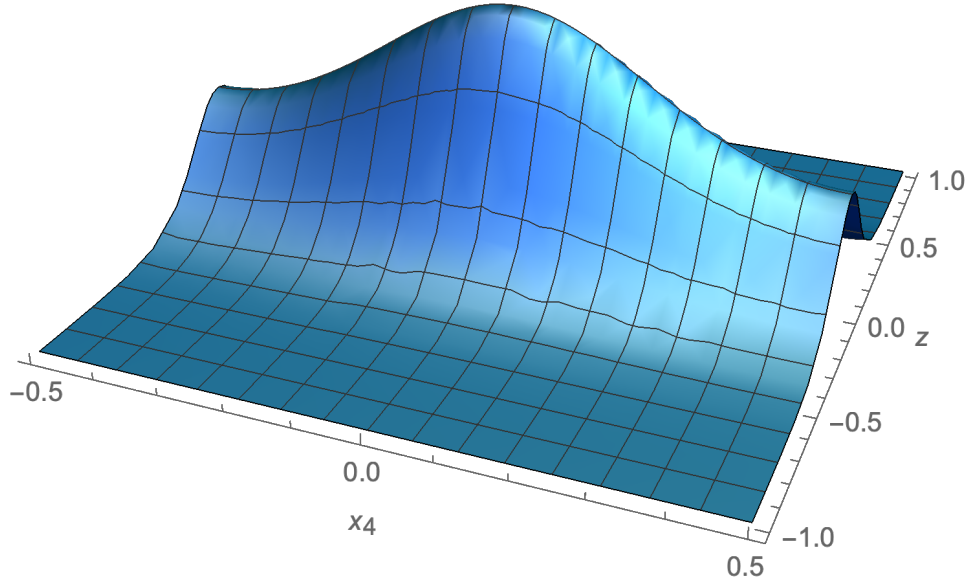


Figure 3.2: Action density of the Harrington-Shepard caloron for $y = z = 0$ and $\rho = 1/T$.

the form

$$\Pi(x) = 1 + \frac{\pi\rho^2 T}{|\vec{x} - \vec{y}|} \frac{\sinh [2\pi T|\vec{x} - \vec{y}|]}{\cosh [2\pi T|\vec{x} - \vec{y}|] - \cos [2\pi T(x_4 - y_4)]}, \quad (3.59)$$

with the H-S caloron being⁹

$$A_\mu^{HS}(x) = -\bar{\eta}_{\mu\nu} \partial_\nu \log \Pi(x). \quad (3.60)$$

One can clearly see that the periodicity in the temporal direction is coming from the cosine term. Just like the BPST-instanton, the caloron has unit topological charge; however, one must not forget that at finite temperature, the temporal direction has been compactified and x_4 must be integrated along the interval $[0, 1/T]$.

In the zero temperature limit, we should expect the caloron field to be reduced to that of the

⁹The anti-caloron is simply obtained with the interchange $\bar{\eta}_{\mu\nu} \rightarrow \eta_{\mu\nu}$.

instanton; which is indeed the case seeing that

$$\lim_{T \rightarrow 0} \Pi(x) = 1 + \frac{\rho^2}{(x-y)^2}. \quad (3.61)$$

The action density $\text{Tr} F_{\mu\nu} F_{\mu\nu}$ is shown on Fig. 3.2. It is periodic in Euclidean time, with a full period being plotted, and symmetric in all spatial directions.

To conclude this section, let us examine the asymptotic behavior of the caloron, in particular its fourth component [89]

$$\lim_{|\vec{x}| \rightarrow \infty} A_4^{HS}(x) = 0, \quad (3.62)$$

which leads to an asymptotic Polyakov Loop (see Eq. (3.6)) of $L(|\vec{x}| \rightarrow \infty) = \mathbb{1}_2 \in Z(2)$. Therefore, the holonomy of the H-S caloron is trivial, and as pointed out in [29], since there is no cancellation of the thermal average $\langle L_\infty \rangle$, the holonomy will never vanish, thus failing to reproduce color confinement.

3.4 MONOPOLES AND DYONS

Historically, non-Abelian magnetic monopoles arise as static solutions [90, 91] to the equations of motion of a Yang-Mills-Higgs theory, also known as the Georgi-Glashow model [92] described by the following Lagrangian¹⁰

$$\mathcal{L} = -\frac{1}{4} F_{\mu\nu}^a F^{\mu\nu,a} + \frac{1}{2} (D_\mu \phi^a) (D^\mu \phi^a) - \lambda (\phi^a \phi^a - v^2)^2, \quad (3.63)$$

with ϕ^a a real scalar field in the adjoint representation of the $SU(2)$ gauge group and where the term $\lambda (\phi^a \phi^a - v^2)^2$ is commonly known as the Higgs potential.

Finiteness of the total energy of the system

$$E = \int d^3x \left[\frac{1}{4} F_{\mu\nu}^a F^{\mu\nu,a} + \frac{1}{2} (D_\mu \phi^a) (D^\mu \phi^a) + \lambda (\phi^a \phi^a - v^2)^2 \right] \quad (3.64)$$

¹⁰Notice the Lagrangian has been written in Minkowski metric.

demands

$$\lim_{|\vec{x}| \rightarrow \infty} \phi^a \phi^a = v^2, \quad (3.65)$$

thus fixing the vacuum expectation value of the scalar Higgs field to $\sqrt{\phi^a \phi^a} = v$. Interesting topological properties can be explored by noticing that the degenerate Higgs field vacuum draws a 2-D sphere of radius v in the 3-D isospace (color space), which shall be called S_{vac}^2 . Moreover, the asymptotic condition Eq. (3.65) implies that in every direction at spatial infinity, i.e., at the boundary of the 3-D physical space, which is described by the 2-D sphere S_{phys}^2 , the field lies on the S_{vac}^2 . The mapping $S_{\text{phys}}^2 \rightarrow S_{\text{vac}}^2$ is characterized by the homotopy group $\pi_2(S^2) = \mathbb{Z}$ which, as was in the case of the instanton, labels the winding number of the mapping to $n = 0, \pm 1, \pm 2, \dots$. The trivial case with $n = 0$ corresponds to that when the asymptotic Higgs field is space-independent and takes a particular direction in isospace, for instance, $\phi = (0, 0, v)$. A much more interesting situation is the topologically non-trivial case of $n = 1$ where the direction of the isovector is parallel to that of the spatial vector, a so called “*hedgehog*” [90]

$$\phi^a = v n^a, \quad n^a = \frac{x^a}{|\vec{x}|}. \quad (3.66)$$

For this type of configuration, based on symmetry arguments, Polyakov and 't Hooft [90, 91] proposed that the solutions to the equations of motion should have the form

$$\phi^a(r) = v \mathcal{H}(r) n^a, \quad A_i^a(r) = \frac{1}{r} [1 - \mathcal{K}(r)] \varepsilon_{aij} n_j, \quad A_0^a = 0, \quad (3.67)$$

where ϕ and A_i are time-independent and $\mathcal{H}(r)$ and $\mathcal{K}(r)$ are unknown functions with the following boundary conditions

$$\begin{aligned} \lim_{r \rightarrow 0} \mathcal{H}(r) &= 0, & \lim_{r \rightarrow 0} \mathcal{K}(r) &= 1, \\ \lim_{r \rightarrow \infty} \mathcal{H}(r) &= 1, & \lim_{r \rightarrow 0} \mathcal{K}(r) &= 0. \end{aligned} \quad (3.68)$$

The resulting system of nonlinear differential equations has no analytic solution; nevertheless, Bogomol'nyi, Prasad and Sommerfield [82, 93] successfully found one in the limit of vanishing

Higgs potential, i.e. $\lambda = 0$, which is now known in the literature as the *BPS limit*.

Despite QCD-like theories without Higgs fields are our main interest; looking at the Georgi-Glashow model turns out to be quite illustrative when realizing the one-to-one correspondence between the system described by this model (in the BPS limit) and the self-dual static equations of Euclidean Yang-Mills theory [94, 95]. This feature, sometimes called the *Julia-Zee correspondence* [96], translates to

$$\phi^a \rightleftharpoons A_4^a, \quad D_i \phi^a \rightleftharpoons F_{4i}^a, \quad (3.69)$$

where the (anti)self-duality condition must be satisfied

$$\tilde{F}_{4i}^a \equiv \frac{1}{2} \varepsilon_{ijk} F_{jk}^a = \pm F_{4i}^a. \quad (3.70)$$

Consequently, the time independent Euclidean Yang-Mills field of interest, must then follow 't Hooft-Polyakov ansatz

$$A_4^a(r) = v \mathcal{H}(r) n^a \quad \text{and} \quad A_i^a(r) = \frac{1}{r} [1 - \mathcal{K}(r)] \varepsilon_{aij} n_j. \quad (3.71)$$

To find the explicit forms of $\mathcal{H}(r)$ and $\mathcal{K}(r)$, rather than using the equations of motion of the vector potential A_μ , it is more convenient to work with the (chromo) electric and magnetic fields defined as

$$E_i^a = F_{4i}^a, \quad B_i^a = \frac{1}{2} \varepsilon_{ijk} F_{jk}^a = \tilde{F}_{4i}^a \quad (3.72)$$

and use the self-duality constraint $E_i^a = B_i^a$. Substituting the ansatz into the field strength tensor $F_{\mu\nu}^a$, which we remember is given by

$$F_{\mu\nu}^a = \partial_\mu A_\nu^a - \partial_\nu A_\mu^a + \varepsilon^{abc} A_\mu^b A_\nu^c, \quad (3.73)$$

the electric field reads

$$\begin{aligned}
E_i^a &= \partial_i A_4^a + \varepsilon_{abc} A_i^b A_4^c \\
&= v \left(\frac{\delta_{ia}}{r} - \frac{n_a n_i}{r} \right) \mathcal{H} + v n_a n_i \mathcal{H}' + \varepsilon_{abc} \varepsilon_{bij} \frac{n_j}{r} (1 - \mathcal{K}) v \mathcal{H} n_c \\
&= \mathcal{H} \mathcal{F} \frac{v}{r} (\delta_{ai} - n_a n_i) + n_a n_i v \mathcal{H}',
\end{aligned} \tag{3.74}$$

where $r = |\vec{x}|$, $\mathcal{H}' \equiv \partial_r \mathcal{H}$ and the identity $\varepsilon_{abc} \varepsilon_{bij} = \delta_{ci} \delta_{aj} - \delta_{cj} \delta_{ai}$ has been used. On the other hand, for the magnetic field we have

$$\begin{aligned}
B_i^a &= \frac{1}{2} \varepsilon_{ijk} \left\{ \varepsilon_{akl} \left[\left(\frac{\delta_{jl}}{r} - \frac{n_l n_j}{r} \right) \frac{1}{r} (1 - \mathcal{K}) - \frac{n_l n_j}{r^2} (1 - \mathcal{K}) - \frac{n_l n_j}{r} \mathcal{K}' \right] \right. \\
&\quad - \varepsilon_{ajl} \left[\left(\frac{\delta_{kl}}{r} - \frac{n_l n_k}{r} \right) \frac{1}{r} (1 - \mathcal{K}) - \frac{n_l n_k}{r^2} (1 - \mathcal{K}) - \frac{n_l n_k}{r} \mathcal{K}' \right] \\
&\quad \left. + \varepsilon_{abc} \varepsilon_{bjl} \varepsilon_{ckm} n_l n_m \frac{1}{r^2} (1 - \mathcal{K})^2 \right\}.
\end{aligned} \tag{3.75}$$

Making use of basic properties of the Levi-Civita tensor and after some straightforward algebraic manipulation, the magnetic field is reduced to

$$B_i^a = \frac{\mathcal{K}'}{r} (\delta_{ai} - n_a n_i) + n_i n_a \frac{\mathcal{K}^2 - 1}{r^2}. \tag{3.76}$$

Combining Eqs. (3.74) and (3.76), we have that the self-dual fields must satisfy

$$\mathcal{K}' = v \mathcal{H} \mathcal{K}, \quad \mathcal{H}' = \frac{\mathcal{K}^2 - 1}{v r^2}. \tag{3.77}$$

These are the differential equations found in the BPS system whose solution have the surprisingly compact form

$$\mathcal{H}(r) = \frac{1}{v r} - \coth(vr), \quad \mathcal{K}(r) = \frac{v r}{\sinh(vr)}. \tag{3.78}$$

One can use instead the anti-self-dual condition $E_i^a = -B_i^a$, and the solution for $\mathcal{K}(r)$ will remain the same, whilst $\mathcal{H}(r)$ will have a flipped sign.

Of course, one of the most important properties of the field is its non-zero magnetic charge

which gives its name of BPS-monopole. However, because the A_4 component is also a source of charge, albeit an “electric” (scalar) one, the configuration is also named *dyon*. Following Diakonov’s nomenclature [29], from now on, we will refer to this dyon field as an M -*dyon*, where its explicit form in the so-called “*hedgehog gauge*” reads

$$\begin{aligned} A_4^{M,\bar{M}}(r) &= \pm \left(\frac{1}{r} - \coth(vr) \right) n_a \frac{\tau^a}{2}, \\ A_i^{M,\bar{M}}(r) &= \left(\frac{1}{r} - \frac{v}{\sinh(vr)} \right) \varepsilon_{aij} n_j \frac{\tau^a}{2}, \end{aligned} \quad (3.79)$$

with the upper sign corresponding to the self-dual M -dyon and the lower sign to the anti-self-dual \bar{M} -dyon.

Even though the hedgehog gauge was found rather convenient to realize the topological structure of the monopole, in the case where there are vacuum configurations with more than two dyons, it is difficult to superpose them in this gauge. Choosing a gauge where all dyons have the same A_4 asymptotics at spatial infinity, thus same color orientation, will prove to be useful later on. Therefore, to “*comb the hedgehog*” we use the following gauge transformations

$$\begin{aligned} S_+ &= e^{-i\frac{\phi}{2}\tau^3} e^{i\frac{\theta}{2}\tau^2} e^{i\frac{\phi}{2}\tau^3}, \\ S_- &= -i\tau^2 S_+ = e^{i\frac{\phi}{2}\tau^3} e^{i\frac{\theta-\pi}{2}\tau^2} e^{i\frac{\phi}{2}\tau^3}, \end{aligned} \quad (3.80)$$

which satisfy the identity $S_{\pm}(n_a \tau^a) S_{\pm}^{\dagger} = \pm \tau^3$, and transform the dyon fields of Eq. (3.79) as

$$A_{\mu}^{M,\bar{M}} \rightarrow S_{\mp} A_{\mu}^{M,\bar{M}} S_{\mp}^{\dagger} + i S_{\mp} \partial_{\mu} S_{\mp}^{\dagger}. \quad (3.81)$$

In spherical coordinates, the dyon solutions in the new gauge take the form

$$\begin{aligned} A_4^{M,\bar{M}} &= \frac{\tau^3}{2} \left(v \coth(vr) - \frac{1}{r} \right), \\ \pm A_i^{M,\bar{M}} &= \begin{cases} A_r &= 0, \\ A_{\theta} &= \frac{v}{2 \sinh(vr)} (\tau^1 \sin \phi + \tau^2 \cos \phi), \\ A_{\phi} &= \frac{v}{2 \sinh(vr)} (\tau^1 \cos \phi - \tau^2 \sin \phi) + \frac{\tau^3 \tan \frac{\theta}{2}}{2r}. \end{cases} \end{aligned} \quad (3.82)$$

One should notice that the A_4 component is now Abelian and equal for both M and \bar{M} with $A_4 \rightarrow v\tau^3/2$ when $r \rightarrow \infty$. Moreover, we have introduced a singularity along the negative x_3 -axis in A_ϕ ; a so called Dirac string which is merely a consequence of the gauge choice, hence the name *stringy gauge*. The nature of the singularity lies in the topological classification of the hedgehog and stringy configurations, where in the latter the A_4 corresponds to the trivial vacuum with winding number $n = 0$ and the former to a non-trivial one with $n = 1$ [91, 96].

It turns out, that we can construct another monopole-like solution out of the BPS monopole field. Although often called a Kaluza-Klein monopole, according to the language used so far, we will name them L and \bar{L} dyons. These solutions are obtained from Eq. (3.82) by replacing $v \rightarrow \bar{v}$ and then apply two gauge transformations: first the time dependent $U_1 = \exp(-i\pi T x_4 \tau^3)$, followed by a global rotation $U_2 = \exp(i\pi\tau^2/2)$ [25, 97, 98]. These will leave the asymptotics of A_4 in the same form as for the M type solutions with the caveat that the spatial components are no longer static; nevertheless, in the large distance limit, neglecting exponentially small terms, the time dependent terms will vanish. The L type dyon fields in the stringy gauge thus are

$$\begin{aligned}
A_4^{L,\bar{L}} &= \frac{\tau^3}{2} \left(2\pi T - \bar{v} \coth(\bar{v}r) + \frac{1}{r} \right), \\
\pm A_i^{L,\bar{L}} &= \begin{cases} A_r &= 0, \\ A_\theta &= \frac{\bar{v}}{2 \sinh(\bar{v}r)} \left[\tau^1 \sin(2\pi T x_4 - \phi) + \tau^2 \cos(2\pi T x_4 - \phi) \right], \\ A_\phi &= \frac{\bar{v}}{2 \sinh(\bar{v}r)} \left[-\tau^1 \cos(2\pi T x_4 - \phi) + \tau^2 \sin(2\pi T x_4 - \phi) \right] \\ &\quad - \frac{\tau^3 \tan \frac{\theta}{2}}{2 r}. \end{cases}
\end{aligned} \tag{3.83}$$

Although the gauge configurations presented here do have the needed non-trivial holonomy, a simple superposition of dyons is not a saddle point of the Yang-Mills action and the semiclassical approach to the partition function is rendered useless. There is merit to this section nonetheless, as it will be seen shortly how these dyonic fields play a significant role in the structure of the KvBLL caloron field.

3.5 THE KVBL CALORON WITH NON-TRIVIAL HOLONOMY

In this section, we will show the generalization of the Harrington-Shepard caloron to a configuration with non-trivial holonomy. Its constituent monopole-like fields, denoted “instanton-dyons”, will be the main ingredient for the statistical ensemble described in Chapters 4 and 5. The construction of the solution, based on the Nahm transform [99, 100] and the ADHM formalism [101], is quite involved and goes beyond the scope of this thesis; however, we will first give a short overview on how the latter¹¹ is used to find the caloron field and then we will introduce the full solution and discuss some of its properties.

3.5.1 The ADHM Construction

The “Atiyah-Hitchin-Drinfeld-Manin (ADHM) formalism” [101], is a very powerful method for constructing all (anti)self-dual Yang-Mills fields in Euclidean space \mathbb{R}^4 , through linear algebraic methods. The construction of $SU(2)$ gauge fields of topological charge k , requires to find the so called *ADHM data* defined as the $(k+1) \times k$ matrix

$$\Delta(x) = \begin{pmatrix} \lambda \\ B - x \end{pmatrix}, \quad (3.84)$$

where λ and B are $1 \times k$ and $k \times k$ matrices, respectively, whose components are given by

$$\lambda_m \equiv \lambda_m^\mu \tau_\mu, \quad B_{mn} = B_{mn}^\mu \tau_\mu \quad \text{with} \quad \lambda_m^\mu, B_{mn}^\mu \in \mathbb{R}, \quad (3.85)$$

for $m, n = 1, \dots, k$ and $\tau_\mu = (i\vec{\tau}, 1)$. Notice that each component is actually a 2×2 matrix, namely, they are written with τ_μ as basis vectors; therefore, λ , B and $x \equiv x_\mu \sigma_\mu$ are in fact quaternionic matrices.

The (anti)self-duality of the solution is realized through the condition that $\Delta^\dagger(x)\Delta(x)$ is non-singular (invertible) and real (it commutes with the quaternions). Once the ADHM data is con-

¹¹Refer to [23, 102, 103] for more in depth reviews on this matter.

structed, the kernel of $\Delta^\dagger(x)$

$$\Delta^\dagger(x)v(x) = 0 \quad (3.86)$$

normalized to $v^\dagger(x)v(x) = \mathbb{1}$, defines the gauge field as

$$A_\mu(x) = iv^\dagger(x)\partial_\mu v(x). \quad (3.87)$$

Although, naively the process may look simple, that is not the case in general. Information about the moduli space of the target solution is needed and only a few cases are known.

3.5.2 The KvBLL Caloron Solution

The caloron field with non-trivial holonomy discovered by Kraan and van Baal [23, 24] and independently by Lee and Lu [25] (therefore also known in the literature as the *KvBLL caloron*), is a classical solution to the $SU(N)$ Yang-Mills equations of motion in $\mathbb{R}^3 \times S^1$. It is a self-dual field with unit topological charge and most importantly, the A_4 component can be gauged to be diagonal and constant at spatial infinity, which leads to a non-trivial Polyakov loop or holonomy.

In the periodic gauge, the $SU(2)$ KvBLL caloron field with period $1/T$ is given by

$$\begin{aligned} A_\mu^{\text{KvBLL}} &= \delta_{\mu 4} v \frac{\tau^3}{2} + \frac{\tau^3}{2} \bar{\eta}_{\mu\nu}^3 \partial_\nu \log \Phi \\ &+ \frac{\Phi}{2} \text{Re} [(\bar{\eta}_{\mu\nu}^1 - i\bar{\eta}_{\mu\nu}^2) (\tau^1 + i\tau^2) (\partial_\nu + iv\delta_{\nu 4}) \tilde{\chi}], \end{aligned} \quad (3.88)$$

where

$$\begin{aligned} \hat{\psi} &= -\cos(2\pi T x_4) + \cosh(\bar{v}r) \cosh(vs) + \frac{r^2 + s^2 - \pi^2 \rho^4 T^2}{2rs} \sinh(\bar{v}r) \sinh(vs), \\ \psi &= \hat{\psi} + \frac{\pi^2 \rho^4 T^2}{rs} \sinh(\bar{v}r) \sinh(vs) + \pi \rho^2 T \left[\frac{\sinh(vs) \cosh(\bar{v}r)}{s} + \frac{\sinh(\bar{v}r) \cosh(vs)}{r} \right], \\ \tilde{\chi} &= \frac{\pi \rho^2 T}{\psi} \left[e^{-2\pi i x_4} \frac{\sinh(vs)}{s} + \frac{\sinh(\bar{v}r)}{r} \right], \\ \Phi &= \frac{\psi}{\hat{\psi}}, \end{aligned} \quad (3.89)$$

and $\bar{\eta}_{\mu\nu}^a$ the 't Hooft symbols, T the temperature, and τ^a the Pauli matrices. The meaning of the s

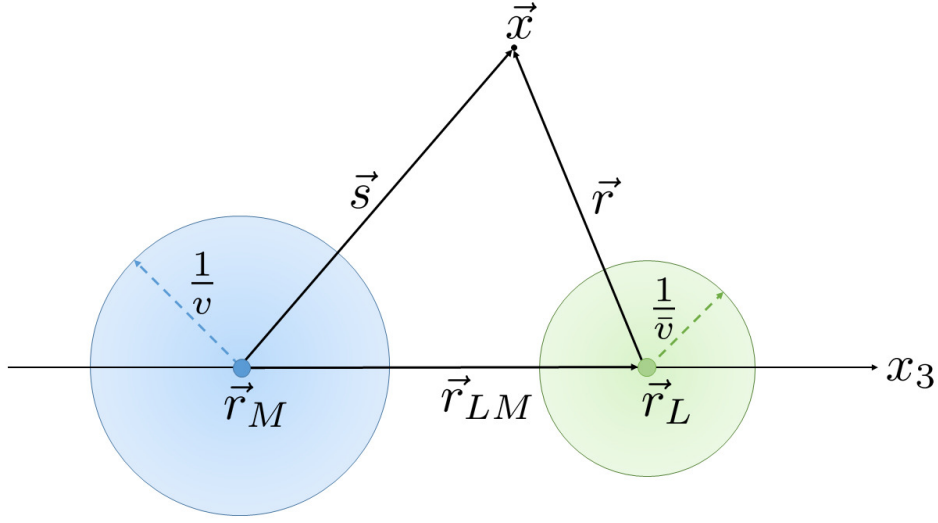


Figure 3.3: Coordinates of the KvBLL caloron in terms of the center of mass positions of its constituent dyon fields.

and r variables will be explained shortly. From this expression, it is not hard to see that at spatial infinity, the fourth component is indeed diagonal and constant $A_4|_{|\vec{x}|\rightarrow\infty} = v\frac{\tau^3}{2}$. This asymptotic value is parametrized as $v \equiv 2\pi T\nu$, with $\nu \in [0, 1]$ and analogously, $\bar{v} = 2\pi T\bar{\nu}$ with $\bar{\nu} = 1 - \nu$. Thus, the trace of the Polyakov loop at spatial infinity has the non-trivial form¹²

$$L_\infty \equiv \lim_{|\vec{x}|\rightarrow\infty} \frac{1}{2} \text{Tr} \mathcal{P} \exp \left(i \int_0^{1/T} dx_4 A_4^{\text{KvBLL}} \right) = \cos(\pi\nu), \quad (3.90)$$

where $\nu = \frac{1}{2}$ corresponds to maximal non-trivial holonomy ($L_\infty = 0$) and $\nu = 0$ trivial holonomy ($L_\infty = 1$). Therefore, ν is naturally called the *holonomy parameter*.

The anti-self-dual caloron or *anticaloron* \bar{A}_μ with negative topological charge is easily obtained from Eq. (3.88) by

$$\begin{aligned} \bar{A}_4^{\text{KvBLL}}(\vec{x}, x_4) &= A_4^{\text{KvBLL}}(-\vec{x}, x_4), \\ \bar{A}_i^{\text{KvBLL}}(\vec{x}, x_4) &= -A_i^{\text{KvBLL}}(-\vec{x}, x_4). \end{aligned} \quad (3.91)$$

In the limit of trivial holonomy ($\nu \rightarrow 0$), the KvBLL field consistently reduces to that of the

¹²For $SU(2)$, in the notation established in Section 3.1, the Polyakov Loop at spatial infinity is generally written as $L(|\vec{x}| \rightarrow \infty) = \text{diag}(e^{2\pi i\mu}, e^{-2\pi i\mu})$. It is useful to define the holonomy in terms of the difference[29] $\nu_m \equiv \mu_{m+1} - \mu_m$, with $\mu_{N_c+1} = \mu_1 + 1$. Therefore, $L(|\vec{x}| \rightarrow \infty) = \text{diag}(e^{\pi i\nu}, e^{-\pi i\nu})$ and the holonomy is simply $L_\infty = \cos(\pi\nu)$.

Table 3.1: Properties of the $SU(2)$ dyons.

	M	\bar{M}	L	\bar{L}
Electric charge	1	1	-1	-1
Magnetic charge	1	-1	-1	1
Action	$\nu \frac{8\pi^2}{g^2}$	$\nu \frac{8\pi^2}{g^2}$	$\bar{\nu} \frac{8\pi^2}{g^2}$	$\bar{\nu} \frac{8\pi^2}{g^2}$
Radius	v^{-1}	v^{-1}	\bar{v}^{-1}	\bar{v}^{-1}

Harrington-Shepard caloron. Furthermore, it becomes a standard BPST instanton of size ρ in the zero temperature limit.

One of the most important properties of this solution becomes relevant when $\rho \gg 1/T$. In this limit, the field is seen as composed of two monopoles separated by a distance $\pi\rho^2T$. As $\rho \rightarrow \infty$, the caloron becomes static and the monopoles are identified as the M and L dyons obtained in Section 3.4; where its opposite electric and magnetic charges cancels out leaving the caloron neutrally charged. In this context, the fields are distinguished as “constituents” of the caloron and are therefore named “*instanton-dyons*”.

The emergence of such configurations suggests to express the caloron in terms of the instanton-dyon’s positions. The coordinates used to write the caloron in Eq. (3.88) are then the positions of the dyon’s center of mass denoted by \vec{r}_L and \vec{r}_M , the dyon separation $r_{LM} \equiv |\vec{r}_L - \vec{r}_M| = \pi\rho^2T$, which for convenience is chosen to be along the x_3 -axis (see Fig. 3.3); i.e. $\vec{r}_{LM} = r_{LM}\hat{e}_3$, and the distances from the observation point \vec{x} to the dyon centers: $\vec{s} = \vec{x} - \vec{r}_M$ and $\vec{r} = \vec{x} - \vec{r}_L$.

This monopole picture is more evident when looking at the caloron in the vicinity of one of its constituent dyons and far away from the other, namely at large separations. For instance, near the L dyon center and far away from the M dyon ($s \gg 1/v$), the caloron field reduces to that of the L dyon, whose asymptotic behavior is given by (see Eq. (3.83))

$$A_4^{L,\bar{L}}|_{r \rightarrow \infty} = \frac{\tau^3}{2} \left(v + \frac{1}{r} \right), \quad A_\phi^{L,\bar{L}}|_{r \rightarrow \infty} = \mp \frac{\tau^3 \tan \frac{\theta}{2}}{2r},$$

where ϕ and θ are the polar and azimuthal angles in spherical coordinates centered at \vec{r}_L . The other components vanish in this limit. Analogously, near the M dyon and far away from the L

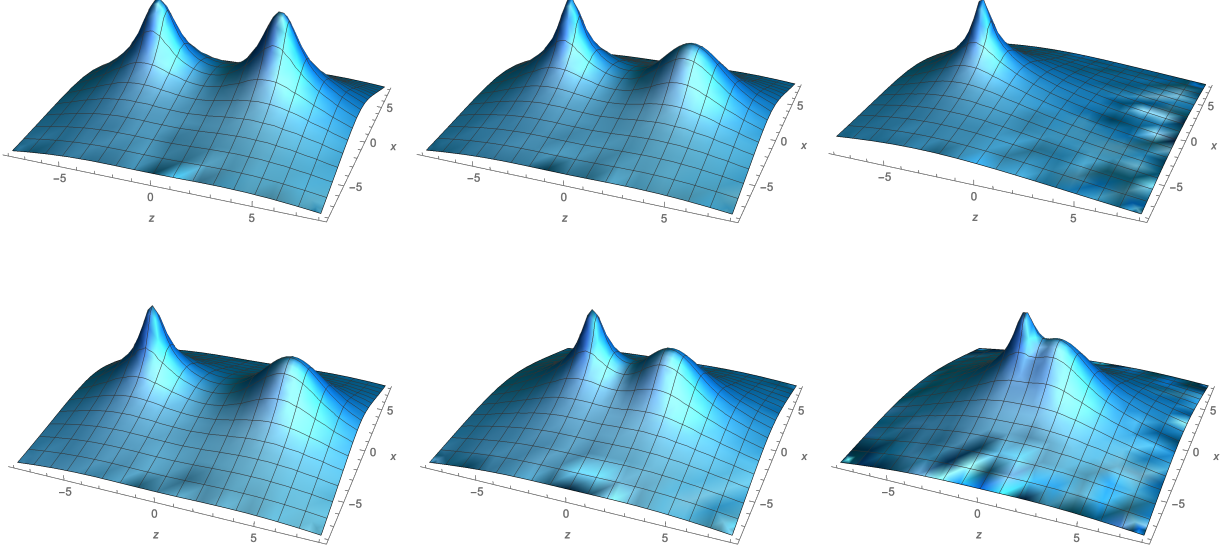


Figure 3.4: Action density of the KvBLL caloron for $x_4 = y = 0$. Top: Dyon separation is fixed to $\rho = 1.5/T$ with different holonomy parameter values $\nu = 1/2, 1/4, 0$ (from left to right). Bottom: For fixed holonomy $\nu = 1/4$, different dyon separations are shown $\rho = (1.6, 1.2, 0.8)/T$ (from left to right).

($r \gg 1/\bar{v}$), the field is that of the M dyon with asymptotics (see Eq. (3.82))

$$A_4^{M, \bar{M}}|_{s \rightarrow \infty} = \frac{\tau^3}{2} \left(v - \frac{1}{s} \right), \quad A_\phi^{M, \bar{M}}|_{r \rightarrow \infty} = \pm \frac{\tau^3 \tan \frac{\theta}{2}}{2s}.$$

In the limits $s \gg 1/v$ and $r \gg 1/\bar{v}$, but not necessarily at large separations r_{LM} ; the KvBLL caloron field also becomes Abelian and takes the form

$$A_\mu^{\text{KvBLL}} = \frac{\tau^3}{2} (\delta_{\mu 4} v + \bar{\eta}_{\mu\nu}^3 \partial_\nu \log \Phi), \quad (3.92)$$

where Φ in this limit reduces to

$$\Phi = \frac{r + s + r_{LM}}{r + s - r_{LM}}. \quad (3.93)$$

The only non-vanishing components of Eq. (3.92) are

$$A_4^{\text{KvBLL}} = \frac{\tau^3}{2} \left(v + \frac{1}{r} - \frac{1}{s} \right),$$

$$A_\phi^{\text{KvBLL}} = -\frac{\tau^3}{2} \left(\frac{1}{r} + \frac{1}{s} \right) \sqrt{\frac{(r_{LM} - r + s)(r_{LM} + r - s)}{(r_{LM} + r + s)(r + s - r_{LM})}}.$$

Finally, it can be quite enlightening to look at the action density of the KvBLL caloron, which can be obtained with the simple formula [23, 103, 104]

$$\text{Tr} F_{\mu\nu} F_{\mu\nu} = -\partial^2 \partial^2 \log \psi(x), \quad (3.94)$$

where $\psi(x)$ is defined in Eq. (3.89). As shown in Fig. 3.4, the constituent monopole picture is clearly visualized in the two lumps whose separation is modulated by the instanton size parameter ρ , indicating that the peaks location correspond to that of the instanton-dyons. As the holonomy parameter decreases, $\nu \rightarrow 0$, one of the dyons becomes larger and its contribution to the action smaller.

Now that we have examined all the useful properties of the gauge configurations relevant to the work presented in the rest of this thesis, we will conclude this chapter here and move forward to the construction of the instanton-dyon ensemble.

CHAPTER 4

THE INSTANTON-DYON ENSEMBLE IN $SU(2)$ YANG-MILLS THEORY

In the framework of a statistical ensemble of correlated instanton-dyons, we present a study of the confinement properties of finite temperature $SU(2)$ Yang-Mills theory. The first section comprises the detailed construction of the partition function of the system and the numerical methods employed for the simulations. In the following section, important physical quantities such as the holonomy potential, the order parameter of the deconfinement phase transition, quark-antiquark potentials, among others, are presented and thoroughly discussed. Finally, we present a series of improvements to the ensemble, allowing to obtain results which are later compared to lattice data. This chapter is based on works [47] (published) and [48] (under review).

4.1 CONSTRUCTION OF THE CORRELATED INSTANTON-DYON ENSEMBLE

4.1.1 The Quantum Weight of the KvBLL Caloron

In a similar fashion as it was done for the BPST instanton (at $T = 0$) [84] and for the Harrington-Shepard caloron [77] (at $T \neq 0$), it is of interest to calculate the contribution of small quantum oscillations of the KvBLL caloron to the Yang-Mills partition function

$$\mathcal{Z} = \int \mathcal{D}A_\mu e^{-S_{\text{YM}}[A_\mu]} = \int \mathcal{D}A_\mu \exp \left[-\frac{1}{2g^2} \int d^4x \text{Tr} F_{\mu\nu} F_{\mu\nu} \right]. \quad (4.1)$$

In broad terms, this semiclassical procedure consists in taking the classical solution as a background field such that the gauge fields in the functional integral are

$$A_\mu(x) = A_\mu^{\text{KvBLL}}(x) + a(x), \quad (4.2)$$

where $a(x)$ is a small quantum fluctuation of the classical solution (the KvBLL field). Then expand the action around the saddle point up to the desired order in a_μ and compute the functional integral.

In [105] Diakonov et al. obtained an analytic expression for the quantum weight of the $SU(2)$ KvBLL caloron in the one-loop approximation. They showed that in the limit of large separation between the constituent dyons (in the temperature scale) $r_{LM} \gg 1/T$, it can be written as

$$\begin{aligned} \mathcal{Z}_{\text{KvBLL}} = & e^{-VP(\nu)/T} \int d^3r_L d^3r_M T^6 C 2\pi \left(\frac{8\pi^2}{g^2}\right)^4 \left(\frac{\Lambda_{\text{PV}} e^{\gamma_E}}{4\pi T}\right)^{\frac{22}{3}} \left(\frac{1}{Tr_{LM}}\right)^{\frac{5}{3}} \\ & \times (1 + 2\pi T \nu \bar{\nu} r_{LM}) (1 + 2\pi T \nu r_{LM})^{\frac{8\nu}{3}-1} (1 + 2\pi T \bar{\nu} r_{LM})^{\frac{8\bar{\nu}}{3}-1}, \end{aligned} \quad (4.3)$$

where $P(\nu) = (4\pi^2/3)T^4\nu^2\bar{\nu}^2|_{\text{mod } 1}$ is the one-loop perturbative potential [77, 106], $C \approx 1.03142$ is a combination of universal constants and the linear term in r_{LM} proportional to $P''(\nu)$ from the exponential factor has been ignored in this work.

This expression can be further simplified in the approximation where the separation between dyons is much larger than their core sizes $r_{LM} \gg \frac{1}{2\pi T\nu}, \frac{1}{2\pi T\bar{\nu}}$; taking the form

$$\mathcal{Z}_{\text{KvBLL}} = e^{-VP(\nu)/T} \int d^3r_L d^3r_M T^6 (2\pi)^{\frac{8}{3}} C \left(\frac{8\pi^2}{g^2}\right)^4 \left(\frac{\Lambda_{\text{PV}} e^{\gamma_E}}{4\pi T}\right)^{\frac{22}{3}} \nu^{\frac{8}{3}} \bar{\nu}^{\frac{8}{3}}. \quad (4.4)$$

To obtain Eq. (4.3), one has to calculate the invariant measure of the moduli space metric of the caloron field denoted as $\sqrt{\det(g)}$. In the general case of $SU(N)$, this is shown to be exactly equal to the determinant of a $N \times N$ matrix \hat{G} [28, 107], which for $SU(2)$ is given by

$$\sqrt{\det(g)} = \det(\hat{G}), \quad (4.5)$$

where

$$\hat{G} = \begin{pmatrix} 4\pi\bar{\nu} + \frac{1}{Tr_{LM}} & -\frac{1}{Tr_{LM}} \\ -\frac{1}{Tr_{LM}} & 4\pi\nu + \frac{1}{Tr_{LM}} \end{pmatrix}, \quad (4.6)$$

$$(4.7)$$

which in the limit of large dyon separation reduces to $\det(\hat{G}) \approx 16\pi^2\nu\bar{\nu}$, and thus the partition

function Eq. (4.4) is rewritten as

$$\begin{aligned} \mathcal{Z}_{\text{KvBLL}} &= e^{-VP(\nu)/T} \int d^3r_L d^3r_M T^6 \frac{(2\pi)^{\frac{2}{3}}}{4} C \det(\hat{G}) \\ &\times \left(\frac{8\pi^2}{g^2}\right)^4 \left(\frac{\Lambda_{\text{PV}} e^{\gamma_E}}{4\pi T}\right)^{\frac{22}{3}} \nu^{\frac{8}{3}\nu-1} \bar{\nu}^{\frac{8}{3}\bar{\nu}-1}. \end{aligned} \quad (4.8)$$

The factor $\left(\frac{\Lambda_{\text{PV}} e^{\gamma_E}}{4\pi T}\right)^{\frac{22}{3}}$, appears from the running of the coupling constant g , in the Pauli-Villars regularization scheme. Namely

$$\left(\frac{\Lambda}{T}\right)^{\frac{22}{3}} = e^{-\frac{8\pi^2}{g^2(T)}}, \quad (4.9)$$

where we have absorbed all constants into Λ . At the one-loop calculation, the g^{-8} coupling in Eq. (4.8) is not renormalized; however, a two-loop improvement (ignoring the effects on $P(\nu)$) will give

$$\left(\frac{8\pi^2}{g^2}\right)^4 \left(\frac{\Lambda}{T}\right)^{\frac{22}{3}} \rightarrow \left(\frac{8\pi^2}{g^2(T)}\right)^4 e^{-\frac{8\pi^2}{g^2(T)} h(T/\Lambda)}, \quad (4.10)$$

where

$$h(T/\Lambda) = \exp \left\{ -\frac{34}{11} \log \left[2 \log \left(\frac{T}{\Lambda} \right) \right] + \frac{510}{1331} \frac{\log \left[\frac{22}{3} \log \left(\frac{T}{\Lambda} \right) \right]}{\log \left(\frac{T}{\Lambda} \right)} \right\}. \quad (4.11)$$

As a first approximation, one can include the two-loop improvement by substituting Eq. (4.10) and absorb the rest of the constant factors into a parameter Γ which is modulated in the simulation and fixed to be $\Gamma \approx 0.119$.

Finally, the caloron quantum weight takes the form

$$\mathcal{Z}_{\text{KvBLL}} = e^{-VP(\nu)/T} \int d^3r_L d^3r_M \det(\hat{G}) T^6 \Gamma^2 S^4 e^{-S} \nu^{\frac{8}{3}\nu-1} \bar{\nu}^{\frac{8}{3}\bar{\nu}-1}, \quad (4.12)$$

with the instanton action given by

$$S(T) = \frac{8\pi^2}{g^2(T)} = \frac{22}{3} \log \left(\frac{T}{\Lambda} \right). \quad (4.13)$$

4.1.2 The Partition Function

The construction of the partition function of the dyon ensemble begins with rewriting the one-loop quantum weight of a single KvBLL caloron in the limit of large dyon separation Eq. (4.12), namely the contribution of a pair of L and M dyons, in the following way:

$$\mathcal{Z} = e^{-VP(\nu)/T} \int (d^3r_L f_L) (d^3r_M f_M) T^6 \det(\hat{G}). \quad (4.14)$$

Here, the fugacities per dyon species are introduced as $f_M = \Gamma S^2 e^{-\nu S} \nu^{\frac{8\nu}{3}-1}$ and $f_L = \Gamma S^2 e^{-\bar{\nu} S} \bar{\nu}^{\frac{8\bar{\nu}}{3}-1}$. Extending this result to arbitrary number of L and M dyons requires the inclusion of the appropriate metric of the moduli space which has not yet been found. Nevertheless, Diakonov and Petrov [28] proposed an approximate metric by merging that of a neutral cluster of dyons of different kind, namely, an L - M pair, with that of dyons of the same kind (originally proposed in [108]). Therefore, the full measure is approximated by the square of the determinant of a symmetric matrix G like $\sqrt{\det(g)} \approx \det(G)$. Despite not being an exact solution, it possesses the interesting property that in the limit of K well separated L - M pairs, the measure factorizes into $\det(G) = \det(\hat{G})^K$, i.e., as the product of K individual KvBLL caloron measures. It is thus straightforward to see that for a single L - M pair, the G matrix reduces to \hat{G} (Eq. (4.5)). In the $SU(2)$ case, when the number of L and M dyons are N_L and N_M respectively, the dimension of this matrix G is $(N_L + N_M) \times (N_L + N_M)$ and its components are given by:

$$G_{mi,nj} = \delta_{mn} \delta_{ij} \left(4\pi\nu_m - \sum_{k \neq i} \frac{2}{T|\vec{r}_{m_i} - \vec{r}_{m_k}|} + \sum_k \frac{2}{T|\vec{r}_{m_i} - \vec{r}_{l_k}|} \Big|_{m \neq l} \right) + \frac{2\delta_{mn}}{T|\vec{r}_{m_i} - \vec{r}_{n_j}|} \Big|_{i \neq j} - \frac{2}{T|\vec{r}_{m_i} - \vec{r}_{n_j}|} \Big|_{m \neq n}, \quad (4.15)$$

where \vec{r}_{m_i} is the position vector of the i^{th} dyon of kind m (either L or M). Furthermore, it should be clear that similar results can be obtained for antidyons.

As pointed out in [29], dyon-antidyon configurations are not saddle points of the Yang-Mills action. The inclusion of anti-self-dual fields in the ensemble is done by factorizing the measure into uncorrelated parts $\det(G_D) \det(G_{\bar{D}})$ (D for dyons and \bar{D} for antidyons) times a correlated

contribution $e^{-V_{D\bar{D}}}$, where $V_{D\bar{D}}$ is the action corresponding to dyon–antidyon interactions. Classical interactions between dyon–antidyon of the same kind was recently introduced in a gradient flow study in [32]. Using the parametrization found in [33] and defining $\zeta_j = 2\pi\nu_j Tr_{j\bar{j}}$, the potential takes the following form

$$\begin{aligned} V_{L\bar{L}} &= -2\bar{\nu}S \left(\frac{1}{\zeta_L} - 1.632e^{-0.704\zeta_L} \right), \\ V_{M\bar{M}} &= -2\nu S \left(\frac{1}{\zeta_M} - 1.632e^{-0.704\zeta_M} \right), \end{aligned} \quad (4.16)$$

for $\zeta_j > \zeta_j^c$ and $r_{j\bar{j}} = |\vec{r}_j - \vec{r}_{\bar{j}}|$. Below the limit $\zeta_j < \zeta_j^c$, the interaction is repulsive and the proposed core potential for this region is given by

$$V_{j\bar{j}}^C = \frac{\nu_j V_c}{1 + e^{(\zeta_j - \zeta_j^c)}}, \quad (4.17)$$

where V_c and ζ_j^c are the two key parameters that quantify the strength and range of the repulsive correlations between dyon–antidyon pairs.

Other interactions that have to be accounted for include the long-range forces due to the Abelian electric and magnetic charges and the nonlinear terms in the field strength tensor $F_{\mu\nu}$, given by

$$V_{ij} = \frac{S}{2\pi Tr_{ij}} (e_i e_j + m_i m_j - 2h_i h_j), \quad (4.18)$$

where e_j and m_j are the electric and magnetic charges (see Table 3.1) and $h_j = 1$ for the M -type (anti)dyons while $h_j = -1$ for the L -type ones. As expected, this gives exactly cancelled classical interaction between the L and M dyons (as well as \bar{L} and \bar{M}) that together make a KvBLL caloron (owing to their BPS nature). On the other hand, there is repulsive interaction for the $L\bar{M}$ and $M\bar{L}$ pairs, while attractive interaction for the $L\bar{L}$ and $M\bar{M}$ pairs.

In the construction of the ensemble, one has to sum over different number of (anti)dyons and also take into account the many-body screening effect which is introduced by means of a Debye screening mass M_D . In doing so, all Coulomb terms appearing in the partition function (including those in the G matrices) are modified into $r^{-1} \rightarrow r^{-1} e^{-M_D r}$. Combining Eqs. (4.16) to (4.18), the

contribution from the inter-particle interactions to the action in the partition function is given by:

$$V_{D\bar{D}} = \begin{cases} -\sum_{j,\bar{j}} 2\nu_j S \left(\frac{1}{\zeta_j} - 1.632 e^{-0.704\zeta_j} \right) e^{-M_D r_{j\bar{j}}} & \text{if } \zeta_j > \zeta_j^c, \text{ for } LL\bar{L}, MM\bar{M} \\ \sum_{\substack{i>j \\ j,\bar{j}}} V_{ij}^C & \text{if } \zeta_j < \zeta_j^c, \text{ for } LL, \bar{L}\bar{L}, MM, \\ & \bar{M}\bar{M}, L\bar{L}, M\bar{M} \\ \sum_{i,\bar{j}} \frac{S}{\pi T r_{i\bar{j}}} e^{-M_D r_{i\bar{j}}} & \text{for } \bar{M}L, \bar{L}M \\ 0 & \text{for } LM, \bar{L}\bar{M}. \end{cases} \quad (4.19)$$

With all the above elements, one finally writes down the following form for the full partition function of the dyon–antidyon ensemble:

$$\begin{aligned} \mathcal{Z} = & e^{-VP(\nu)/T} \sum_{\substack{N_M, N_L, \\ N_{\bar{L}}, N_{\bar{M}}}} \frac{1}{N_L! N_M! N_{\bar{L}}! N_{\bar{M}}!} \int \prod_{l=1}^{N_L} f_L T^3 d^3 r_{L_l} \prod_{m=1}^{N_M} f_M T^3 d^3 r_{M_m} \\ & \times \prod_{\bar{l}=1}^{N_{\bar{L}}} f_{\bar{L}} T^3 d^3 r_{\bar{L}_{\bar{l}}} \prod_{\bar{m}=1}^{N_{\bar{M}}} f_{\bar{M}} T^3 d^3 r_{\bar{M}_{\bar{m}}} \det(G_D) \det(G_{\bar{D}}) e^{-V_{D\bar{D}}}, \end{aligned} \quad (4.20)$$

where the factorial terms are needed to avoid duplicate counting of identical configurations with given numbers of dyons and antidyons. By requiring neutrality condition, i.e., equal number of dyons and antidyons of the same kind, the above expression can be further simplified into:

$$\mathcal{Z} = e^{-VP(\nu)/T} \sum_{N_L, N_M} \left[\frac{(f_L V T^3)^{N_L}}{N_L!} \frac{(f_M V T^3)^{N_M}}{N_M!} \right]^2 e^{-VT^3 \mathcal{F}(T, \nu)}, \quad (4.21)$$

where V is the 3D volume available and

$$e^{-VT^3 \mathcal{F}(T, \nu)} \equiv \int \prod_{l,m,\bar{l},\bar{m}}^{N_L, N_M} \frac{d^3 r_{L_l}}{V} \frac{d^3 r_{M_m}}{V} \frac{d^3 r_{\bar{L}_{\bar{l}}}}{V} \frac{d^3 r_{\bar{M}_{\bar{m}}}}{V} \exp \{ \log [\det(G_D) \det(G_{\bar{D}})] - V_{D\bar{D}} \} \quad (4.22)$$

is obtained after performing integrals over all dyon positions. Finally, using Stirling's approximation $\log N! \approx N \log N - N + \log \sqrt{2\pi N}$ and defining the dimensionless dyon densities as $n_D = N_D / VT^3$,

we rewrite \mathcal{Z} as a sum of weights running over number of dyons as

$$\begin{aligned} \mathcal{Z} &= \sum_{N_L, N_M} \exp \left[-VT^3 \left(\frac{4\pi^2}{3} \nu \bar{\nu} + 2n_L \log \left(\frac{n_L}{f_L} \right) + 2n_M \log \left(\frac{n_M}{f_M} \right) \right. \right. \\ &\quad \left. \left. + 2(n_L + n_M) + \frac{\log(4\pi^2 N_L N_M)}{VT^3} + \mathcal{F}(T, \nu) \right) \right] \\ &\equiv \sum_{N_L, N_M} \mathcal{Z}_{LM}. \end{aligned} \tag{4.23}$$

In this framework, there are three key parameters as theoretical inputs: the screening mass M_D , as well as the strength parameter V_C and range parameter ζ_j^c for the dyon–antidyon interaction potential. In principle these parameters could be constrained by comparing relevant observables from the dyon ensemble with lattice simulations. Such quantitative comparison will be shown in Section 4.4, while the present section focuses on qualitative question of demonstrating how the confinement is driven to occur in the correlated dyon ensemble.

4.1.3 The Monte-Carlo Simulations

Let us now discuss the details of the Monte-Carlo simulations to be used for evaluating the dyon ensemble partition function. Different from the implementation in [33, 40, 41], in our simulation we used a flat geometry, namely a box with periodic boundary conditions which shall be a more “realistic” approach and a more direct way to compare the results with e.g. lattice simulations.

From Eq. (4.23), it can be seen that all explicit dependence on the temperature T can be absorbed by rescaling $rT \rightarrow r$, $VT^3 \rightarrow V$, $M_D/T \rightarrow M_D$ and the free energy $F/T \equiv -\log \mathcal{Z} \rightarrow F$. Since this simplifies the calculations, all the simulations are done using such scaled dimensionless variables. In doing so, the temperature T superficially disappears from the explicit simulations. However, the temperature dependence implicitly affects the system properties through the running coupling constant in the caloron action S , which as was discussed in the previous section, at the one-loop level is given by

$$S(T) = \frac{8\pi^2}{g^2(T)} = \frac{22}{3} \log \left(\frac{T}{\Lambda} \right), \tag{4.24}$$

where Λ is the scale parameter in the regularization. Therefore, by varying S as a parameter in

the simulation, one is essentially varying the system temperature. It is straightforward to convert S into T/Λ . To further put temperature in e.g. MeV unit, one would then have to make a physical choice for the value of Λ . For example, one may choose Λ such that the critical temperature T_c matches the lattice obtained value for $SU(2)$ Yang-Mills theory. Once T_c is fixed, one can then measure temperature T in terms of T/T_c (note this is equivalent to specifying the ratio T_c/Λ).

The computation of all the observables are performed through Monte Carlo simulations using the well known Metropolis-Hastings algorithm [109, 110]. Each configuration is generated by first randomly varying the 3-D positions of a single dyon or antidyon of each kind (and accounting for the periodic boundary conditions), then applying the acceptance algorithm, and moving to the next set of dyons/antidions by repeating the same procedure. Once all positions have been swept, we then move to compute the observables with this new configuration and repeat all over again until the ensemble has been thermalized with enough statistics. It has been found that after about 2000 Monte Carlo configurations, the system is typically stabilized, after which the ensemble average would be calculated with the 10000 subsequent new configurations. The determined autocorrelation time was close to 5 configurations; therefore, the observables are averaged over 2000 configurations. On Fig. 4.3 we compare the free energy density calculated with a smaller number of Monte Carlo configurations for both confined and deconfined phases. The results are obviously consistent with each other and the small discrepancy between the two data sets is merely at a level of approximately 0.54% in the order parameter calculation $\langle L_\infty \rangle$. This comparison clearly demonstrates that with 12000 configurations one obtains very reliable results with rather small statistical uncertainty.

One technical issue in the Monte Carlo sampling process is about the measure factors $\det(G)$. As it is an approximation to the actual moduli space metric, it may happen that some of the eigenvalues of the G matrices become negative thus violating the positive definiteness of the metric. This issue has been addressed in detail by [29, 34, 111]. To avoid configurations with negative eigenvalues in the simulations, the approach taken was to use the Metropolis-Hastings algorithm to reject such “wrong” configurations by assigning them a small statistical weight, i.e. if either G_D or $G_{\bar{D}}$ has at least one negative eigenvalue, then the weight $\exp(\log \det(G))$ is substituted by e^{-100} , which was found to be enough to suppress these and to ensure an ensemble of sufficient configurations with all positive eigenvalues. It may be noted that this procedure effectively introduces a modification of the action, the impact of which is currently not well controlled and requires further investigation

in the future.

One of the most important quantities to be calculated from the simulations is the holonomy potential or free energy density F/V at a given temperature. Due to the way it is defined, the calculation through Monte Carlo is not straightforward. However, there is a common method to evaluate it [32] which we will adopt here. Note that the only term that needs to be evaluated from the Monte Carlo configurations is $e^{-V\mathcal{F}}$ since it is the only one depending upon spatial positions of the dyons/antidions, while all other terms do not have such dependence. In the calculation, according to the standard thermodynamic integration, one introduces an auxiliary parameter ξ as

$$e^{-V\mathcal{F}_\xi(\xi)} = \frac{\int \mathcal{D}r e^{-\xi S_r}}{V^{2(N_L+N_M)}}, \quad (4.25)$$

where

$$S_r \equiv V_{D\bar{D}} - \log [\det(G_D) \det(G_{\bar{D}})], \quad (4.26)$$

and $\mathcal{D}r$ is just the integration measure over all dyons' and antidions' positions (for a total of $2(N_L + N_M)$ of these particles in the simulation). It should be emphasized that for $\xi = 1$, the above Eq. (4.25) is exactly equal to Eq. (4.22). The normalization factor $V^{2(N_L+N_M)}$ in the denominator above, is *not* introduced arbitrarily but rather comes directly from the construction of the partition function by correctly counting the “ $1/V$ ” factors in the Eq. (4.22). This proper normalization factor also automatically gives $\mathcal{F}_\xi(0) = 0$. Then, via standard Monte Carlo simulation procedure, one can compute the ensemble average of the following quantity:

$$\langle S_r \rangle (\xi) \equiv \frac{\int \mathcal{D}r S_r e^{-\xi S_r}}{\int \mathcal{D}r e^{-\xi S_r}} = V \frac{\partial \mathcal{F}_\xi}{\partial \xi}. \quad (4.27)$$

Lastly, by integrating out the ξ dependence of the above, one arrives at the desired free energy:

$$\mathcal{F} = \frac{1}{V} \int_0^1 d\xi \langle S_r \rangle (\xi) = \mathcal{F}_\xi(1), \quad (4.28)$$

given that $\mathcal{F}_\xi(0) = 0$ by definition. We emphasize again that for $\xi = 1$, Eq. (4.25) reduces to Eq. (4.22), where the denominator $V^{2(N_L+N_M)}$ appears naturally from the construction of the

partition function (Eqs. (4.20) to (4.22)), allowing to set $\mathcal{F}_\xi(0) = 0$ unambiguously, regardless of the dyon numbers N_L and N_M .

Finally, we discuss the choice of the parameters in this framework. For most of the results to be presented, we use a (dimensionless) spatial volume of the box to be $V = 43.37$. After several tests, it was determined that the optimal range of (anti)dyon density of each kind was $n_D \in [0, 0.5]$ (corresponding to $N_D \in [0, 22]$ number of (anti)dyons). Configurations with larger n_D were found to have a rather small contribution to the partition function; therefore, discarded in the simulations (— see Section 4.3.1). We choose the three key parameters as Debye mass $M_D = 2$, the core potential strength $V_c = 20$ and size $\zeta_j^c = 2$; however, in Sections 4.3.1 to 4.3.3, we will vary these quantities to explore the finite volume effects as well as the influence of the three key parameters.

4.2 CONFINEMENT-DECONFINEMENT TRANSITION

4.2.1 The Holonomy Potential

It is known from lattice simulations that the $SU(2)$ pure gauge theory has a certain critical temperature T_c , with a confined phase at $T < T_c$, a deconfined phase at $T > T_c$, and a 2nd order phase transition connecting the two phases at $T = T_c$. The relevant order parameter is the expectation value of the Polyakov loop at spatial infinity L_∞ (see Sections 2.2.1 and 3.1) which is related to holonomy parameter ν by $\langle L_\infty \rangle = \cos(\pi\nu)$. An expectation value of $L_\infty = 0$ or $\nu = 1/2$ would correspond to the low temperature Z_2 center-symmetric, confined phase.

A first important check is to examine whether such expected phase transition indeed occurs in the dyon ensemble. In order to see that, one needs to compute the holonomy potential, that is, the free energy density as a function of the holonomy $F(\nu) = -T \log \mathcal{Z}$ at varied temperature. Such holonomy potential determines the Polyakov loop dynamics and is a crucial input for a class of chiral models to incorporate confinement dynamics [112–115]. For any given temperature, the minimum of the holonomy potential determines the thermodynamically realized expectation value of the holonomy value which as order parameter thus tells us about the different phases of the theory. As mentioned earlier, the temperature dependence of all the observables in the ensemble comes from the instanton action S (Eq. (4.24)) which is an input parameter in the simulation.

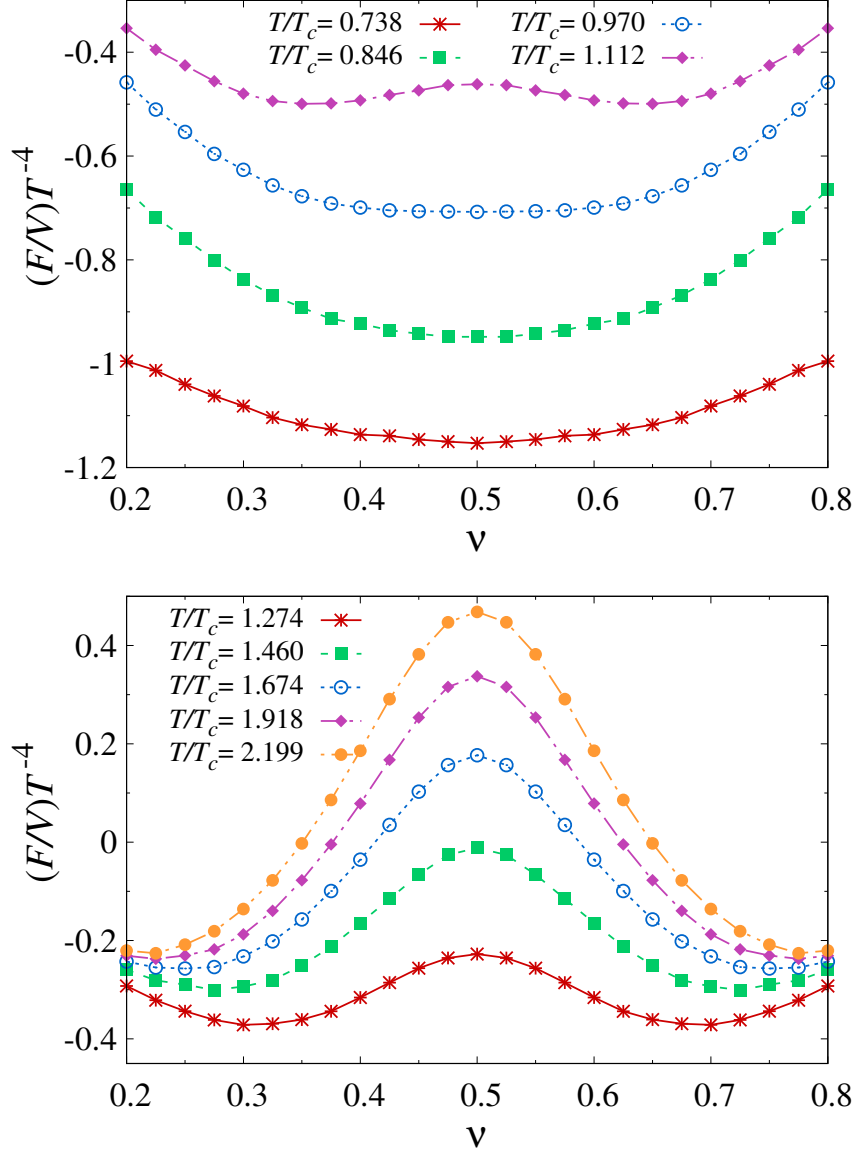


Figure 4.1: Free energy density F/V as a function of holonomy ν at various values of temperature. The corresponding action parameters, from bottom top, are $S = 5, 6, 7, 8$ (top plot) and $S = 9, 10, 11, 12, 13$ (bottom plot).

Fig. 4.1 shows the free energy density for $S = 5, 6, \dots, 13$. It is found that for $S = 5 \sim 7$, the minimum of the free energy density lies at $\nu_{\min} = 0.5$, namely maximal non-trivial holonomy corresponding to the confined phase. For $S > 7$, the shape of F/V becomes that of a symmetric double well potential with two minima located at $\nu_{\min} < 0.5$ and $\nu_{\min} > 0.5$ in a symmetric way. It shall be mentioned that as expected for an $SU(2)$ pure gauge theory, F/V is symmetric under the interchange $\nu \rightarrow \bar{\nu} = 1 - \nu$, and this feature has indeed been validated explicitly in the numerical

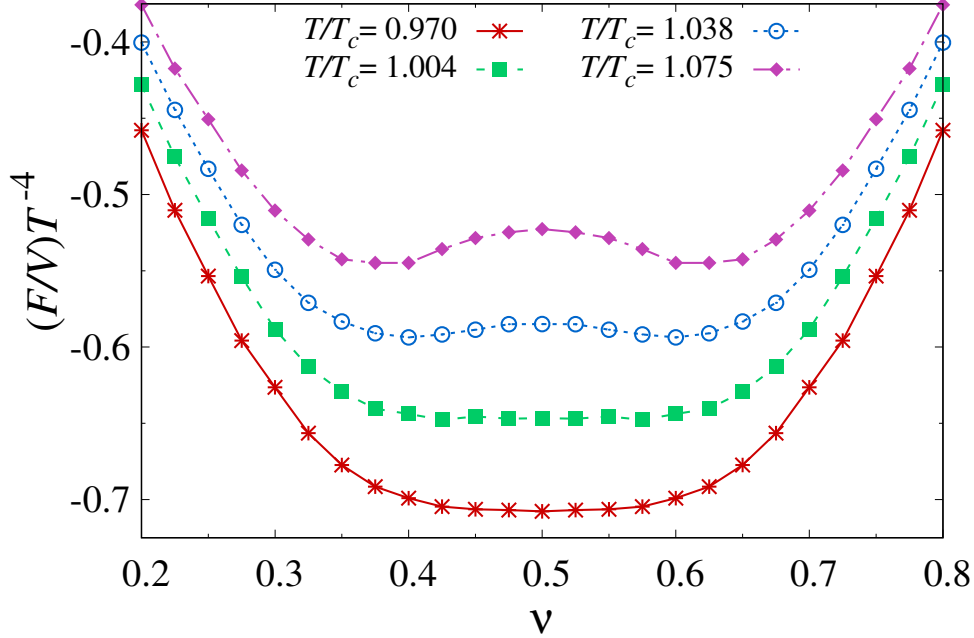


Figure 4.2: Free energy density F/V as a function of holonomy ν at several values of temperature near the phase transition point, with the corresponding action parameters $S = 7.00, 7.25, 7.50, 7.75$, from bottom to top.

calculations. So the results clearly reveal a confined phase at low temperature while a deconfined phase at high temperature.

To more accurately locate the critical action (or equivalently the critical temperature T_c), we further run the simulation for $S = 7.25, 7.5$ and 7.75 . As shown on Fig. 4.2, for $S \geq 7.5$ the Z_2 symmetry is clearly broken and the minimum of the free energy density is shifted away from the $\nu = \bar{\nu} = 0.5$. For $S = 7.25$, more points were necessary to examine the minimum, and despite the potential on Fig. 4.2 exhibits a very flat dependence around $\nu = 0.5$, the minimum was actually found around $\nu_{\min} \approx 0.453$. Thus, at the present numerical precision, we determine the critical temperature at $S_c = 7.25$, which fixes our scale parameter from Eq. (4.24) at $\Lambda = 0.373T_c$ and allows us to express all temperature dependent quantities in terms of the ratio T/T_c .

We next come to the expectation value $\langle L_\infty \rangle = \cos(\pi\nu)$, which can be determined from the position of the minimum of the holonomy potential. This is done by fitting the free energy density near the minima to a quadratic function with 9 to 15 points and then, through a derivative test on the fit, finding its minimum accurately.

As an important and insightful check of the role of L_∞ as an order parameter for the expected

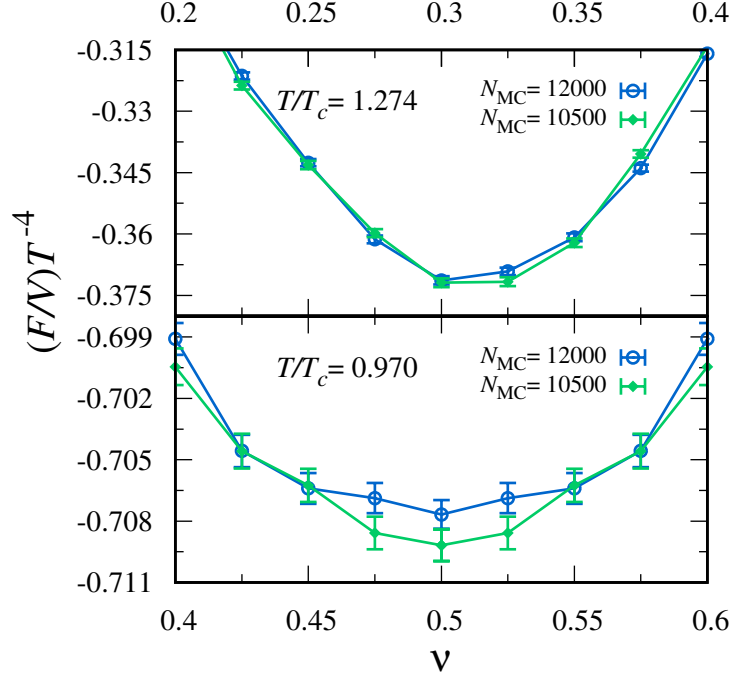


Figure 4.3: Free energy density F/V as a function of holonomy ν computed with different choices for the number N_{MC} of the Monte Carlo configurations in the simulations, in the confined (bottom) and deconfined (top) phases.

2nd order phase transition, we quantitatively examine whether its dependence on temperature near the transition point follows the proper universality class. As already discussed in Chapter 2, the well known Svetitsky-Yaffe conjecture [61], relates $SU(2)$ pure gauge theory in $(3 + 1)$ dimensions to the 3-D Ising model of ferromagnetism by categorizing both in the same universality class. In this sense, L_∞ becomes the analog of the magnetization, thus its critical behavior must follow the same universal power law

$$\langle L_\infty \rangle = b(T/T_c - 1)^\beta [1 + d(T/T_c - 1)^\Delta], \quad (4.29)$$

with b and d the fitting parameters.

Using the well established values of the critical exponents of the 3-D Ising model $\beta \approx 0.3265(3)$ and $\Delta \approx 0.530(16)$ [116], on Fig. 4.4 we show the fitted curve obtained from the numerical results of the dyon ensemble in the near- T_c region, namely $1 \leq T/T_c \leq 1.274$. The very low value of $\chi^2 = 1.44 \times 10^{-4}$ of the fit (which is partly due to the sizable error bar because of limited statistics) suggests an almost perfect agreement between the confinement/deconfinement phase transition be-

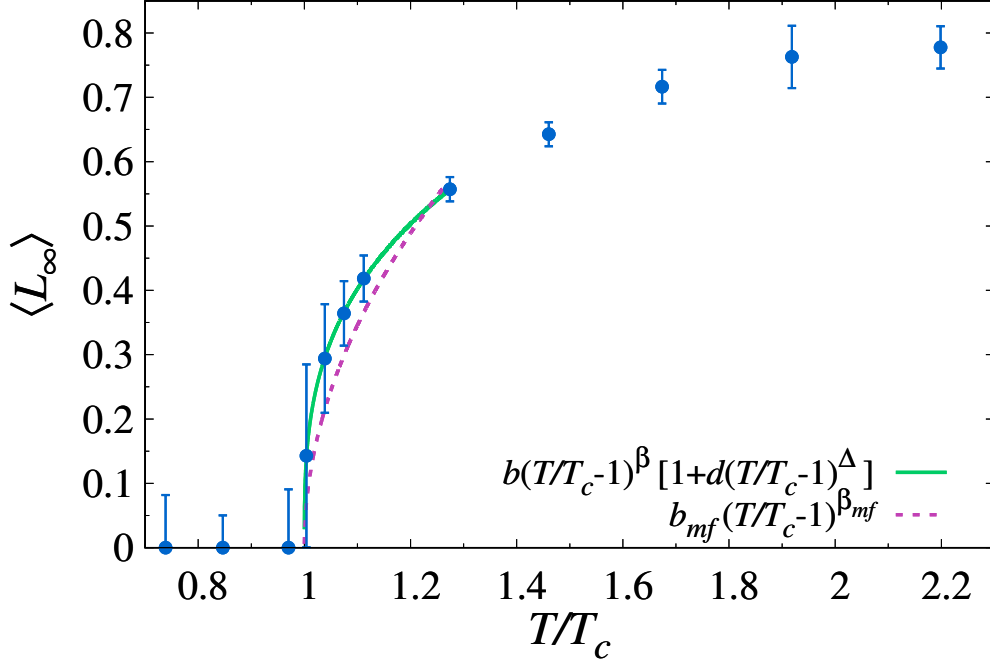


Figure 4.4: L_∞ as an order parameter of the 2nd order phase transition with $b = 0.858(142)$ and $d = -0.017(348)$ as the fitting parameters to the power law Eq. (4.29) and $b_{mf} = 1.094(33)$ the corresponding one to the mean-field fit.

havior with the anticipated critical behavior of the 3-D Ising model's 2nd order phase transition. It also demonstrates qualitative agreement with the lattice results from [117, 118]. For completeness and comparison, we also show the fit using the mean-field critical exponent $\beta_{mf} = 1/2$, which shows a qualitatively similar trend but a significantly larger value of $\chi^2 = 0.13$. The comparison favors the former fitting and implies that the transition from the dyon ensembles captures the beyond-mean-field critical behavior of a 2nd order phase transition.

We now report the results for the expectation values of dyon densities, shown in Fig. 4.5. One can see that at $T < T_c$, the L and M type densities are equal as expected. In the confined phase, the preferred holonomy corresponds to the maximally non-trivial one where both dyon types have the same core radius as well as equal action share and therefore equal weight in the partition function. For $T > T_c$, the preferred holonomy starts to shift away from the symmetric point towards the trivial holonomy ($\nu \rightarrow 0$ in this case) and the M dyons become larger and larger. Recalling from the KvBLL caloron solution, in the limit of trivial holonomy, the L dyon disappears and the field becomes that of the Harrington-Shepard caloron. A similar situation is observed in the ensemble as temperature is increased, with the L dyon density decreasing much faster than M type. The total

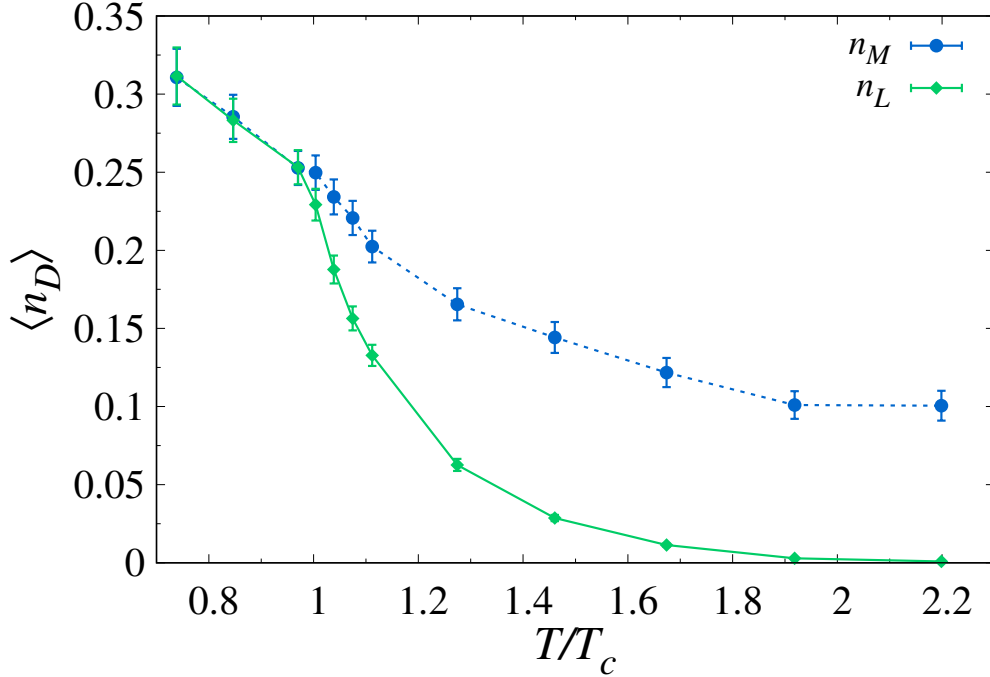


Figure 4.5: Temperature dependence of the ensemble average of dyon densities.

density of all these magnetically charged objects demonstrates a strong temperature dependence with very rapid increase from high temperature toward near T_c regime, in consistency with the magnetic scenario.

4.2.2 The Dyon and Antidyon Spatial Correlations

The interactions between dyons and antidyons are essential for the properties of the ensemble and in particular for driving the system toward confinement at high dyon density (i.e. low temperature) regime. The effect of such interactions can be illustrated by examining the spatial density density correlations among various pairs of dyons/antidyons, as defined in the following:

$$G_{DD'}(|\vec{x}|) = \frac{\frac{1}{V} \left\langle \sum_{i=1}^{N_D} \sum_{j=1}^{N_{D'}} \Theta_{\delta x}(r_{ij} - |\vec{x}|) \right\rangle}{n_D n_{D'} \frac{4\pi}{3} [(|\vec{x}| + \delta x)^3 - |\vec{x}|^3]}, \quad (4.30)$$

which is normalized to that of an uncorrelated ideal gas and where the step function $\Theta_{\delta x}(\xi) = 1$ for $0 < \xi < \delta x$ and 0 otherwise. A value of unity for the $G_{DD'}$ would indicate a situation without correlations as is characteristic for a free gas ensemble. The numerical results are shown in Fig. 4.6

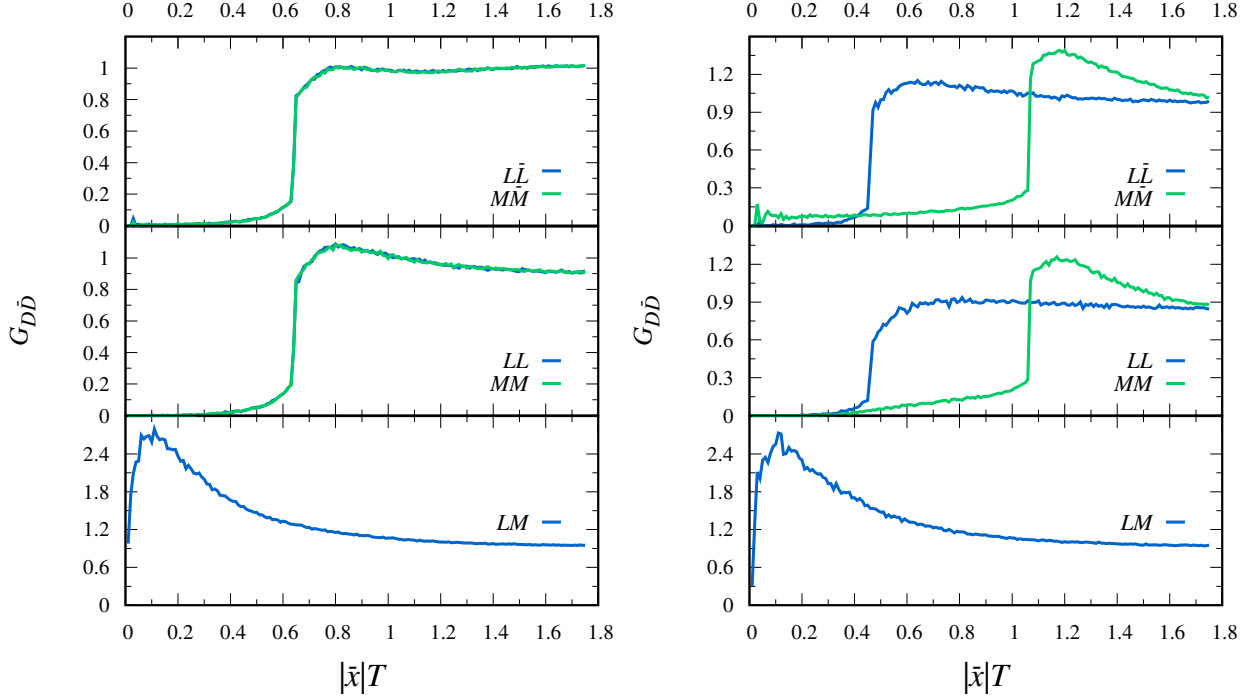


Figure 4.6: 2-particle spatial correlations for dyon–dyon and dyon–antidyon pairs at $T < T_c$ (left) and $T > T_c$ (right).

for all different (anti)dyon pairs combinations, each computed at one temperature value below T_c and another one above T_c . These results are obtained under equilibrium conditions for given temperature, i.e. with holonomy parameter ν being the one at minimal free energy and the number of dyons N_D fixed at the ensemble averaged values.

The presence of the repulsive core is clearly observed for all the dyon pairs, besides the LM for which there is none. At distances right above the core size $\zeta_j^c/2\pi\nu_j$ the correlation functions seem to have a small bump that rapidly goes to unity at larger distance, indicating at a short-range correlation pattern arising from the repulsive core.

4.2.3 The Polyakov Loop Correlator

Besides the Polyakov loop expectation value itself, another important “indicator” of the confinement/deconfinement transition is the static (quark-antiquark) potential which essentially is evaluated from a temporal Wilson loop or equivalently the spatial correlator of the Polyakov loop. In particular the so-obtained static potential is expected, at large spatial separation, to exhibit

a linearly rising behavior in the confined phase while to level off in the deconfined phase. It is important to evaluate this observable in the dyon ensemble.

The computation is however technically tricky in the present framework. In the large distance limit ($|\vec{x}| \rightarrow \infty$), the A_4 component of the dyon fields becomes Abelian. However, the total A_4 of the ensemble (far away from their individual cores) cannot be given by a superposition of the individual fields of all dyons yet. Since the asymptotic condition $A_4|_{|\vec{x}| \rightarrow \infty} = \pi\nu\tau^3$ must be satisfied, one has to eliminate the holonomy parameter term in the gauge field associated with individual dyon by means of the time dependent gauge transformation $U = \exp(-i\pi\nu x_4\tau^3)$, after which one can then superimpose all dyonic fields and finally restore the asymptotic term with the inverse gauge transformation U^\dagger [32]. This procedure leads to

$$A_4(\vec{x}) = \frac{\tau^3}{2} [2\pi\nu + l(\vec{x})], \quad (4.31)$$

where $l(\vec{x})$ is the sum of all Coulomb terms of dyons and antidyons

$$l(\vec{x}) \equiv \sum_{l,m}^{N_L, N_M} \left(\frac{1}{|\vec{x} - \vec{r}_{L_l}|} - \frac{1}{|\vec{x} - \vec{r}_{M_m}|} + \frac{1}{|\vec{x} - \vec{r}_{\bar{L}_l}|} - \frac{1}{|\vec{x} - \vec{r}_{\bar{M}_m}|} \right). \quad (4.32)$$

At finite temperature, the color averaged heavy quark-antiquark free energy $F_{q\bar{q}}^{\text{avg}}$ is defined through the expectation value of traced Polyakov loop correlators. For quarks in the fundamental representation, from Eqs. (4.31) and (4.32) and the definition of the Polyakov loop, it is straightforward to see that

$$\frac{1}{2} \text{Tr} L^f(\vec{x}) = \cos \left[\pi\nu + \frac{1}{2} l(\vec{x}) \right]. \quad (4.33)$$

Thus, the color averaged static quark-antiquark potential in the dyon ensemble is given by

$$\begin{aligned} e^{-F_{q\bar{q}}^{\text{avg}}} &\equiv \frac{1}{4} \left\langle \text{Tr} L^{\dagger f}(\vec{x}) \text{Tr} L^f(\vec{y}) \right\rangle \\ &= \left\langle \cos \left[\pi\nu + \frac{1}{2} l(\vec{x}) \right] \cos \left[\pi\nu + \frac{1}{2} l(\vec{y}) \right] \right\rangle. \end{aligned} \quad (4.34)$$

The above static potential, though, is different from a color-singlet static potential which is the one relevant for linear behavior at large separation. According to the color decomposition

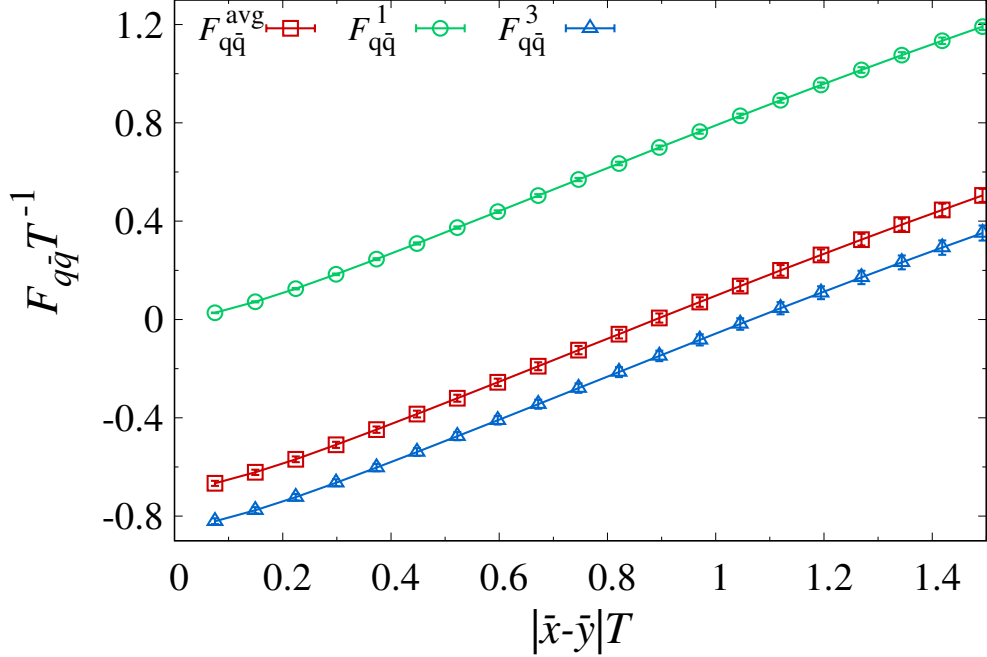


Figure 4.7: The color-averaged static quark-antiquark potential as well as its decomposed singlet and triplet channel components in the confined phase at $T/T_c = 0.970$ and $\nu = 0.5$.

$2 \otimes \bar{2} = 1 \oplus 3$, an $SU(2)$ quark-antiquark pair can interact through a singlet and a triplet channel [119], meaning that $F_{q\bar{q}}^{avg}$ is decomposed into

$$e^{F_{q\bar{q}}^{avg}} = \frac{1}{4}e^{-F_{q\bar{q}}^1} + \frac{3}{4}e^{-F_{q\bar{q}}^3}, \quad (4.35)$$

where the singlet free energy is obtained from the following:

$$e^{-F_{q\bar{q}}^1} \equiv \frac{1}{2} \left\langle \text{Tr} \left[L^{\dagger f}(\vec{x}) L^f(\vec{y}) \right] \right\rangle = \left\langle \cos \left[\frac{l(\vec{x}) - l(\vec{y})}{2} \right] \right\rangle \quad (4.36)$$

and the triplet contribution follows trivially from Eq. (4.35).

Due to the periodic boundary conditions imposed in our geometry, the maximum allowed distance is $|\vec{x} - \vec{y}| \leq R/2$, where $R \approx 3.51$ is the size of the box of volume $V = 43.37$. To compute these observables, a total of 3000 Monte Carlo configurations are used for each combination of number of dyons ($N_L, N_M = 0, \dots, 22$). To account for isotropy, for each interquark separation we averaged the contribution to the Polyakov loop correlator from 13 different orientations. At each temperature, the holonomy parameter ν is fixed to be the equilibrium value that the one which

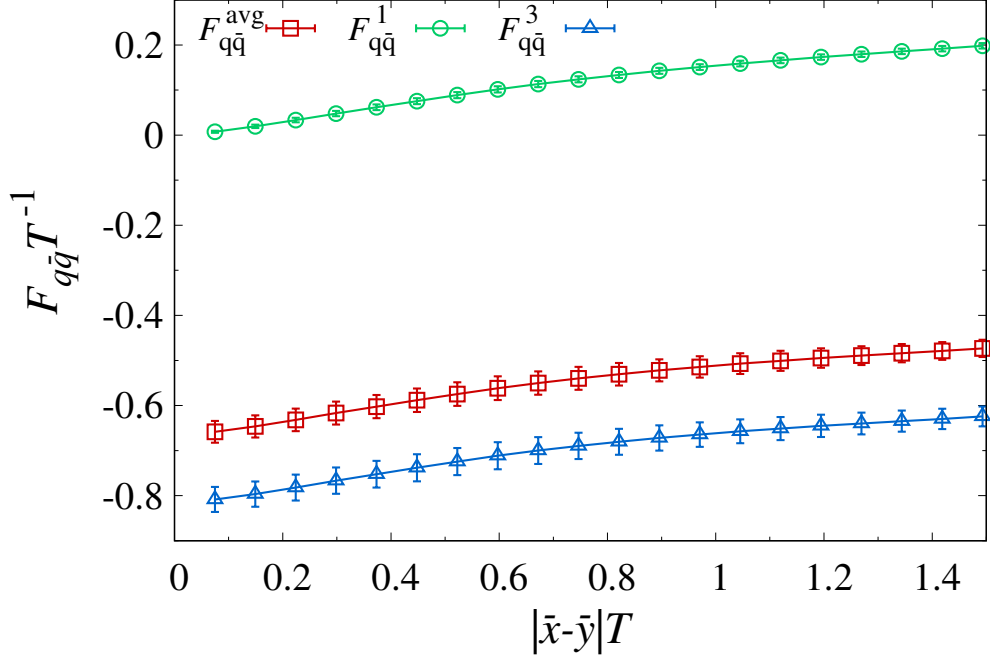


Figure 4.8: The color-averaged static quark-antiquark potential as well as its decomposed singlet and triplet channel components in the deconfined phase at $T/T_c = 1.674$ and $\nu = 0.250$.

minimizes the ensemble free energy. In Figs. 4.7 and 4.8, we show the color averaged potential and its singlet and triplet contributions for the confined and deconfined phases at $T/T_c = 0.970$ and $T/T_c = 1.674$ respectively. In Fig. 4.9 we show the singlet channel free energy alone as a function of interquark separation $|\vec{x} - \vec{y}|$ for several temperatures below and above T_c . It may be noted that the color-averaged static potential above T_c appears not fully saturated at large distance, due to two factors. The first is the finite volume effect (as will be discussed later in Section 4.3.1) which would limit the largest possible distance we could explore. The second is that in the high temperature deconfined phase, the perturbative thermal gluons (which are absent in the current framework) would contribute more and more importantly with increasing temperature to the screening of the static potentials.

An interesting comparison is with the static potential of quarks and antiquarks in the adjoint representation, in which case no linear rising at large distance is expected as the gluons (themselves being adjoint) can screen out the potential. Following [114], one can obtain the adjoint static

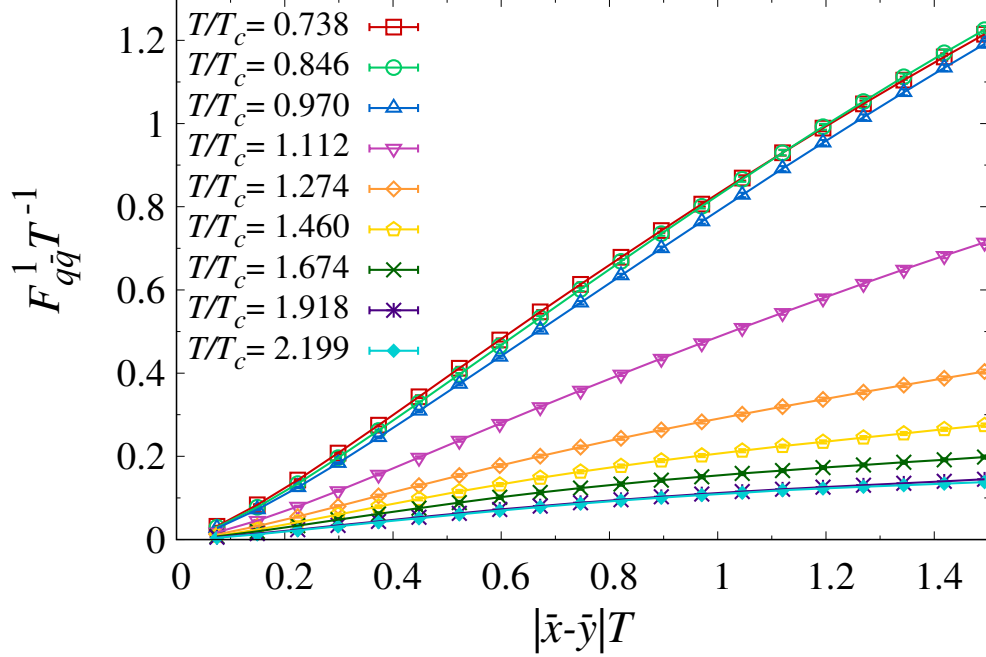


Figure 4.9: The singlet channel of the static quark-antiquark potential for the fundamental representation in both confined and deconfined phases for $\nu = 0.5, 0.5, 0.5, 0.35, 0.3, 0.275, 0.25, 0.225$ and 0.225 , in order of increasing temperature.

potential via the following relation with the fundamental one L^f :

$$L_{ij}^a = \frac{1}{2} \text{Tr} \left(\tau_i L^f \tau_j L^{f\dagger} \right), \quad (4.37)$$

where τ_i are the Pauli matrices. Given that $L \in SU(2)$, the fundamental representation is generally defined as

$$L^f = a_0 \mathbf{1} + i a_j \tau_j, \quad (4.38)$$

with $a_\mu a_\mu = 1$. Thus Eq. (4.37) can be rewritten as

$$L_{ij}^a = 2 \left[a_0 a_k \varepsilon_{ijk} + a_i a_j + \delta_{ij} \left(a_0^2 - \frac{1}{2} \right) \right], \quad (4.39)$$

and it is easy to see that its trace is expressed in terms of the fundamental one as

$$\text{Tr} L^a(\vec{x}) = \left| \text{Tr} L^f(\vec{x}) \right|^2 - 1. \quad (4.40)$$

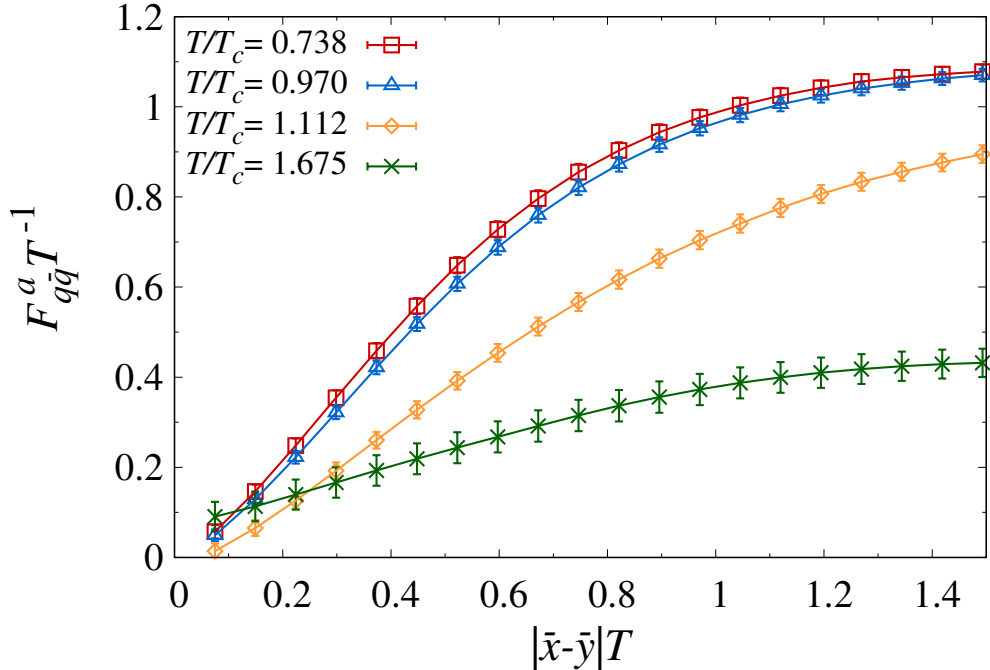


Figure 4.10: The static quark-antiquark potential for the adjoint representation in both confined and deconfined phases for $\nu = 0.5, 0.5, 0.3$ and 0.25 , in order of increasing temperature.

Therefore, the adjoint static quark-antiquark free energy is then given by

$$e^{-F_{q\bar{q}}^a} = \frac{\langle \text{Tr} L^{\dagger a}(\vec{x}) \text{Tr} L^a(\vec{y}) \rangle}{\langle |\text{Tr} L^a(0)|^2 \rangle}. \quad (4.41)$$

Notice we have included a normalization factor $\langle |\text{Tr} L^a(0)|^2 \rangle$ in the correlator such that $F_{q\bar{q}}^a = 0$ at $|\vec{x} - \vec{y}| = 0$. The resulting potentials are shown in Fig. 4.10 for different temperatures.

As pointed out already, at large separation in the confined phase, one expects the (fundamental representation) singlet static potential to have a linear rising behavior of the following form:

$$F_{q\bar{q}}|_{|\vec{x}-\vec{y}|\rightarrow\infty} \approx \sigma |\vec{x} - \vec{y}|, \quad (4.42)$$

where σ is the so called *string tension*. This is clearly observed in the fundamental representation (Fig. 4.9) at $T/T_c < 1$. However, at temperatures above T_c , the slope σ drops toward zero, as expected. In Fig. 4.11, we show the extracted string tensions for the singlet potential for several temperatures. In extracting the slope, we use linear fits for the large distance part but ignore the “curved” tails observed at the largest distances, which are most likely due to finite volume effects

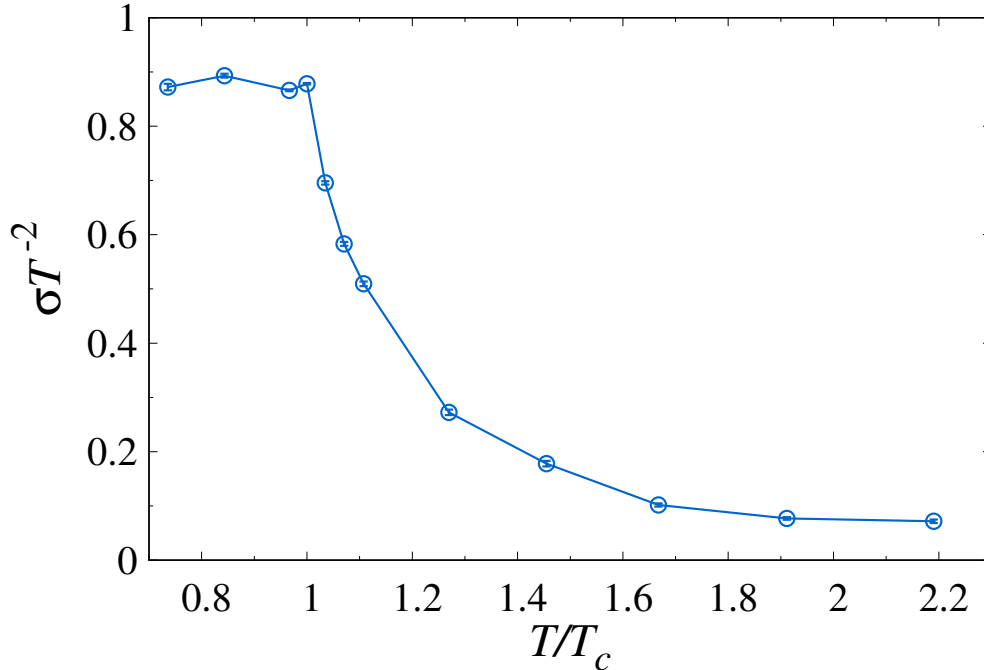


Figure 4.11: Temperature dependence of the string tension σ extracted from the singlet static quark-antiquark potential $F_{q\bar{q}}^1$ in the fundamental representation.

(see Section 4.3.1 for an extended discussion). It may also be mentioned that our results show a relatively slow decrease of σ above T_c , an effect which may also be due to finite volume issues. In contrast, the adjoint static potential does not show any linear rising at large separation. In short, our results from the dyon ensemble for the static quark-antiquark potentials in both representations are consistent with the expected behavior of an $SU(2)$ pure gauge theory.

4.2.4 The Spatial Wilson Loop

Another interesting quantity to explore is the spatial Wilson loop. It is known that the spatial Wilson loop at finite temperature shows area law behavior with a finite spatial string tension σ_s both below and above T_c and thus by itself does not serve as an “indicator” of confinement transition [120–123]. Nonetheless, the restoration of Lorentz symmetry (Euclidean $O(4)$) at $T \rightarrow 0$ suggests that in this limit, σ_s should coincide with the string tension of the static potential Eq. (4.42) extracted from Polyakov loop correlators. The $SU(2)$ traced spatial Wilson loop is defined as

$$W_C \equiv \frac{1}{2} \text{Tr} \mathcal{P} \exp \left[i \oint_C dx_i A_i(x) \right]. \quad (4.43)$$

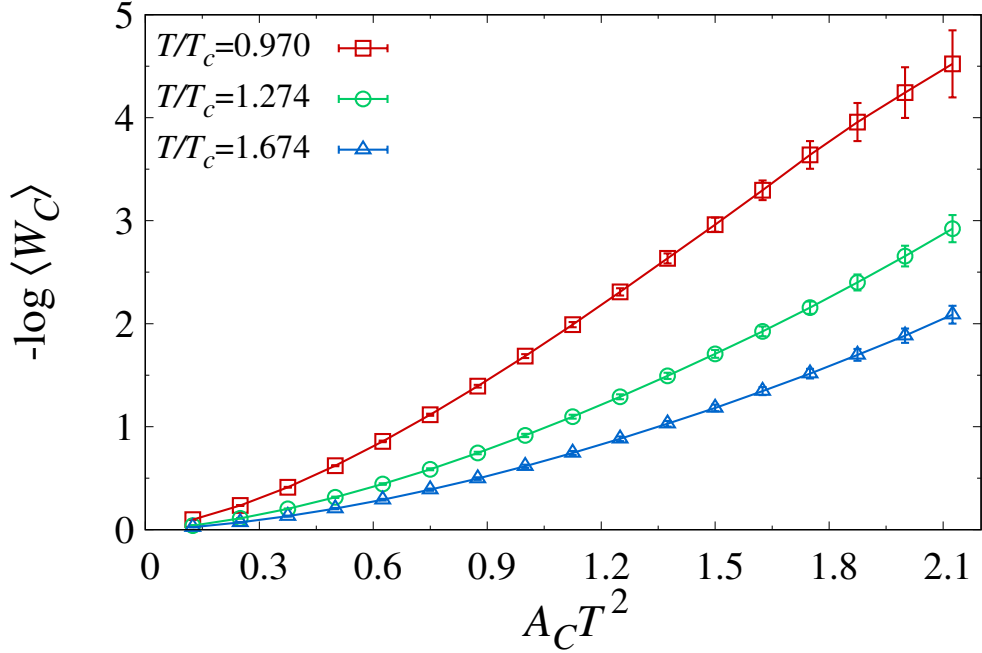


Figure 4.12: The spatial Wilson loop (in the form of its negative logarithm) for the fundamental representation in both confined and deconfined phases.

In the gauge where $A_4(x)$ is diagonal, the only non-vanishing spatial component of the dyon fields, in the asymptotic limit, is

$$A_\phi^j(\vec{x}) = m_j \frac{\tan \frac{\theta}{2} \tau^3}{r} \frac{1}{2}, \quad (4.44)$$

where $m_j = \pm 1$ is the corresponding magnetic charge (Table 3.1) and $r = \sqrt{x_i x_i}$. The Dirac string singularity along the negative x_3 -axis, although a gauge artifact, might be an inconvenience for the numerical simulations. Therefore, for computing W_C it is more suitable to use the corresponding magnetic field (instead of the gauge potential). For this, the Abelian Stokes theorem can be used to rewrite the spatial Wilson Loop in the so called ‘‘Abelian dominance’’ approximation [124]

$$W_C \approx \frac{1}{2} \text{Tr} \exp \left[i \int_{A_C} da_i B_i(x) \right], \quad (4.45)$$

where $B_i \equiv \frac{1}{2} \varepsilon_{ijk} F_{jk}$ and A_C is the area enclosed by a rectangular contour C . Therefore, the

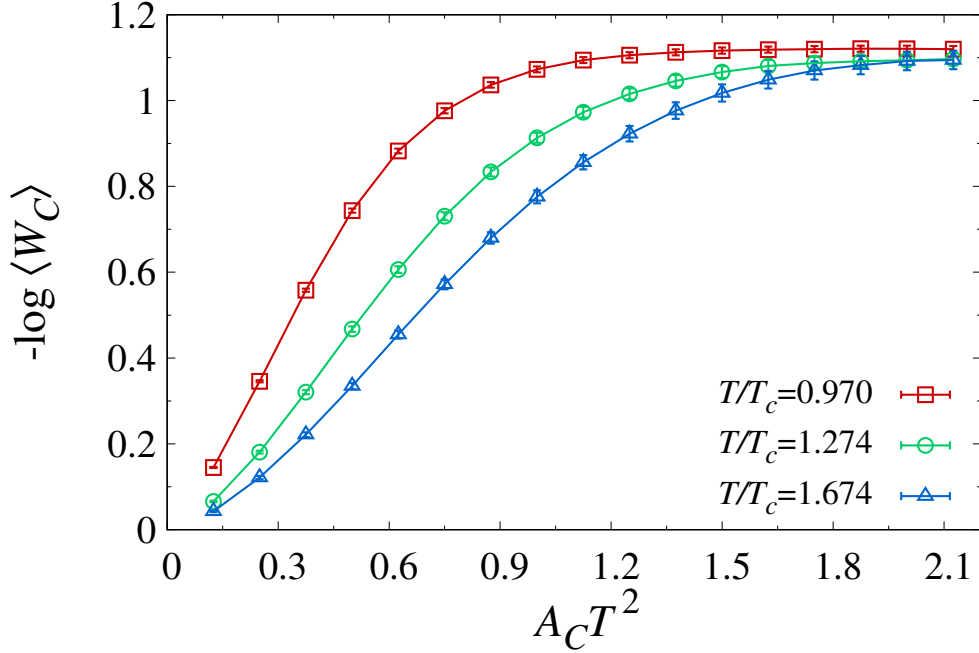


Figure 4.13: The spatial Wilson loop (in the form of its negative logarithm) for the adjoint representation in both confined and deconfined phases.

corresponding magnetic field to Eq. (4.44) is

$$B_r^j = \frac{m_j \tau^3}{r^2} \frac{1}{2}, \quad (4.46)$$

and $B_\phi = B_\theta = 0$. The total field strength from the whole ensemble will thus be

$$B_i(\vec{x}) = \frac{\tau^3}{2} \sum_{l,m}^{N_L, N_M} \left[\frac{(\vec{x} - \vec{r}_{L_l})_i}{|\vec{x} - \vec{r}_{L_l}|^3} - \frac{(\vec{x} - \vec{r}_{M_m})_i}{|\vec{x} - \vec{r}_{M_m}|^3} - \frac{(\vec{x} - \vec{r}_{\bar{L}_l})_i}{|\vec{x} - \vec{r}_{\bar{L}_l}|^3} + \frac{(\vec{x} - \vec{r}_{\bar{M}_m})_i}{|\vec{x} - \vec{r}_{\bar{M}_m}|^3} \right]. \quad (4.47)$$

It is interesting to examine whether the spatial Wilson loop computed from the dyon ensemble will follow the area law in both confining and deconfined phases, i.e.

$$\langle W_C \rangle \propto e^{-\sigma_s A_C}. \quad (4.48)$$

In Fig. 4.12, the negative logarithm of $\langle W_C \rangle$ in the fundamental representation is plotted as a function of the spatial loop area A_C , which indeed demonstrates an almost linear rising behavior at large contour areas.

Recalling the units used in this work, the string tension obtained here is dimensionless after rescaling all quantities by temperature. To restore physical units, one makes the change $\sigma_s \rightarrow \sigma_s/T^2$. As has been established before [122], σ_s increases with increasing T , however, σ_s/T^2 should decrease with increasing temperature. Such a trend is consistent with our results from dyon ensemble. Finally, we've also examined the spatial Wilson loop for the adjoint representation, shown in Fig. 4.13. It is observed that the curve rises rapidly with loop area and reaches a plateau much faster than that of $F_{q\bar{q}}^a$, again an indication of the screening effects for adjoint sources.

4.3 DISCUSSIONS

4.3.1 Finite Volume Effects

A rigorous study of all thermodynamic quantities in principle requires an infinite volume limit, which is obviously impossible for any realistic numerical simulations. In the case of the present study on the dyon ensemble, using a larger volume requires an increased number of dyons/antidions in the simulations thus costing significantly more computing power. A practical approach would be to examine the finite size effect by perform tests with increasing volume of the box. In this Subsection we compare results obtained with two and three times the originally used volume, denoted as $V_0 = 43.37$.

One important feature to check is the (relative) contribution from various terms \mathcal{Z}_{LM} in the partition function \mathcal{Z} Eq. (4.23). Note that for different volumes, each term with fixed number of dyons/antidions $N_{L,M}$ would have different density. The better way to compare results computed with different volume would be to examine the contribution from given dyon/antidyon densities. In Fig. 4.14, we show how the contribution to partition function (from individual fixed-density terms in the ensemble sum) is changed with the increased volume. As expected, the maximum peak of the distribution becomes sharper around the most probable densities. Most importantly the location of the maximum does not change much with increased volume. Table 4.1 summarizes and compares numerical values of ensemble averages of the dyon densities at different temperatures as well as the free energy density for ν_{\min} obtained at the three different volumes. It can be seen that going from V_0 up to $3V_0$, there is a small shift (at few percent level) of the free energy density while small changes in the dyon densities. Such comparison clearly demonstrates that our thermodynamic

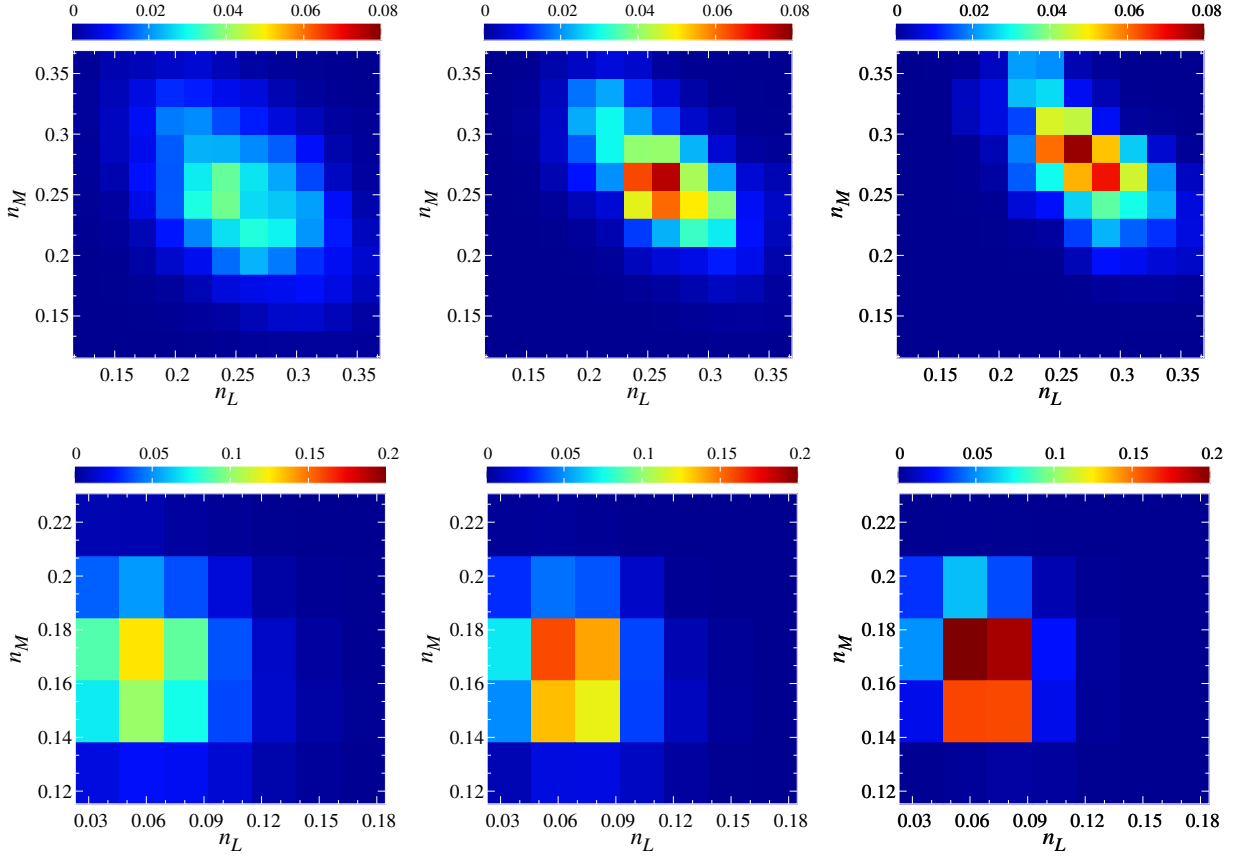


Figure 4.14: Dyon density dependence of $\mathcal{Z}_{\text{LM}}/\mathcal{Z}$ at different volumes (from left to right: $V_0, 2V_0$ and $3V_0$). Top: confined phase at $T/T_c = 0.970$ and $\nu = 0.5$. Bottom: deconfined phase at $T/T_c = 1.274$ and $\nu = 0.3$.

results are quite stable with increasing system volume, which is an indication that our results shall be a very good approximation to the thermodynamic limit.

The finite volume also bears influence on the evaluation of spatial correlation observables, in particular the static quark-antiquark potential. As mentioned in the previous section, it exhibits unnatural behavior near the largest distances that are allowed by the finite volume. To test if this could indeed be a consequence of the finite volume, we've computed these observables with enlarged volume for comparison. In Fig. 4.15 we show the results of the singlet channel potential calculated in a box twice the volume of the original volume V_0 . For comparison, we also include the results from the original volume. One can see that indeed, the curved tails only appear at the edge of the box and at intermediate distances both potentials match substantially well. This comparison justifies our previous extraction of string tension via linear fit in intermediate distance regime and

Table 4.1: Volume dependence of the free energy density and ensemble averages of dyon densities at several temperatures, for $V = V_0, 2V_0$ and $3V_0$ (with $V_0 = 43.37$) respectively.

	T/T_c	V_0	$2V_0$	$3V_0$
$\frac{F}{VT^4}$	0.970	-0.7077(7)	-0.7782(6)	-0.8271(7)
	1.274	-0.3713(10)	-0.3977(8)	-0.4227(9)
$\langle n_L \rangle$	0.970	0.253(11)	0.260(19)	0.289(35)
	1.274	0.063(4)	0.066(7)	0.069(12)
$\langle n_M \rangle$	0.970	0.253(11)	0.264(19)	0.259(31)
	1.274	0.165(10)	0.165(16)	0.172(29)

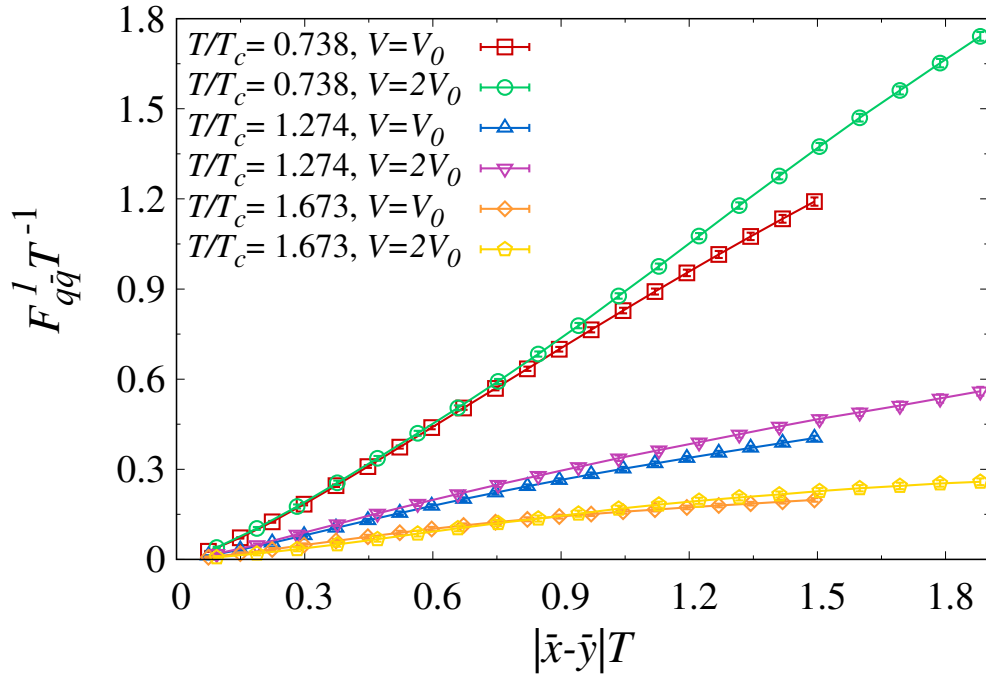


Figure 4.15: Volume effects on the singlet static quark-antiquark potential in both confined and deconfined phases.

do suggest that for such spatial correlations, a significantly larger volume may be needed for their accurate evaluation.

4.3.2 The Influence of Dyon–antidyon Short-Range Correlation

A key ingredient in the confinement mechanism of dyon ensemble is the repulsive core potential V_{jj}^C . As defined in Eq. (4.17), there are two parameters which quantify such interaction: V_c is the strength and ζ_j^c the size of the core. It is important to understand the influence of these parameters on the various observables. In Fig. 4.16 we show the free energy density as a function of ν for

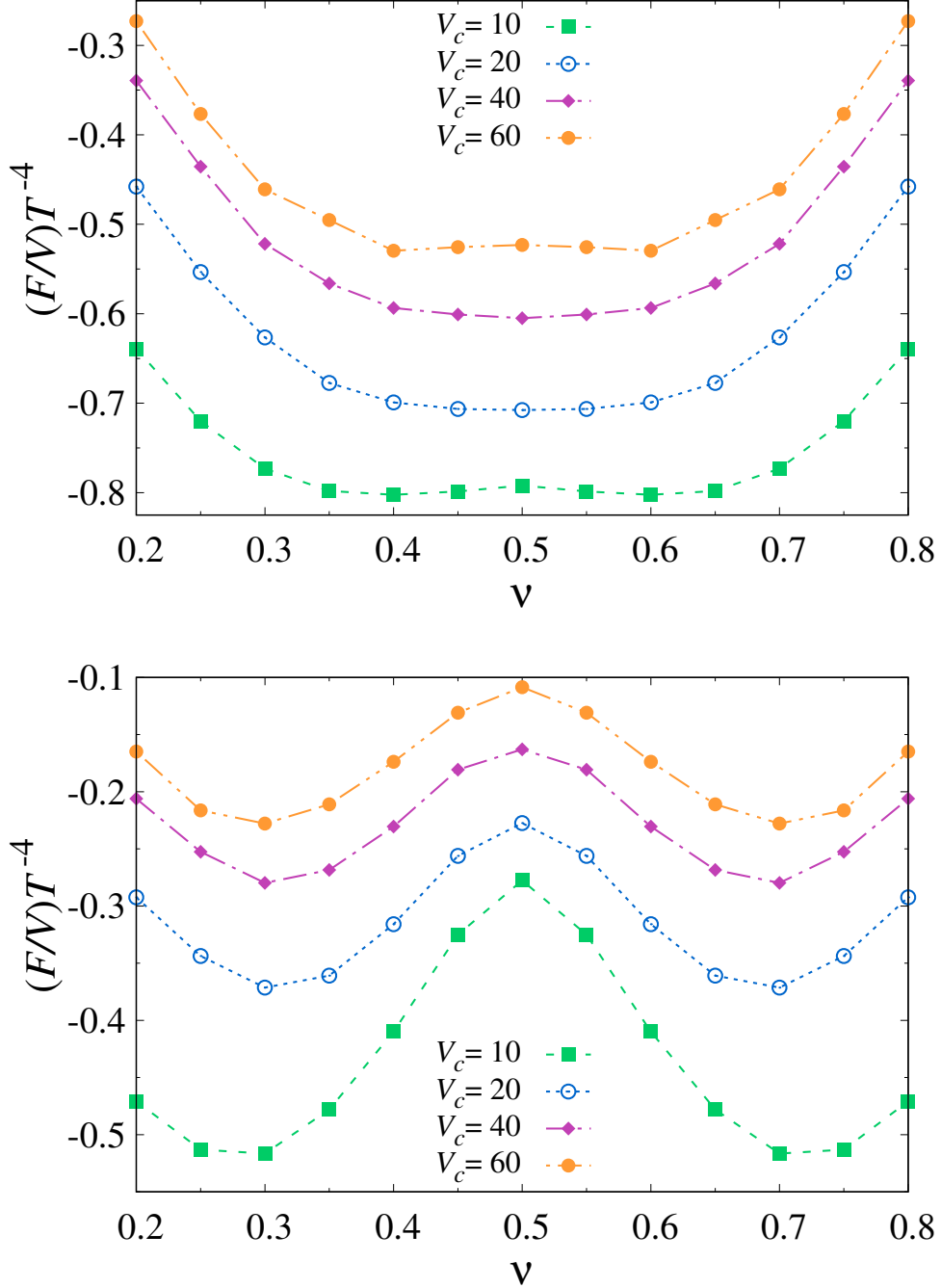


Figure 4.16: The free energy density versus holonomy for several different values of core potential strength V_c . Top: $T/T_c = 0.970$ ($S = 7$). Bottom: $T/T_c = 1.274$ ($S = 9$).

different values of V_c at both low and high temperatures. A general observation is that a larger core strength V_c always favors more the confining holonomy $\nu = \bar{\nu} = 1/2$. A smaller V_c , on the other hand, weakens the correlation and makes confinement harder to occur. Indeed for the $V_c = 10$ case, even with the lowest temperature we explore, the system is still in the deconfined phase. These

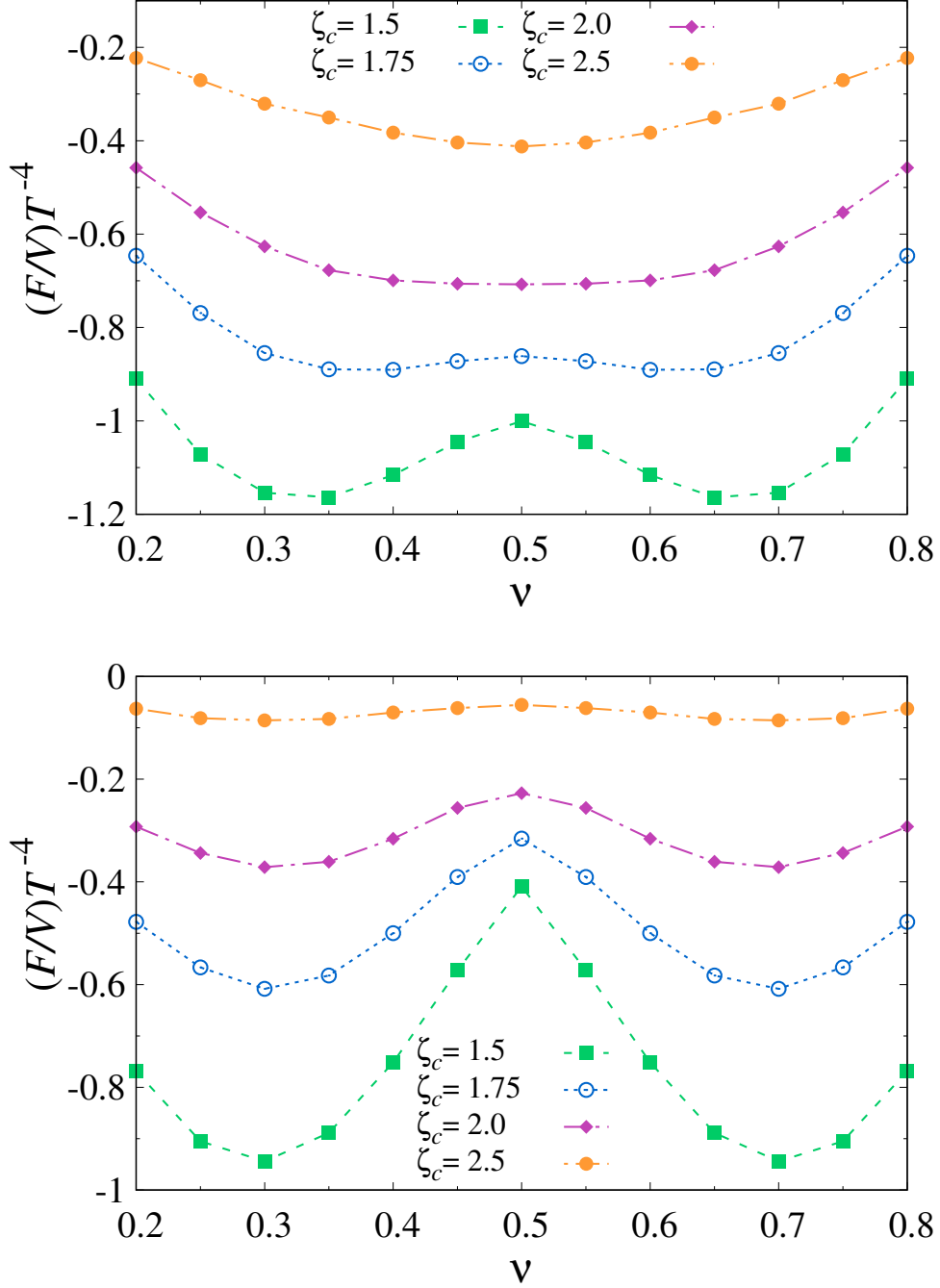


Figure 4.17: The free energy density versus holonomy for several different values of core potential range ζ_j^c . Top: $T/T_c = 0.970$ ($S = 7$). Bottom: $T/T_c = 1.274$ ($S = 9$).

results also imply that the critical action S_c needed for the confinement transition will shift toward larger values with increasing V_c .

In a similar fashion, a change in the core size parameter ζ_j^c , will also result in considerable effect on the behavior of the free energy density.

To investigate the influence of this parameter, we have computed the ν dependence of the free energy density for $\zeta_j^c = 1.5, 1.75$ and 2.5 (in comparison with the standard choice of $\zeta_j^c = 2$) with the results shown in Fig. 4.17 for both low and high temperatures. (Due to the finite volume limitation, it is technically difficult to explore even larger core size values.)

As can be seen, when the core size is decreased, the free energy density's minimum shifts further and further away from the confining holonomy value $\nu = \bar{\nu} = 1/2$. If the core size is too small then the system would be in deconfined phase even at the low temperature value computed here. With a large core size, the system could maintain a holonomy value near the confining one even at high temperature. The comparison clearly demonstrates the importance of the repulsive core. It is a strong repulsive core that drives the system toward favoring the confining holonomy at low temperature.

4.3.3 The Debye Screening Mass

Finally, we investigate another important parameter for the ensemble, namely, the Debye mass M_D used to regularize the large distance behavior of the Coulomb terms and therefore to account for the screening effect. This parameter plays an important role in controlling the contributions to the free energy from the long range Coulomb interactions among the dyons/antidions. To see its effect, we compare the free energy density versus holonomy from dyon ensembles with three different choices of the M_D in Fig. 4.18 at both low and high temperatures. The results show that a smaller screening mass would disfavor the confining holonomy while a larger screening mass would help strengthen the confinement. This could be understood as follows: with a large screening mass the contribution to the free energy from many-body long-range Coulomb interactions get suppressed and thus the contribution from the short range correlations via the repulsive core, which essentially drives confinement, become relatively more important.

4.4 NEXT-TO-LEADING ORDER CORRECTIONS AND OTHER IMPROVEMENTS

After successfully reproducing some of the expected behavior of a confining $SU(2)$ theory, we are prompted to improve the instanton-dyon model in order to explore its viability to describe such features in a more quantitative way, by comparing the consistency of its predictions with those

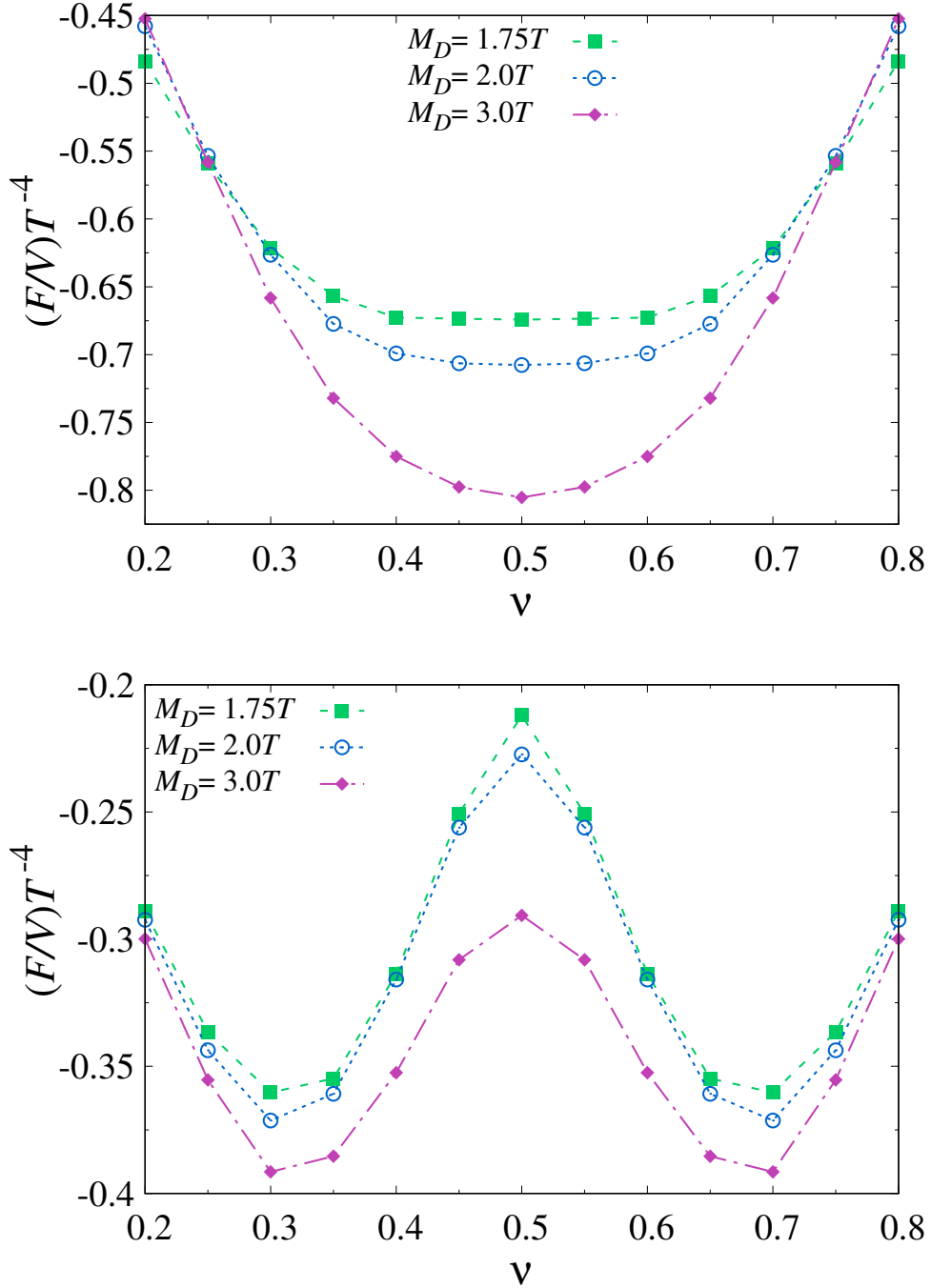


Figure 4.18: The free energy density versus holonomy at for several different values of Debye screening mass M_D . Top: $T/T_c = 0.970$ ($S = 7$). Bottom: $T/T_c = 1.274$ ($S = 9$).

from first-principle calculations such as lattice gauge theory.

The first refinement to the model consists of a better introduction of “two-loop” effects in the quantum weight. Let us recall from Section 4.1.1 that the one-loop contribution of the KvBLL

caloron is given by Eq. (4.8)

$$\begin{aligned} \mathcal{Z}_{\text{KvBLL}} &= e^{-VP_I(\nu)/T} \int d^3r_L d^3r_M T^6 C \frac{(2\pi)^{\frac{2}{3}}}{4} \det(\hat{G}) \\ &\times \left(\frac{8\pi^2}{g^2}\right)^4 \left(\frac{\Lambda_{\text{PV}} e^{\gamma_E}}{4\pi T}\right)^{\frac{22}{3}} \nu^{\frac{8}{3}\nu-1} \bar{\nu}^{\frac{8}{3}\bar{\nu}-1}. \end{aligned}$$

The factor $\left(\frac{\Lambda_{\text{PV}} e^{\gamma_E}}{4\pi T}\right)^{\frac{22}{3}}$, appears from the renormalization of the coupling at one-loop precision, namely

$$\frac{8\pi^2}{g^2(T)} \xrightarrow{\text{one-loop}} \beta_I(T) = b_1 \log\left(\frac{T}{\Lambda}\right) \implies \left(\frac{\Lambda}{T}\right)^{b_1} = e^{-\frac{8\pi^2}{g^2(T)}}, \quad b_1 = \frac{11}{3}N_c \quad (4.49)$$

where $\Lambda = \Lambda_{\text{PV}} e^{\gamma_E}/4\pi$. However, the factor g^{-8} in $\mathcal{Z}_{\text{KvBLL}}$ corresponds to the bare coupling and it is renormalized for two-loop corrections. We previously handled this issue by taking

$$\left(\frac{8\pi^2}{g^2}\right)^4 \left(\frac{\Lambda}{T}\right)^{\frac{22}{3}} \rightarrow \beta_I(T)^4 e^{-\beta_I(T)} \Gamma^2, \quad (4.50)$$

and introducing the constant factor $\Gamma = 0.119$ and with β_I equal to the instanton action parameter S , acting as a control parameter for the temperature dependence. According to Diakonov et al [105], a proper way to introduce the running of the coupling in the g^{-8} factor and hence determine the two-loop quantum weight of the caloron, is achieved by the replacement

$$\left(\frac{8\pi^2}{g^2(T)}\right)^{2N_c} e^{-\frac{8\pi^2}{g^2(T)}} \rightarrow \beta_I^{2N_c} \exp\left[-\beta_{II} + \left(2N_c - \frac{b_1}{2b_2}\right) \frac{b_1}{2b_2} \frac{\log \beta_I}{\beta_I} + \mathcal{O}\left(\frac{1}{\beta_I}\right)\right], \quad (4.51)$$

where

$$\beta_{II}(T) = \beta_I(T) + \frac{b_2}{b_1} \log \frac{2\beta_I(T)}{b_1}, \quad b_2 = \frac{34}{3}N_c^2. \quad (4.52)$$

For the instanton-dyon ensemble, we include such two-loop contribution (for $N_c = 2$) as

$$\left(\frac{8\pi^2}{g^2(T)}\right)^4 e^{-\frac{8\pi^2}{g^2(T)}} \rightarrow S^4 e^{-S} \Gamma^2(S), \quad (4.53)$$

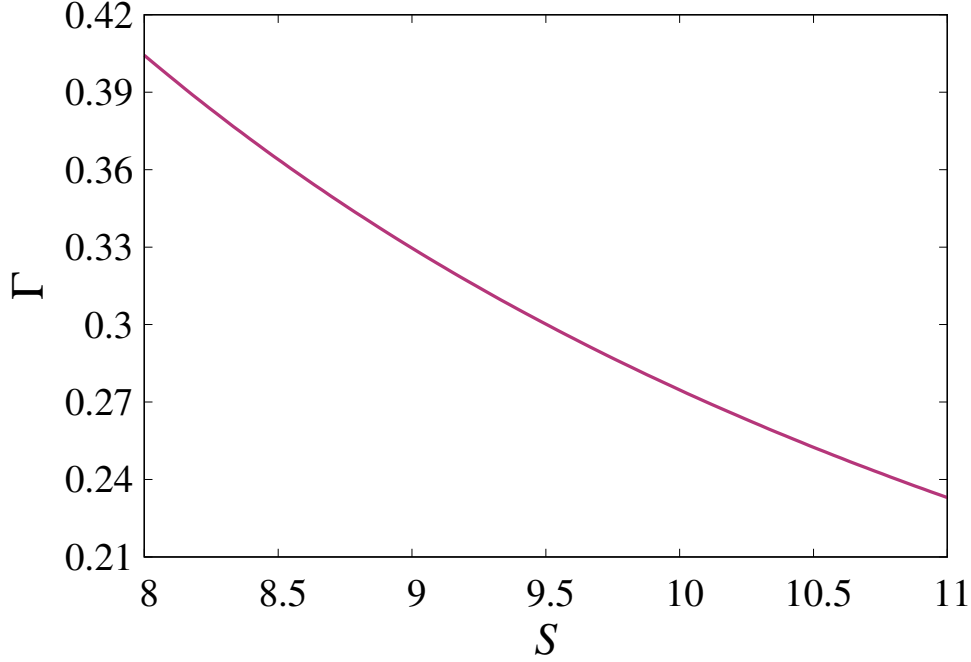


Figure 4.19: Γ -factor of the two-loop improvement as a function of the action parameter S . The plotted function contains the constant factor $\sqrt{C(2\pi)^{\frac{2}{3}}/4}$.

with

$$\Gamma(S) = \exp \left[-\frac{17}{11} \log \left(\frac{3S}{11} \right) + \frac{170 \log S}{121 S} \right], \quad (4.54)$$

and the action parameter $S(T) = \beta_I(T) = \frac{22}{3} \log \left(\frac{T}{\Lambda} \right)$. Therefore, the mapping between S and temperature is the same as before; however, Γ is not constant anymore, it is temperature dependent (see Fig. 4.19) and it portrays more accurately next-to-leading order effects. For simplicity, we redefine Γ by absorbing the constant $\sqrt{C(2\pi)^{\frac{2}{3}}/4}$ into it and rewrite the caloron partition function as

$$\mathcal{Z}_{\text{KvBLL}} = e^{-V P_I(\nu)/T} \int (d^3 r_L f_L) (d^3 r_M f_M) T^6 \det(\hat{G}) \quad (4.55)$$

with

$$f_M = \Gamma(S) S^2 e^{-\nu S} \nu^{\frac{8\nu}{3}-1}, \quad f_L = \Gamma(S) S^2 e^{-\bar{\nu} S} \bar{\nu}^{\frac{8\bar{\nu}}{3}-1}. \quad (4.56)$$

Furthermore, for this set of calculations, the interaction term $V_{D\bar{D}}$, in particular, the dyon-antidyon interaction between $L-\bar{L}$ and $M-\bar{M}$ pairs, is simplified in such manner that all classical interactions are of the Coulomb-type (see Eq. (4.18)) with a screening effect carried out by a Debye mass parameter M_D . Therefore, $V_{D\bar{D}}$ is reduced to

$$V_{D\bar{D}} = \begin{cases} \sum_{i,\bar{j}} \frac{S}{\pi T r_{i\bar{j}}} e^{-M_D r_{i\bar{j}}} & \text{for } \bar{M}L, \bar{L}M \\ \sum_{i,\bar{j}} \frac{-S}{\pi T r_{i\bar{j}}} e^{-M_D r_{i\bar{j}}} & \text{if } \zeta_j > \zeta_j^c, \text{ for } L\bar{L}, M\bar{M} \\ \sum_{\substack{i>j \\ j,\bar{j}}} V_{ij}^C & \text{if } \zeta_j < \zeta_j^c, \text{ for } LL, MM, \bar{L}\bar{L}, \bar{M}\bar{M}, L\bar{L}, M\bar{M} \\ 0 & \text{for } LM, \bar{L}\bar{M}. \end{cases} \quad (4.57)$$

with V_{jj}^C the already introduced repulsive core potential (see Eq. (4.17))

$$V_{jj}^C = \frac{\nu_j V_c}{1 + e^{(\zeta_j - \zeta_c)}}, \quad \zeta_j = 2\pi\nu_j T r_{j\bar{j}}$$

Notice then, that the full partition function of the ensemble will have the same form as in Eq. (4.20), with the replacements of the dyon fugacities Eq. (4.56) and the $V_{D\bar{D}}$ potential defined above.

The instanton-dyon ensemble contains a set of parameters which are free to be tuned in the simulations and, in principle, might produce different results. These are the screening mass M_D , the strength parameter of the repulsive core potential V_c , and the range parameter that separates the long and short-distance regions, namely, the core size ζ_c . Our goal here is to characterize the set of parameters which will give the most accurate description of the computed quantities.

4.4.1 Temperature Dependence of the Order Parameter

One of the main observables of interest is the order parameter of the deconfinement phase transition, i.e., the thermal average of the holonomy $\langle L_\infty \rangle$, which as we know, it follows the power law (see

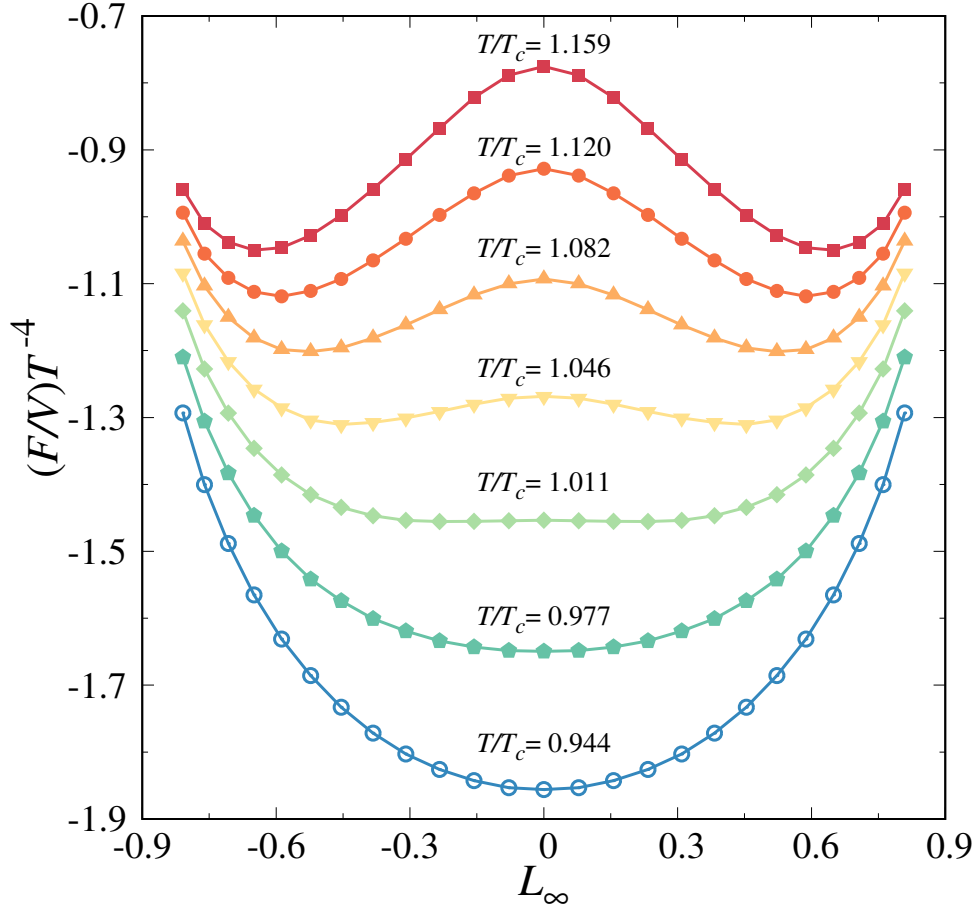


Figure 4.20: Free energy density of the instanton-dyon ensemble for $V_c = 5$, $M_D = 3.0$ and $\zeta_c = 2$

Eq. (4.29))

$$\langle L_{\infty} \rangle = b(T/T_c - 1)^{\beta} [1 + d(T/T_c - 1)^{\Delta}],$$

with $\beta = 0.3265(3)$ and $\Delta = 0.530(16)$ the critical exponents of the universality class.

As previously described in Section 4.2.1, for a fixed value of S , it is determined by the minimum of the holonomy potential. An example of this potential is shown in Fig. 4.20 for the particular case of $V_c = 5$, $M_D = 3.0$ and $\zeta_c = 2$; however, the observed behavior which characterizes the second order phase transition, is observed in all the parameter combinations explored in this section.

Since the temperature dependence is extracted via the control parameter S , this entails to fix

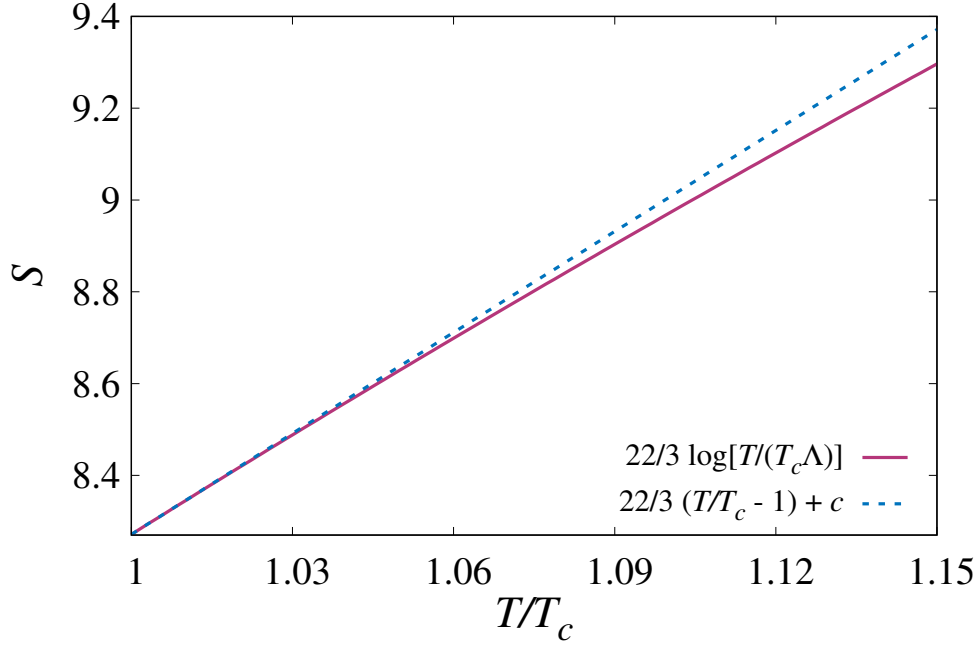


Figure 4.21: Linear approximation to the instanton action $S(T)$ near T_c .

the scale Λ as

$$\frac{\Lambda}{T_c} = \exp\left(-\frac{3}{22}S_c\right), \quad (4.58)$$

rendering the specification of the critical action S_c essential. As opposed to the previous set of calculations, where the critical action was found up to a precision of 0.25; this time, the process of determining S_c consists of first narrowing the range of S from the confined (below) and deconfined (above) phases, and then to extrapolate its value, following the ansatz

$$\langle L_\infty \rangle \propto (S - S_c)^\beta. \quad (4.59)$$

This assertion would only be true if close to T_c , the action parameter is proportional to T , i.e., if the linear expansion around the point $T = T_c$

$$S(T) = \frac{22}{3} \log\left(\frac{T}{T_c \Lambda}\right) \approx \frac{22}{3} \left(\frac{T}{T_c} - 1\right) + \text{const.} \quad (4.60)$$

proves to be a good approximation. That is the case for the temperature range explored in this

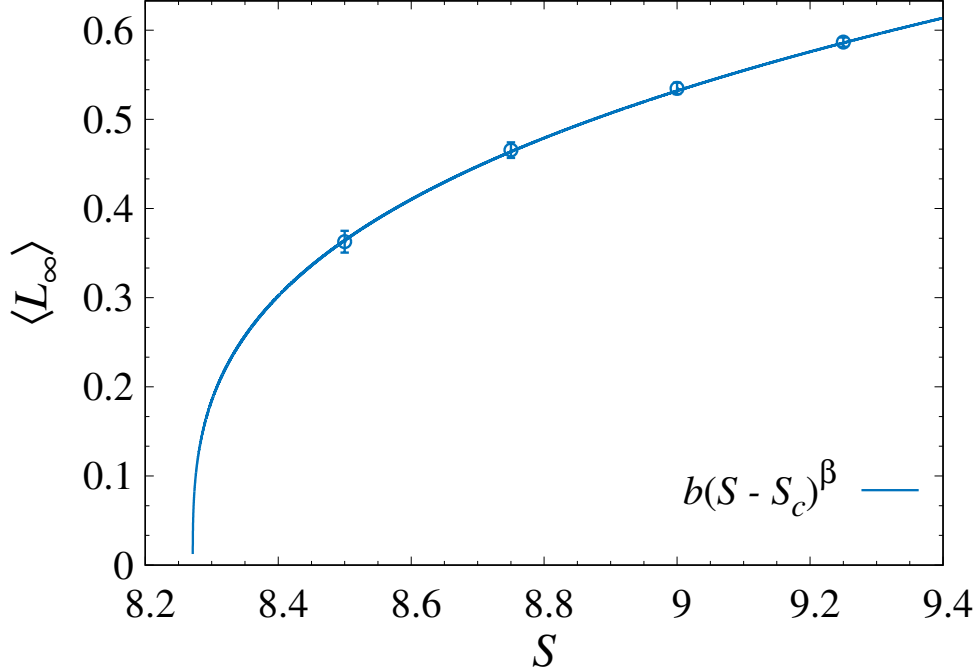


Figure 4.22: Fit of the holonomy as a function of S to determine the critical action S_c .

work, and a clear example for $\Lambda = 0.32$ is depicted on Fig. 4.21. Therefore, it is safe to expect the critical scaling of Eq. (4.59). On Fig. 4.22 we show an example of the fit used to determine the critical action.

The instanton-dyon ensemble predictions for the temperature dependence of $\langle L_\infty \rangle$ will be compared against two independent calculations on the lattice, which to our knowledge, are the most recent and state of the art simulations. Throughout the plots, the data points extracted from [117] are referred to as Latt.[DFP,2003] and those from [118] as Latt.[HP,2008]. It should be noticed that only the data points from Latt.[DFP,2003] are shown with error bars, since those from Latt.[HP,2008] were significantly small to be extracted from the available plot figure. Given the not so small discrepancy between both lattice simulations, the grey shaded area on the plots shows the desired region where we want our results to lay in. The borders of the mentioned area correspond to their respective critical scaling fit, which is showed in each of their sources [117, 118].

The reference curve used for the quantitative comparison corresponds to the average fit between the two lattice ones, which is denoted as “Latt. Avg. Fit”. To quantify the accuracy of our results,

Table 4.2: Fit parameters corresponding to results shown in Fig. 4.23.

V_c	b	d	S_c	$\chi_f^2/\text{d.o.f.}$	$\chi_L^2/\text{d.o.f.}$
5	1.381(50)	-0.312(92)	8.591(21)	0.196	17.713
10	1.325(47)	-0.232(86)	9.210(36)	0.643	12.177
15	1.286(42)	-0.160(85)	9.477(29)	0.636	8.780
20	1.115(38)	0.151(106)	9.479(32)	0.978	5.392

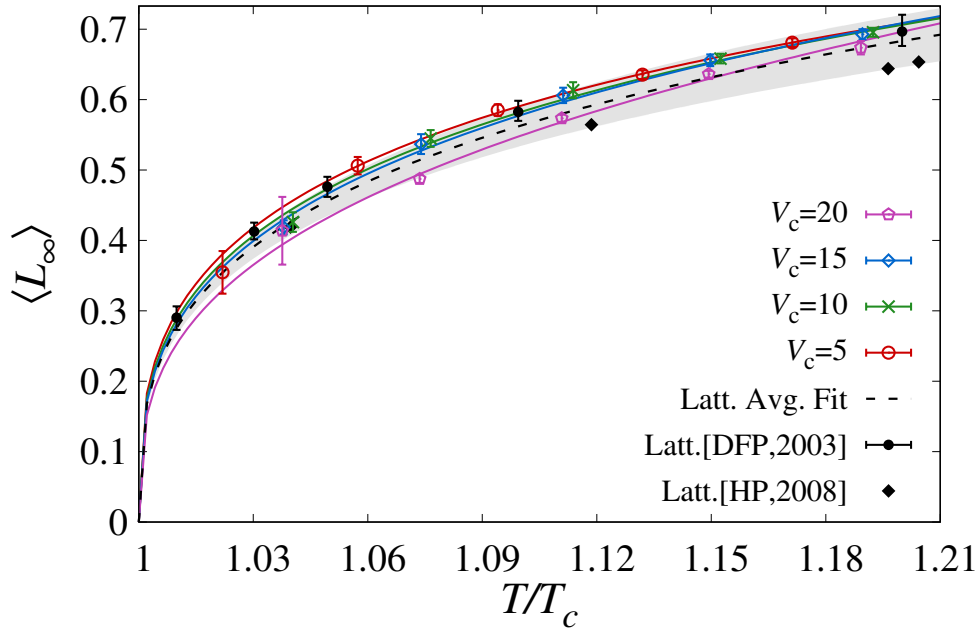


Figure 4.23: The Polyakov loop at spatial infinity with $\zeta_c = 2.1$ and $M_D = 3$, for different core strengths V_c . Continuous lines correspond to fits from critical behavior.

we follow the standard procedure of minimizing the χ^2 statistic, defined as

$$\chi^2 = \sum_{i=1}^{\text{d.o.f.}} \frac{(\langle L_\infty \rangle_i^{\text{DE}} - \langle L_\infty \rangle_i^{\text{fit}})^2}{\sigma_i^2}, \quad (4.61)$$

where d.o.f. stands for degrees of freedom, $\langle L_\infty \rangle^{\text{DE}}$ are the dyon ensemble data points, $\langle L_\infty \rangle^{\text{fit}}$ the fit used for comparison, and σ_i^2 the variance of the $\langle L_\infty \rangle^{\text{DE}}$ data points.

We will now show the effects of the three key parameters of the ensemble in the deconfinement phase transition. Tables 4.2 to 4.4 contain the details of the fitting parameters, the corresponding critical action S_c , as well as the χ^2 associated to their fitted function χ_f^2 and that to the lattice average fit χ_L^2 .

Table 4.3: Fit parameters corresponding to results shown in Fig. 4.24.

M_D	b	d	S_c	$\chi_f^2/\text{d.o.f.}$	$\chi_L^2/\text{d.o.f.}$
2.5	1.291(38)	-0.271(70)	8.737(18)	0.283	0.429
3.0	1.381(50)	-0.312(92)	8.419(25)	0.196	17.713
3.5	1.357(39)	-0.334(65)	8.442(41)	0.795	9.178

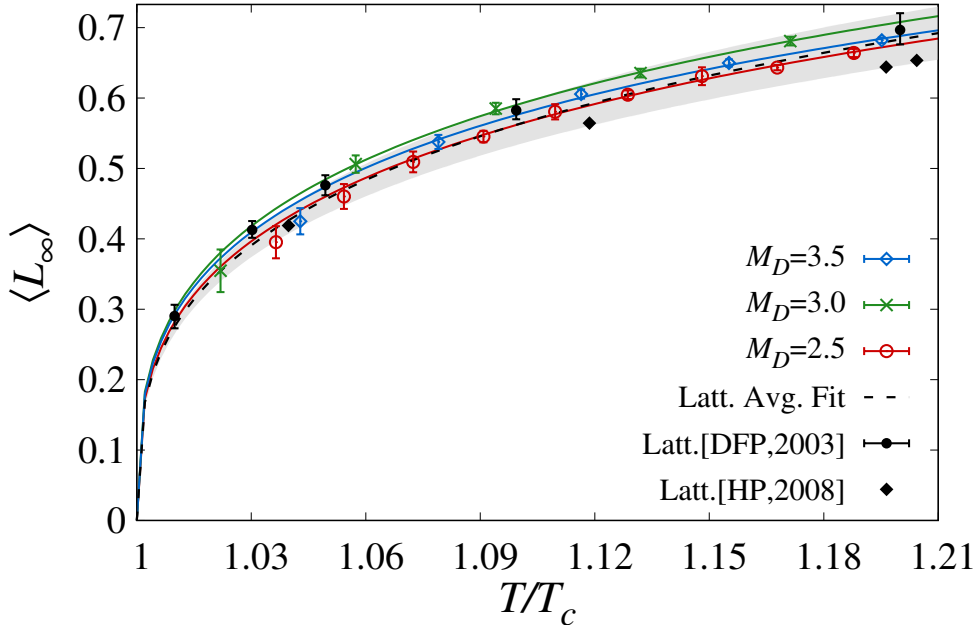


Figure 4.24: The Polyakov loop at spatial infinity with $\zeta_c = 2.1$ and $V_c = 5$, for different screening masses M_D . Continuous lines correspond to fits from critical behavior.

We explore first the dependence on the core strength V_c portrayed on Fig. 4.23. At fixed screening mass and core size ($M_D = 3$ and $\zeta_c = 2.1$), the phase transition is enhanced as V_c decreases; however, it was found that around $V_c = 15$ the enhancement effect is saturated. As the core strength decreases, the dyon densities must increase to balance the necessary repulsion to generate confinement and the critical action gets smaller. Therefore, we conclude that the core potential should be strong enough to generate confinement and simultaneously weak to have the faster growth in the order parameter observed in lattice simulations.

Next, fixing the core strength and size to $V_c = 5$ and $\zeta_c = 2.1$, we dive into the effects produced by the screening mass M_D . As seen in Fig. 4.24, a larger mass enhances the phase transition. Given that M_D regulates the long range interactions of Coulomb terms such as in a Yukawa potential, a small increase will make the exponential term sufficiently small, thus suppressing its contribution

Table 4.4: Fit parameters corresponding to results shown in Fig. 4.25.

ζ_c	b	d	S_c	$\chi_f^2/\text{d.o.f.}$	$\chi_L^2/\text{d.o.f.}$
1.7	1.048(53)	0.009(138)	8.200(7)	0.089	24.363
1.8	1.163(37)	-0.140(86)	8.271(7)	0.098	18.924
2.0	1.277(33)	-0.272(60)	8.419(25)	0.443	0.850
2.1	1.381(50)	-0.312(92)	8.591(21)	0.196	17.713
2.2	1.465(32)	-0.444(47)	8.681(35)	0.647	40.155
2.4	1.705(37)	-0.659(49)	8.879(41)	0.584	192.594

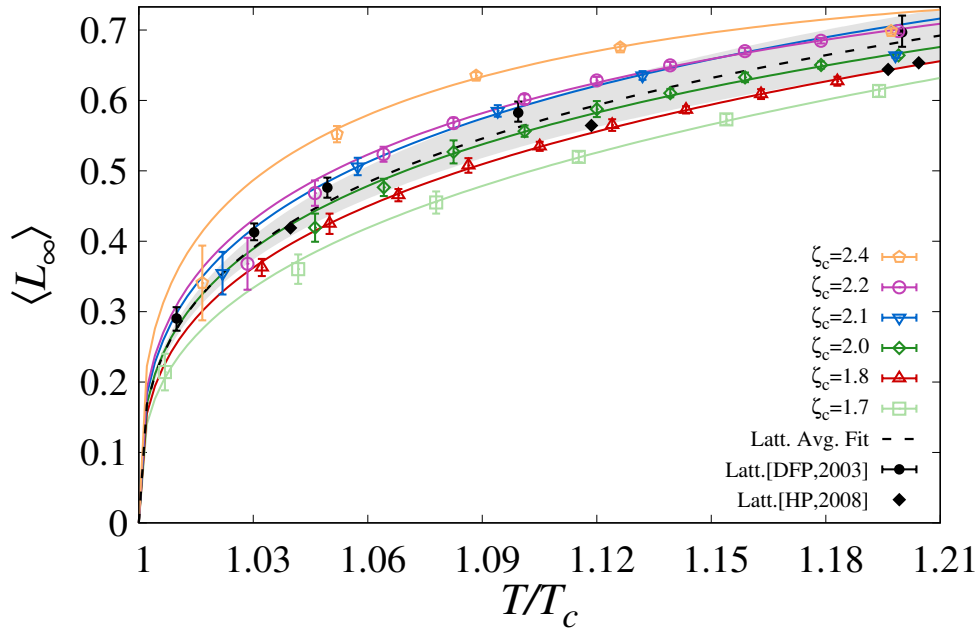


Figure 4.25: The Polyakov loop at spatial infinity with $V_c = 5$ and $M_D = 3$, for different core sizes ζ_c . Continuous lines correspond to fits from critical behavior.

faster. This suggests that there is a saturation point for large enough M_D , which we set up to be approximately at $M_D = 3.0$. The curve obtained for $M_D = 2.5$, remarkably agrees with the lattice average fit, having the lowest $\chi_L^2/\text{d.o.f.}$ of all the results presented. Regarding S_c , it was observed that the more the phase transition is enhanced, the smaller the value, i.e. the critical action grows as the screening mass decreases.

To finish cover the parameter space, we now look at ζ_c with the screening mass and the core strength being fixed at $V_c = 5$ and $M_D = 3$. As shown in Fig. 4.25, the dyon ensemble is significantly more sensitive to this parameter than the previous ones. It is clearly seen that the phase transition is enhanced with larger core sizes, even above the Latt.[DFP,2003] curve; which is no surprising

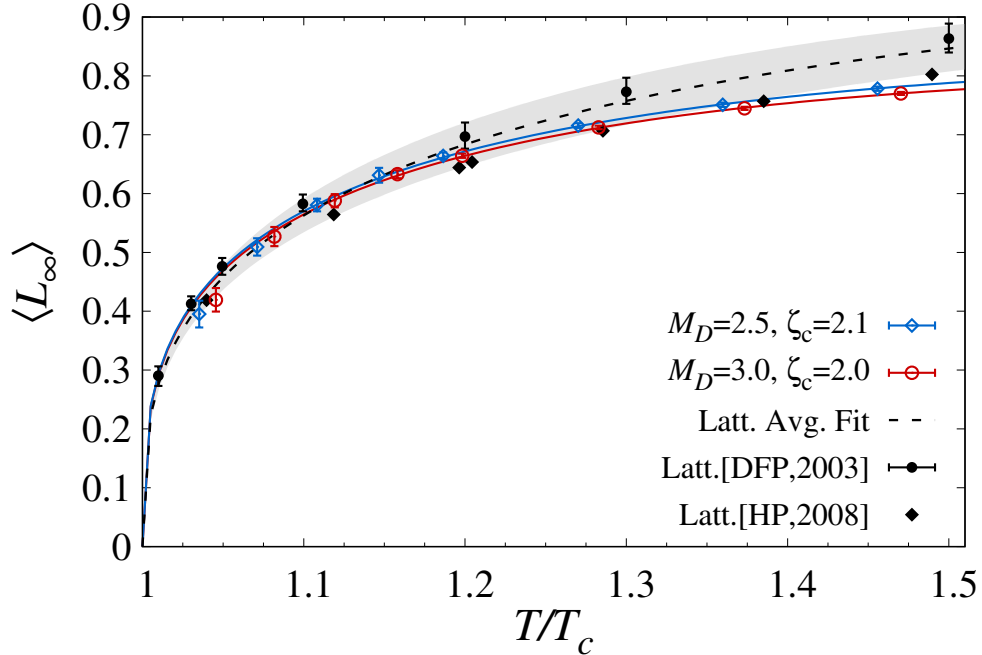


Figure 4.26: The Polyakov at spatial infinity in a higher temperature regime.

given that larger core sizes result in configurations with more repulsive interactions, hence favoring confinement and reducing dyon densities. On the other hand, with increasingly strong coupling, it costs less action to create these objects; as a result, the ensemble would eventually become dense enough so that the short-range repulsive force becomes important.

From the standard χ^2 -test, it was found that the points (5, 2.5, 2.1) and (5, 3, 2) of the parameter space (V_c, M_D, ζ_c) had the best agreement with our target function, i.e. the lattice average fit, with remarkable χ_L^2 values of 0.429 and 0.850, respectively.

Using those two sets of optimal parameters, we explore the behavior at higher temperatures. Depicted in Fig. 4.26, it is observed that as temperature grows larger than T_c , the order parameter appears to grow slower than what it is observed on the lattice. Nevertheless, one must have in mind that this is a non-perturbative approach, namely, the validity of this ensemble relies on a strong coupling; therefore, it does not take into account higher temperature phenomena such as thermal gluons, whose contribution to the partition function becomes more relevant as temperature increases. Moreover, as discussed in the following section, the dyon density is small at higher temperatures and so the dyon's contribution to the dynamics of the system.

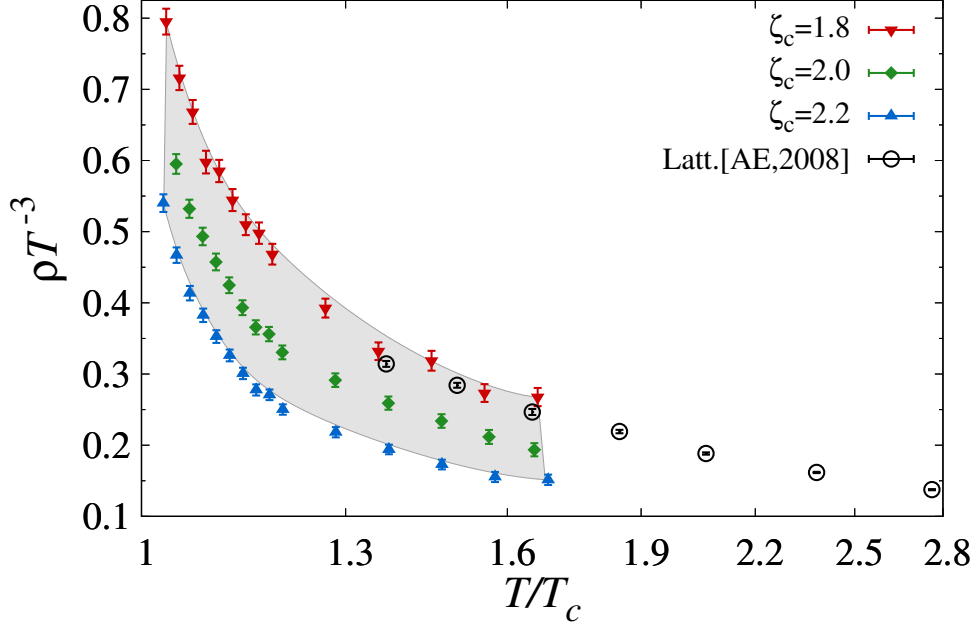


Figure 4.27: Temperature dependence of the total instanton-dyon density for different core sizes ζ_c and fixed $M_D = 3.0$, $V_c = 5$. Latt.[AE,2008] points correspond to the thermal monopole density on the lattice from [125].

4.4.2 Instanton-Dyon Density and Correlations

With the key parameters of the instanton-dyon ensemble being characterized above, we now examine its consistency with other relevant information. One such example is the density of chromo-magnetically charged objects, which in this framework is defined as the total dyonic density

$$\rho = \frac{N_M + N_L}{V}. \quad (4.62)$$

This quantity has been studied on the lattice for $SU(2)$ Yang-Mills theory and in Fig. 4.27, we compare such density from our instanton-dyon ensemble with that from a lattice calculation in [125]. As one can see, in the same parameter range for ζ_c where the confinement transition can be quantitatively described, we also see excellent agreement for the magnetic density with lattice results. It may be noted that recent phenomenological studies of jet energy loss observables and heavy flavor transport at the RHIC and LHC, provide interesting evidence for the presence of a chromo-magnetic component in the near- T_c region [126–131]. The density of magnetic charges extracted from those studies in the vicinity of T_c [131] is about $\rho T^{-3} \simeq (N_c - 1) \cdot (0.4 \sim 0.6)$, which

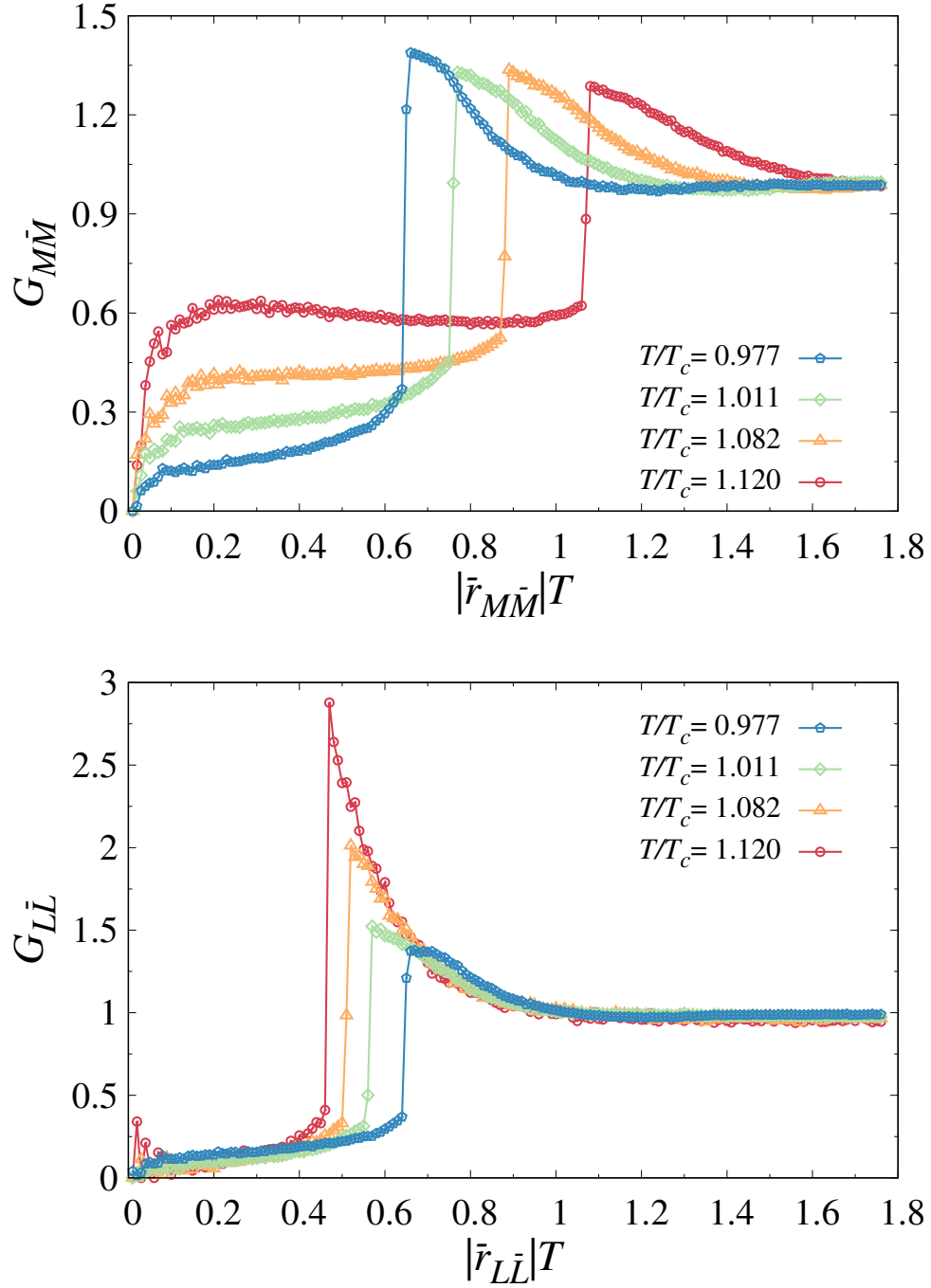


Figure 4.28: Spatial correlation functions between M - \bar{M} (top) and L - \bar{L} (bottom) pairs at different temperatures for $V_c = 5$, $M_D = 3.0$ and $\zeta_c = 2.0$.

is also in consistency with the instanton-dyon ensemble results.

Finally, we have also computed the spatial density-density correlations between dyons and antidyons in the ensemble (see Fig. 4.28). These correlations feature a typical liquid-like behavior

in the near- T_c region, with a correlation length on the order of $(0.5 \sim 1) \cdot 1/T$. Such observations, again, appear to be viable with experimental observations of the quark-gluon plasma as a nearly perfect liquid at the RHIC and LHC [132–135] and with phenomenological studies that suggest the chromo-magnetic component to play a key role in such observed transport property [126, 136, 137].

In summary, in the framework of a statistical ensemble of correlated instanton-dyons, we have presented an in-depth study of the thermodynamical properties of the deconfinement phase transition in $SU(2)$ pure gauge theory. Such objects, with non-trivial topology, not only have proven to be relevant in the qualitative description of confinement, but have successfully been able to produce quantitatively accurate results which were found in outstanding agreement with data obtained from first-principle lattice calculations. It is worth mentioning, that this work was based on an extensive numerical analysis consisting of more than 3.5 million independent Monte Carlo simulations which required over 7 million CPU hours; a task which clearly would not have been possible without the use of a high-performance parallel computing system, such as Indiana University’s Big Red II.

CHAPTER 5

FERMIONS IN THE INSTANTON-DYON ENSEMBLE

Incorporating fermions into a Yang-Mills theory constitutes the next logical step towards the study of full Quantum Chromodynamics. In this chapter, we continue our focus on the $SU(2)$ gauge group and present an analysis on how fermions in the fundamental representation are introduced in the instanton-dyon ensemble. In the first section, we will present an analytic formula for the matrix elements T_{IJ} used for the calculation of the fermion determinant. The following sections contain the details of the numerical simulations and a discussion of the results obtained for the particular case of $N_f = 1$, regarding the fermion effects in the deconfinement phase transition and their role in the chiral symmetry restoration.

5.1 THE FERMION DETERMINANT

Let us recall that the general Euclidean action of a QCD-like theory is given

$$\mathcal{S} = S_{\text{YM}} + S_F = \int d^4x \left[\frac{1}{4g^2} F_{\mu\nu}^a F_{\mu\nu}^a + \sum_{k=1}^{N_f} \psi_{(k)}^\dagger (-i\not{D} - im_k) \psi_{(k)} \right], \quad (5.1)$$

where S_{YM} is the Yang-Mills action which describes the dynamics of only color degrees of freedom and S_F is the corresponding action of the dynamical fermion fields ψ of N_f flavors. Naturally, in the particular case where the gauge group is $SU(3)$, \mathcal{S} becomes the Euclidean QCD action.

Integrating out the fermion fields in the general partition function yields

$$\begin{aligned} \mathcal{Z} &= \int \mathcal{D}A_\mu \mathcal{D}\psi \mathcal{D}\psi^\dagger e^{-S_{\text{YM}} - S_F} \\ &= \int \mathcal{D}A_\mu [\det(i\not{D} + im_k)]^{N_f} \exp \left[- \int d^4x \frac{1}{4g^2} F_{\mu\nu}^a F_{\mu\nu}^a \right], \end{aligned} \quad (5.2)$$

where we have ignored all terms associated to gauge fixing and Faddeev-Popov ghosts. The fermionic determinant can be quite difficult to compute due its non-trivial dependence on the gauge field A_μ . Nevertheless, similarly to the Instanton Liquid Model [21] (ILM), where the background field in the Dirac operator $i\mathcal{D} \equiv \gamma_\mu(\partial_\mu - iA_\mu)$ is assumed to be a superposition of self and anti-self-dual pseudoparticles, the determinant is approximated to

$$\det(i\mathcal{D} + im_{(k)}) \approx \det \hat{\mathbf{T}}, \quad (5.3)$$

by truncating the functional fermionic space to that spanned only by the zero modes. When antiperiodic boundary conditions are imposed on the fermion fields, only the L and \bar{L} dyons have zero modes with right and left chiralities, respectively¹. Hence, in the instanton-dyon ensemble, the background field in the Dirac operator is written as

$$A_\mu(x) = \sum_{i=1}^{N_L} A_\mu^L(x - x_i) + \sum_{\bar{j}=1}^{N_{\bar{L}}} A_\mu^{\bar{L}}(x - x_{\bar{j}}), \quad (5.4)$$

with \vec{x}_i and $\vec{x}_{\bar{j}}$ denoting the locations of the i^{th} and \bar{j}^{th} dyons.

In this context, $\hat{\mathbf{T}}$ is thus an $(N_L + N_{\bar{L}}) \times (N_L + N_{\bar{L}})$ matrix defined as [54]

$$\hat{\mathbf{T}} = \begin{pmatrix} K_{11} & \dots & K_{1N} & T_{1\bar{1}} & \dots & T_{1\bar{N}} \\ \vdots & \ddots & \vdots & \vdots & \ddots & \vdots \\ K_{N1} & \dots & K_{NN} & T_{N\bar{1}} & \dots & T_{N\bar{N}} \\ T_{\bar{1}1} & \dots & T_{\bar{1}N} & K_{\bar{1}\bar{1}} & \dots & K_{\bar{1}\bar{N}} \\ \vdots & \ddots & \vdots & \vdots & \ddots & \vdots \\ T_{\bar{N}1} & \dots & T_{\bar{N}N} & K_{\bar{N}\bar{1}} & \dots & K_{\bar{N}\bar{N}} \end{pmatrix}, \quad (5.5)$$

where $T_{I\bar{J}}$ is often called in the literature “*hopping matrix element*” or “*overlap matrix element*”.

¹Appendix C contains a detail derivation of the fermion zero modes in the background of instanton-dyons fields.

For ψ_I the zero mode corresponding to the I^{th} dyon, the overlap integral is²

$$T_{I\bar{J}} \equiv \int d^4x \psi_I^\dagger(x - x_I) i \not{D} \psi_{\bar{J}}(x - x_{\bar{J}}) \approx \int d^4x \psi_I^\dagger(x - x_I) i \not{\phi} \psi_{\bar{J}}(x - x_{\bar{J}}), \quad (5.6)$$

and, under the assumption of equal mass for all quark flavors,

$$K_{I\bar{J}} = im \int d^4x \psi_I^\dagger(x - x_I) \psi_{\bar{J}}(x - x_{\bar{J}}) \approx im \delta_{I\bar{J}}. \quad (5.7)$$

For the sake of simplicity, the $\hat{\mathbf{T}}$ matrix is then often written in the more compact and familiar form

$$\hat{\mathbf{T}} = \begin{pmatrix} im & T_{I\bar{J}} \\ T_{\bar{J}I} & im \end{pmatrix}. \quad (5.8)$$

The $T_{I\bar{J}}$ matrix elements are non-vanishing only between fermions of opposite chirality, which in the chiral representation will take the form

$$T_{I\bar{J}} = - \int d^4x \chi_R^\dagger \sigma_\mu^+ \partial_\mu \chi_L \quad \text{and} \quad T_{\bar{J}I} = \int d^4x \chi_L^\dagger \sigma_\mu^- \partial_\mu \chi_R. \quad (5.9)$$

As discussed in Appendix C, while examining the asymptotic behavior of the zero modes, it was found that its chirality is such that for antiperiodic boundary conditions, there is only one right-handed zero mode on the self-dual dyon L

$$\chi_R^{(L)} = \frac{\bar{v} \tanh\left(\frac{\bar{v}r}{2}\right)}{\sqrt{8\pi r \sinh(\bar{v}r)}} e^{-i\pi T x_4 n_i \tau^i} \epsilon \quad (5.10)$$

²Let us take the simple example of a dyon-antidyon pair. The total gauge field, according to Eq. (5.4), is $A_\mu = A_\mu^L + A_\mu^{\bar{L}}$, then the overlap integral will take the form

$$T_{I\bar{J}} = \int d^4x \psi_I^\dagger (i \not{\phi} + \not{A}^I + \not{A}^{\bar{J}}) \psi_{\bar{J}} = \int d^4x \psi_I^\dagger \not{A}^I \psi_{\bar{J}} = - \int d^4x (i \not{\phi} \psi_I^\dagger) \psi_{\bar{J}} = \int d^4x \psi_I^\dagger i \not{\phi} \psi_{\bar{J}},$$

where we have used the equations of motion of the zero modes $(i \not{\phi} + \not{A}^{\bar{J}}) \psi_{\bar{J}} = \psi_I^\dagger (i \not{\phi} + \not{A}^I) = 0$. When extending the calculation to arbitrary number of dyons, the cross terms of the form $\psi_I^\dagger \not{A}^K \psi_J$ with $I \neq J \neq K$, are too small and can be conveniently neglected [138]. The covariant derivative in $T_{I\bar{J}}$ can thus be approximated to an ordinary partial derivative.

and a left-handed one on the anti-self-dual \bar{L}

$$\chi_L^{(\bar{L})} = \frac{\bar{v} \tanh\left(\frac{\bar{v}r}{2}\right)}{\sqrt{8\pi r \sinh(\bar{v}r)}} e^{i\pi T x_4 n_i \tau^i} \epsilon, \quad (5.11)$$

where $\epsilon = i\tau^2$ satisfies $\epsilon\vec{\sigma}\epsilon = \vec{\sigma}^T$ and $\epsilon\vec{\sigma}^T\epsilon = \vec{\sigma}$.

Moreover, one should notice that these solutions were obtained in the hedgehog gauge which happens to be inconvenient for superimposing the dyon fields as in Eq. (5.4); therefore, we must change the gauge to the so called *stringy gauge*, where all dyons have the same asymptotics in the A_4 component. This is achieved by using the gauge transformations S_{\pm} defined in Section 3.4, rewritten here for convenience

$$\begin{aligned} S_+ &= e^{-i\frac{\phi}{2}\tau^3} e^{i\frac{\theta}{2}\tau^2} e^{i\frac{\phi}{2}\tau^3} = \begin{pmatrix} \cos\frac{\theta}{2} & \sin\frac{\theta}{2}e^{-i\phi} \\ -\sin\frac{\theta}{2}e^{i\phi} & \cos\frac{\theta}{2} \end{pmatrix}, \\ S_- &= e^{i\frac{\phi}{2}\tau^3} e^{i\frac{\theta-\pi}{2}\tau^2} e^{i\frac{\phi}{2}\tau^3} = \begin{pmatrix} \sin\frac{\theta}{2}e^{i\phi} & -\cos\frac{\theta}{2} \\ \cos\frac{\theta}{2} & \sin\frac{\theta}{2}e^{-i\phi} \end{pmatrix}, \end{aligned} \quad (5.12)$$

and the transform the zero modes of the L -dyon with S_- and S_+ for the antidyon \bar{L} . Since they satisfy the relations $S_{\pm}(n_a\tau^a)S_{\pm}^{\dagger} = \pm\tau^3$, the holonomy in this gauge is thus oriented in the third direction of color space.

Hence, the matrix elements that need to be computed are

$$\begin{aligned} T_{I\bar{J}} &= - \int d^4x \chi_R^{\dagger}(\vec{r} - \vec{r}_I) S_-^{\dagger}(\theta_I, \phi_I) \sigma_{\mu}^{+} \partial_{\mu} [S_+(\theta_{\bar{J}}, \phi_{\bar{J}}) \chi_L(\vec{r} - \vec{r}_{\bar{J}})], \\ T_{\bar{J}I} &= \int d^4x \chi_L^{\dagger}(\vec{r} - \vec{r}_{\bar{J}}) S_+^{\dagger}(\theta_{\bar{J}}, \phi_{\bar{J}}) \sigma_{\mu}^{-} \partial_{\mu} [S_-(\theta_I, \phi_I) \chi_R(\vec{r} - \vec{r}_I)]. \end{aligned} \quad (5.13)$$

To simplify the calculations, we are free to choose the frame of reference where one of the dyons sits at the origin (see Fig. 5.1). Keeping in mind that (r, θ, ϕ) are the integration variables, we then have $r_I = r$, $\theta = \theta_I$ and $\phi_I = \phi$ and the unit vector $\hat{n} = (\sin\theta \cos\phi, \sin\theta \sin\phi, \cos\theta)$. In order to properly handle the color and spinor indices, one must be careful when dealing with the spin matrices σ_{μ} and recall that they satisfy the identities $\epsilon\vec{\sigma}\epsilon = \vec{\sigma}^T$ and $\epsilon\vec{\sigma}^T\epsilon = \vec{\sigma}$. With this in mind

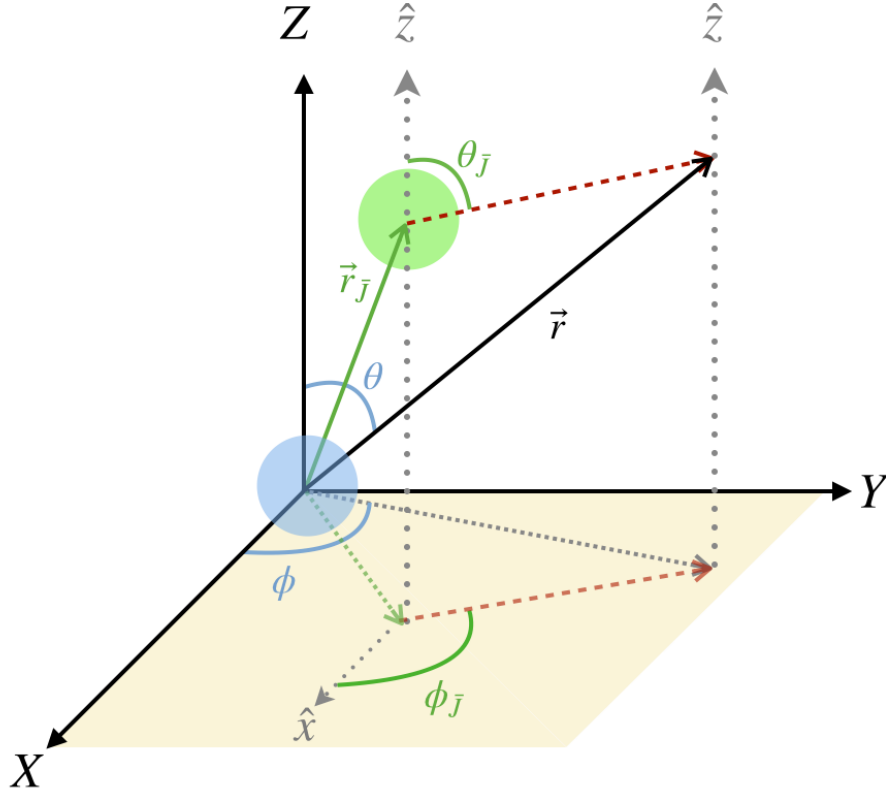


Figure 5.1: Coordinate system for the calculation of $T_{\bar{J}I}$, where \vec{r} is the observation point, $\theta_{\bar{J}}$ and $\phi_{\bar{J}}$ are the polar and azimuthal angle between the \bar{J} antidyon center and the observation point.

and defining $\gamma = \pi T x_4$, we obtain

$$\begin{aligned}
\sigma_{\mu}^{-} \partial_{\mu} [S_{-}(\theta, \phi) \chi_R(\vec{r})] &= (\sigma_{\mu}^{-})^{\alpha\beta} \partial_{\mu} \left[S_{-}^{AB} \left(\epsilon^{B\beta} \cos \gamma - i n_m (\tau^m \epsilon)^{B\beta} \sin \gamma \right) \xi \right] \\
&= \partial_{\mu} \left\{ \left[(S_{-} \epsilon \sigma_{\mu}^T)^{A\alpha} \cos \gamma - i n_m (S_{-} \tau^m \epsilon \sigma_{\mu}^T)^{A\alpha} \sin \gamma \right] \xi \right\} \\
&= i \partial_4 \left[(S_{-} \epsilon)^{A\alpha} \cos \gamma - i [S_{-} (\hat{n} \cdot \vec{\sigma}) \epsilon]^{A\alpha} \sin \gamma \right] \xi \\
&+ \partial_r \xi \left\{ [S_{-} \epsilon (\hat{n} \cdot \vec{\sigma})^T]^{A\alpha} \cos \gamma - i [S_{-} (\hat{n} \cdot \vec{\sigma}) \epsilon (\hat{n} \cdot \vec{\sigma})^T]^{A\alpha} \sin \gamma \right\}, \quad (5.14)
\end{aligned}$$

where we have used $\sigma^i \partial_i = (\hat{n} \cdot \vec{\sigma}) \partial_r$ and $\xi(r) = \bar{v} \tanh\left(\frac{\bar{v}r}{2}\right) [8\pi r \sinh(\bar{v}r)]^{-1/2}$. After some careful algebra, its explicit form is found to be

$$\sigma_{\mu}^{-} \partial_{\mu} [S_{-}(\theta, \phi) \chi_R(\vec{r})] = (\partial_r \xi - \pi T \xi) \begin{pmatrix} \cos \frac{\theta}{2} e^{i\pi T x_4} & \sin \frac{\theta}{2} e^{i(\pi T x_4 + \phi)} \\ \sin \frac{\theta}{2} e^{-i(\pi T x_4 + \phi)} & -\cos \frac{\theta}{2} e^{-i\pi T x_4} \end{pmatrix}. \quad (5.15)$$

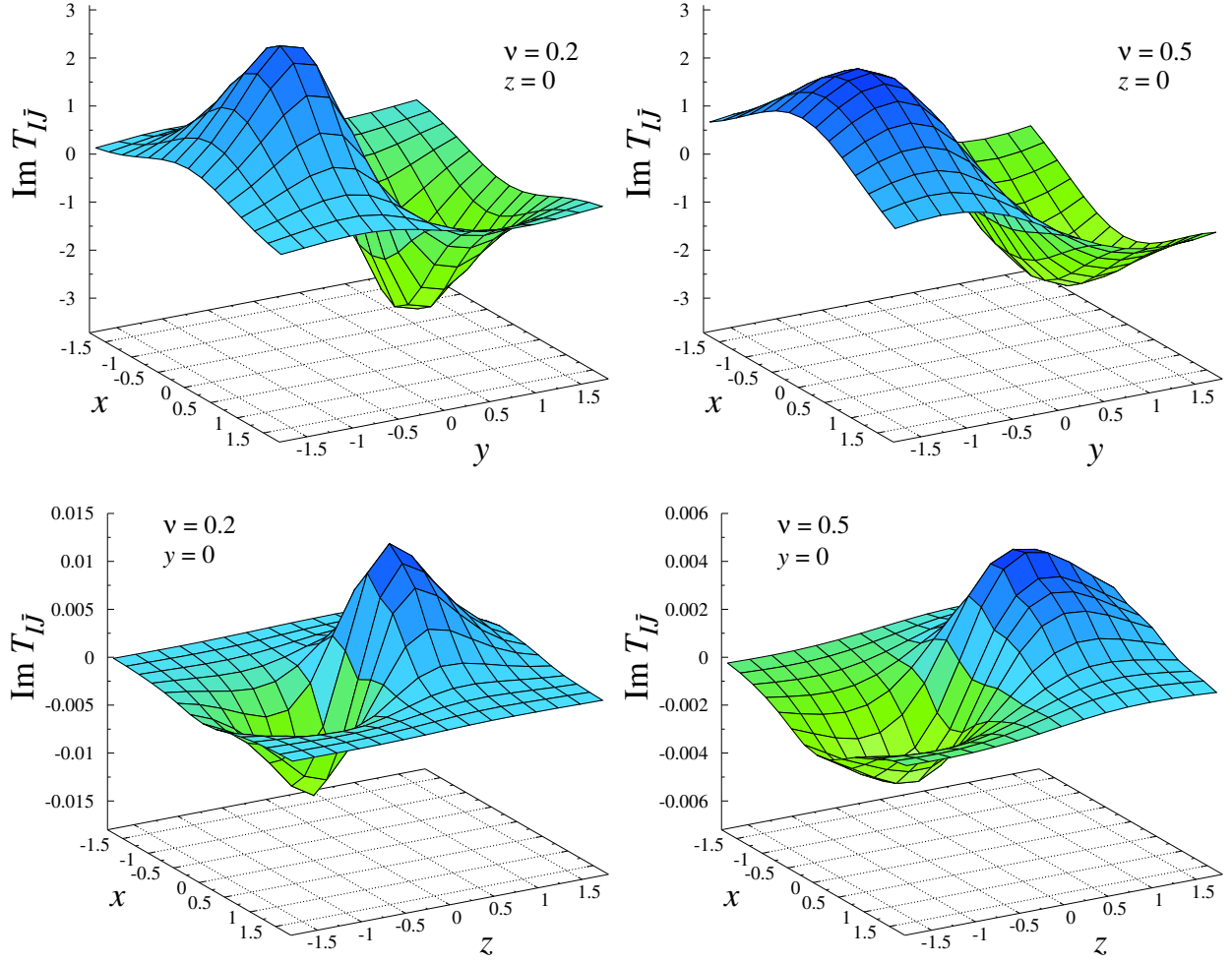


Figure 5.2: The $T_{I\bar{J}}$ matrix elements as a function of the dyon's position.

Let $t_{\bar{J}I}$ be the integrand in $T_{\bar{J}I}$, then

$$\begin{aligned}
t_{\bar{J}I} &\equiv \text{Tr} \left\{ \chi_L^\dagger (\vec{r} - \vec{r}_{\bar{J}}) S_+^\dagger(\theta_{\bar{J}}, \phi_{\bar{J}}) \sigma_\mu^- \partial_\mu [S_-(\theta, \phi) \chi_R(\vec{r})] \right\} \\
&= \frac{2e^{-i\phi_{\bar{J}}}}{T} [\partial_r \xi(r) - \pi T \xi(r)] \xi(|\vec{r} - \vec{r}_{\bar{J}}|) \left[\left(e^{2i\phi_{\bar{J}}} - 1 \right) \cos \frac{\theta}{2} \sin \frac{\theta_{\bar{J}}}{2} \right. \\
&\quad \left. - 2ie^{i\phi_{\bar{J}}} \cos \frac{\theta_{\bar{J}}}{2} \sin \frac{\theta}{2} \sin \phi \right] \\
&= 4i [\partial_r \xi(r) - \pi T \xi(r)] \xi(|\vec{r} - \vec{r}_{\bar{J}}|) \left[\cos \frac{\theta}{2} \sin \frac{\theta_{\bar{J}}}{2} \sin \phi_{\bar{J}} - \cos \frac{\theta_{\bar{J}}}{2} \sin \frac{\theta}{2} \sin \phi \right]. \quad (5.16)
\end{aligned}$$

Interestingly, not only has the temporal dependence disappeared, but we have found that $t_{\bar{J}I}$ is purely imaginary.

The integration over $t_{\bar{J}I}$ is quite intricate and requires numerical approximations. For the

general case, since $\theta_{\bar{j}}$ and $\phi_{\bar{j}}$ depend non-trivially on the integration variables θ and ϕ , the best way to do the numerical integration seems to be in Cartesian coordinates. However, as usual, one needs to be careful with the definition of the azimuthal angle $\phi = \tan^{-1}(y/x)$, since it is clearly undefined at $x = y = 0$. In Fig. 5.2 we show the numerical results as a function the dyon's position for different values of holonomy.

5.2 CONSTRUCTION OF THE INSTANTON-DYON ENSEMBLE

Similarly to what was done in Chapter 4, the general partition function Eq. (5.2) for $SU(2)$, is approximated by that of an ensemble of instanton-dyons which takes the form

$$\begin{aligned} \mathcal{Z} = & e^{-[P(\nu)+P_{\text{F}}(\nu)]V/T} \sum_{\substack{N_M, N_L, \\ N_{\bar{L}}, N_{\bar{M}}}} \frac{1}{N_L! N_M! N_{\bar{L}}! N_{\bar{M}}!} \int \prod_{l=1}^{N_L} f_L T^3 d^3 r_{L_l} \prod_{m=1}^{N_M} f_M T^3 d^3 r_{M_m} \\ & \times \prod_{\bar{l}=1}^{N_{\bar{L}}} f_{\bar{L}} T^3 d^3 r_{\bar{L}_{\bar{l}}} \prod_{\bar{m}=1}^{N_{\bar{M}}} f_{\bar{M}} T^3 d^3 r_{\bar{M}_{\bar{m}}} \det(G_D) \det(G_{\bar{D}}) \left(\det \hat{\mathbf{T}}\right)^{N_f} e^{-V_{D\bar{D}}}. \end{aligned} \quad (5.17)$$

The first thing to notice is that the exponential factor outside the integrals, now contains two functions: the already considered perturbative potential from the Yang-Mills contribution [77, 106]

$$P(\nu) = \frac{4\pi^2}{3} T^4 \nu^2 (1 - \nu)^2 \Big|_{\text{mod } 1} \quad (5.18)$$

and the new fermionic perturbative potential [139–141]

$$P_{\text{F}}(\nu) = -N_f \frac{\pi^2}{6} T^4 \left[(1 - \nu^2)^2 - 1 \right]_{\text{mod } 2}. \quad (5.19)$$

The total perturbative contribution, as shown in Fig. 5.3, is no longer symmetric under the substitution $\nu \rightarrow 1 - \nu$, an indication that the center symmetry is now broken.

The most important element for the fermion dynamics is of course $\det \hat{\mathbf{T}}$, which as we just saw, is the approximation to the full fermionic determinant coming from the functional integration of the spinor fields. The $\hat{\mathbf{T}}$ -matrix of dimension $(N_L + N_{\bar{L}}) \times (N_L + N_{\bar{L}})$ is antisymmetric³ and depends on the L and \bar{L} dyons positions.

³We only explore the case of massless fermions.

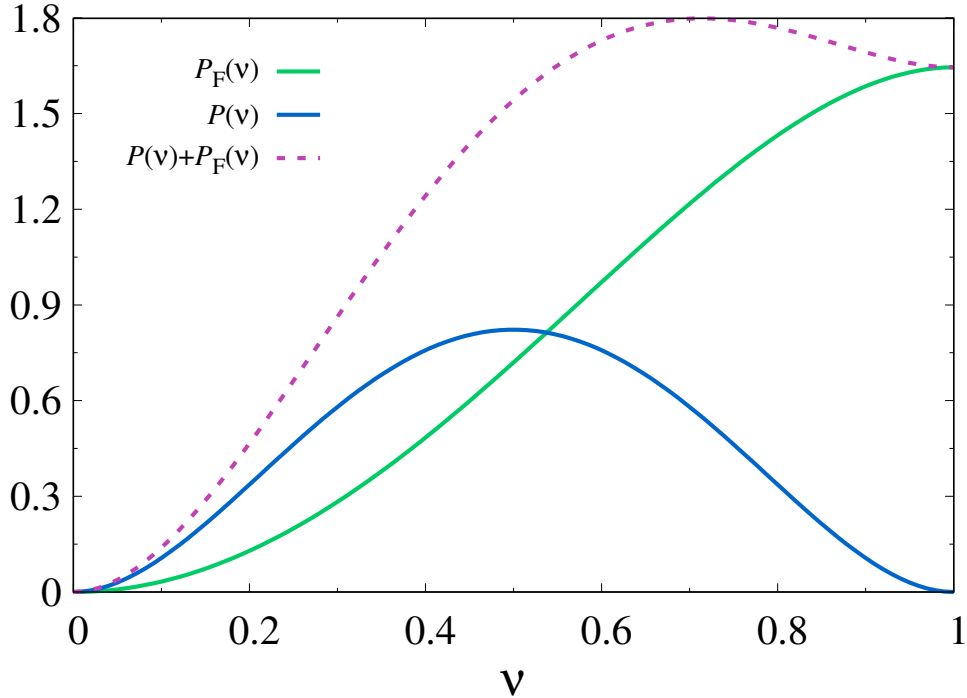


Figure 5.3: Perturbative contributions from the pure Yang-Mills fields $P(\nu)$ and from fundamental quarks $P_F(\nu)$. For the latter, $N_f = 1$ has been used.

The rest of the components in the ensemble remain the same as for the pure Yang-Mills case, namely, $\det(G_D)$ and $\det(G_{\bar{D}})$ are the many-dyon measure approximation referred to as Diakonov's determinant. The $V_{D\bar{D}}$ term regulates the classical interactions between instanton-dyons: at long distances, via a Coulomb-like potential with screening effects implemented through a Debye mass M_D (see Eq. (4.57))

$$V_{ij} = \pm \frac{S}{\pi T r_{i\bar{j}}} e^{-M_D r_{i\bar{j}}}, \quad (5.20)$$

and a short-range core-like interaction defined as

$$V_{jj}^C = \frac{\nu_j V_c}{1 + e^{(\zeta_j - \zeta_c)}}, \quad \zeta_j = 2\pi\nu_j T r_{j\bar{j}}.$$

5.3 NUMERICAL SIMULATIONS

The ensemble is once again simulated using a 3-D box with periodic boundary conditions. The definition of parameters and observables is simplified by eliminating the explicit dependence on

temperature via the rescaling $rT \rightarrow r$, $VT^3 \rightarrow V$, $M_D/T \rightarrow M_D$, and $F/T \rightarrow F$. However, there is an implicit temperature dependence controlled by the instanton action parameter S , which at one-loop level, is now N_f -dependent, and given by

$$S(T) = \left(\frac{22}{3} - \frac{2N_f}{3} \right) \log \left(\frac{T}{\Lambda} \right). \quad (5.21)$$

Therefore, analogously to the pure gauge simulations, variations in S are essentially variations in temperature.

The free energy density $F/V = -\log(\mathcal{Z})/V$, a pivotal quantity in the ensemble, is first computed at fixed number dyons N_D , holonomy ν , and integration parameter ξ , by means of a Monte Carlo simulation. The configurations are generated with the random variation of the spatial position of a single (anti)dyon of each kind, followed by the implementation of the acceptance criterion of the Metropolis-Hastings algorithm [109, 110], and then proceed to update the next set of dyon positions. Once all dyons have been swept by the algorithm, which is regarded as a single Monte Carlo configuration, the value of the free energy $F(N_D, \nu, \xi)$ is saved to be averaged afterwards. Each Monte Carlo simulation consisted of 15000 sweeps with 5000 thermalization steps and 5 of autocorrelation, leading to a total 2000 generated configurations used for averaging.

In principle, since the $T_{I\bar{J}}$ matrix elements depend explicitly on dyon positions, they should be calculated at each one of the Monte Carlo sweeps, thus prolonging substantially the required computing time. Instead, we followed the more economical approach of computing each $T_{I\bar{J}}$ independently by discretizing the 3-D volume into cells, place an $L\text{-}\bar{L}$ dyon pair in distinct cells, and using a standard low-dimensional numerical integration method, calculate the matrix element. Spanning the discretized volume will generate an array containing the dyon-antidyon positions (or cell location) and its associated $T_{I\bar{J}}$. Therefore, during the Monte Carlo simulation, the matrix elements are simply read out from the array by identifying the dyon-antidyon pair in their respective cells.

After the Monte Carlo average has been obtained, using the standard technique of thermodynamical integration (described in Section 4.1.3), the ξ parameter is integrated out and the free energy is averaged over the dyon numbers N_L and N_M .

The characteristic parameters of the ensemble used in the simulations correspond to those

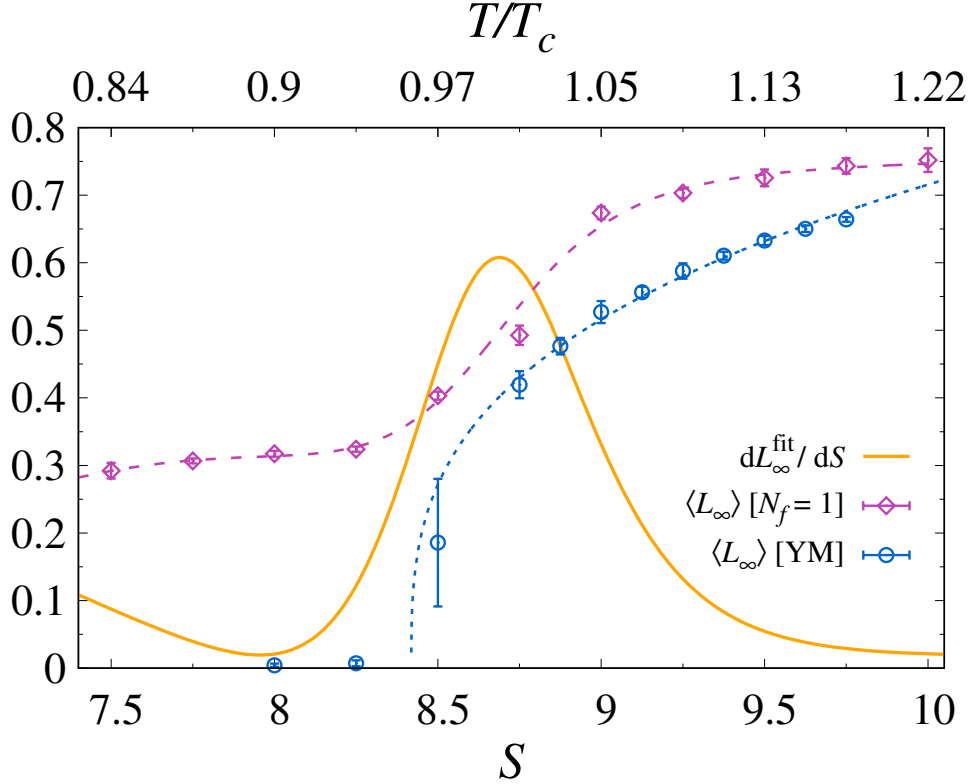


Figure 5.4: The holonomy L_∞ from the instanton-dyon ensemble with $N_f = 1$ quarks. The pure Yang-Mills points and its critical scaling fit are added for comparison.

optimized for the Yang-Mills case, namely $M_D = 3.0$, $V_c = 5.0$, and $\zeta_c = 2.0$; this will allow a direct comparison of the physical results and identify the influence of dynamical fermions in the system. We will limit this study to a single quark flavor, i.e. $N_f = 1$, and zero quark mass. In contrast with the pure gauge simulations, a larger density of L -dyons was needed, resulting in a reduced volume of $V = 30.36$ and optimal range of dyon numbers $N_L \in [2, 26]$ and $N_M \in [0, 22]$, in increments of 2.

5.3.1 Holonomy and Dyon Densities

In pure gauge theories, the confined and deconfined phases are characterized by the spontaneous breaking of center symmetry, with the Polyakov loop at spatial infinity, or holonomy, acting as the order parameter of the phase transition. However, adding dynamical quarks to such theories causes the symmetry to be explicitly broken and the phase transition becomes a rapid crossover, a phenomenon that has been observed in lattice simulations, e.g. [142].

The ensemble average of the holonomy, defined as $\langle L_\infty \rangle = \cos(\pi\nu_{\min})$ with ν_{\min} the holonomy

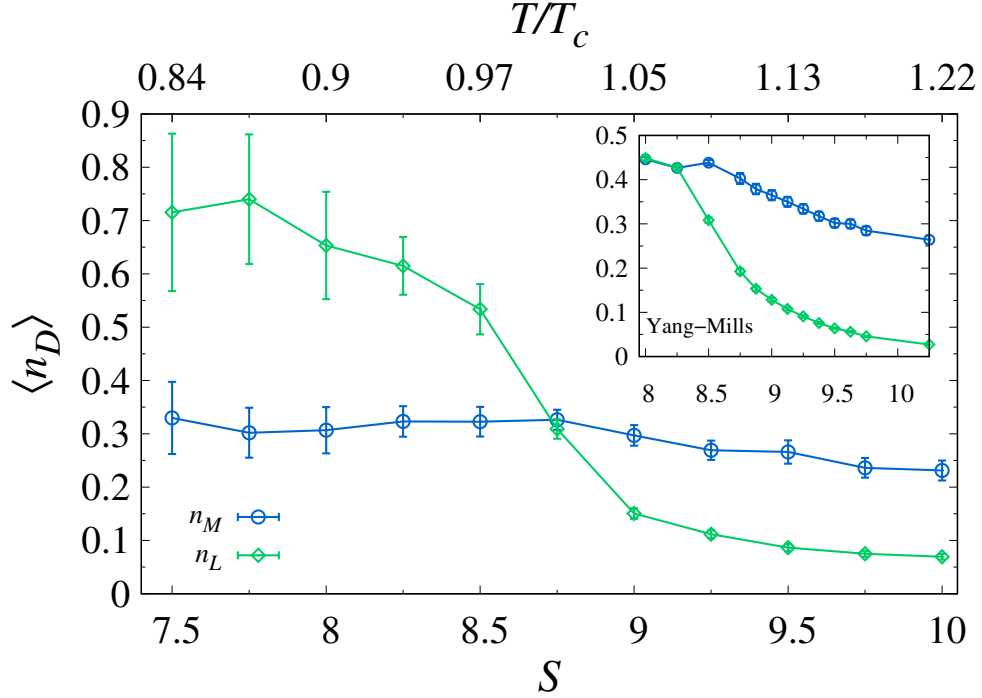


Figure 5.5: Dimensionless spatial densities of the L and M instanton-dyons. Subplot contains the Yang-Mills results from Section 4.4.1, for comparison.

parameter which minimizes the free energy density, is depicted in Fig. 5.4 as a function of the action parameter S .

As expected, L_∞ no longer behaves as an order parameter; the non-analytic phase transition observed in pure Yang-Mills (blue circles), is now a smooth crossover with a non-vanishing holonomy in the confining region of pure gauge theory. The latter is physically consistent, since a static test quark can now bind to a dynamical quark to form a meson-like system; therefore, its free energy is finite and the holonomy non-zero. Such behavior makes the definition of the critical action S_c somewhat vague; nevertheless, for the sake of completeness, we define the temperature dependence of our results by extracting a *crossover action* with a non-physical fit of the holonomy of the form

$$L_\infty^{\text{fit}} = \frac{a_1 S^3 + b_1 S^2 + c_1 S + d_1}{a_2 S^3 + b_2 S^2 + c_2 S + d_2}, \quad (5.22)$$

and simply computing its inflection point, leading to $S_c = 8.689$. The solid orange line in Fig. 5.4 is included to show such point as the local maximum of the curve. The mapping to T/T_c is then done via Eq. (5.21).

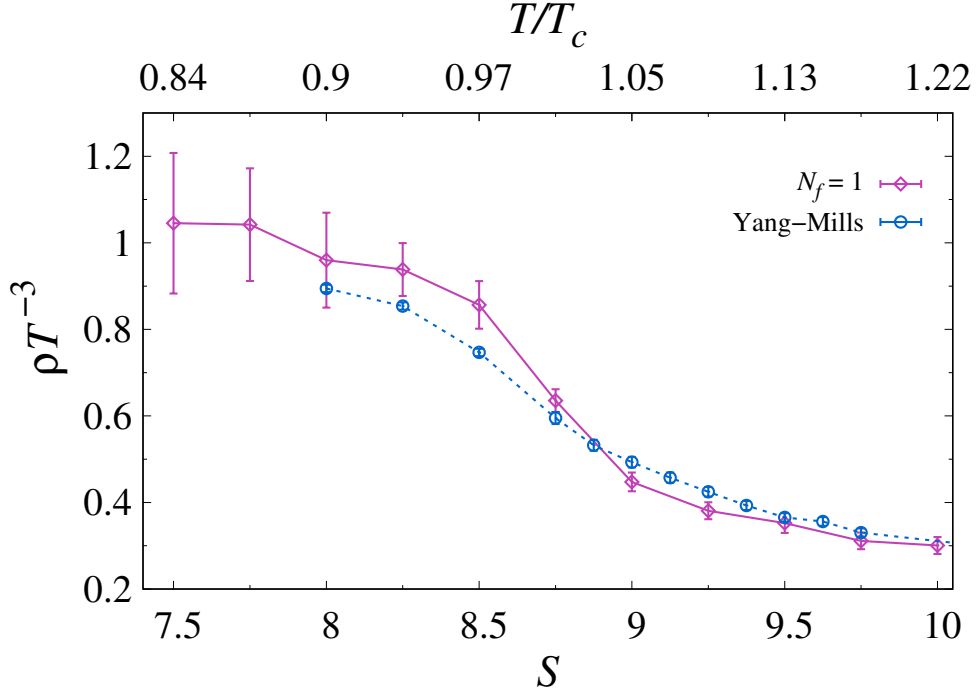


Figure 5.6: Total density of instanton-dyons for the $N_f = 1$ case and pure Yang-Mills theory.

The dyon densities, portrayed in Fig. 5.5, show an interesting difference with the Yang-Mills results. In the latter case, the dyon densities were equal in the confinement region since the holonomy, at its confining value $\nu = 1/2$, sets equal dyon sizes such that the core potential is equally likely to be triggered by any type of dyon. When fermions are added to the ensemble, the holonomy never vanishes and the dyon cores are always different between dyon kinds. Moreover, dynamical quarks contribute to the action via the fermion determinant defined in the zero-mode basis of only L -dyons (for antiperiodic fermion fields), this asymmetry seems to trigger the increase in L -dyon density in order to compensate the determinant contribution. It is quite surprising, however, how the total density $\rho T^{-3} = \langle n_L \rangle + \langle n_M \rangle$ seems to be quite similar between the two cases, in other words, the density of chromo-magnetically charged objects is found to be the same between Yang-Mills and 2-Color-QCD with a single quark flavor.

5.3.2 The Chiral Phase Transition

The state of chiral symmetry is determined by the quark condensate⁴ $\langle \bar{q}q \rangle$, which is conveniently related to the spectral density of the eigenvalues of the Dirac operator by the Banks-Casher relation [74] (see Section 2.3)

$$\langle \bar{q}q \rangle = -\pi \rho_\lambda(0), \quad (5.23)$$

where $\rho_\lambda(\lambda) = \langle \sum_n \delta(\lambda - \lambda_n) \rangle$ is the spectral density and should not be confused with the total dyon density discussed above. In the instanton-dyon ensemble, this quantity is computed at fixed dyon density and holonomy, using the optimal values which minimize the free energy density at a given action parameter S . The important features of chiral symmetry are observed in the region of near-zero eigenvalues; therefore, the simulations were set up to run 1005000 total Monte Carlo sweeps with 5000 of thermalization. Autocorrelation effects were avoided by saving configurations every 100 steps. The goal was to obtain a total of 5000 eigenvalues in the range $0 \leq \lambda \leq 1$.

Our results are presented in Fig. 5.7 for different temperatures, namely, different action parameters. We only show the positive eigenvalues since $\rho_\lambda(\lambda) = \rho_\lambda(-\lambda)$. The normalization was chosen such that $\int_0^1 d\lambda \rho_\lambda(\lambda) = 1$. The first thing to notice is that the behavior of the eigenvalue distribution is relatively similar among the range $7.5 \leq S \leq 8.5$: the spectral density appears to have a near-linear rise as the eigenvalues become smaller, then at $\lambda \approx 0.2$, a rapid fall-off yields to a vanishing ρ_λ at $\lambda = 0$. Such steep drop is attributable to finite volume effects since the lowest eigenvalues are bounded from below by $\lambda \propto 1/V$ [40, 42].

The famous result by Smilga and Stern [143], which gives the approximate slope of the spectral density near zero eigenvalues, namely

$$\rho_\lambda(\lambda) = -\frac{\langle \bar{q}q \rangle}{\pi} + \frac{N_f^2 - 4}{32\pi^2 N_f} \left(\frac{\langle \bar{q}q \rangle}{F_\pi^2} \right)^2 |\lambda| + \mathcal{O}(\lambda) \quad (5.24)$$

is derived under the assumption that $N_f \geq 2$; however, an analytic continuation of the above formula [144] will result in a negative slope just as the one observed in our results for $0.2 \lesssim \lambda \leq 1$,

⁴We use here the standard notation found in the literature, defining the Euclidean quark condensate as $\langle \bar{q}q \rangle = \langle \psi^\dagger \psi \rangle$.

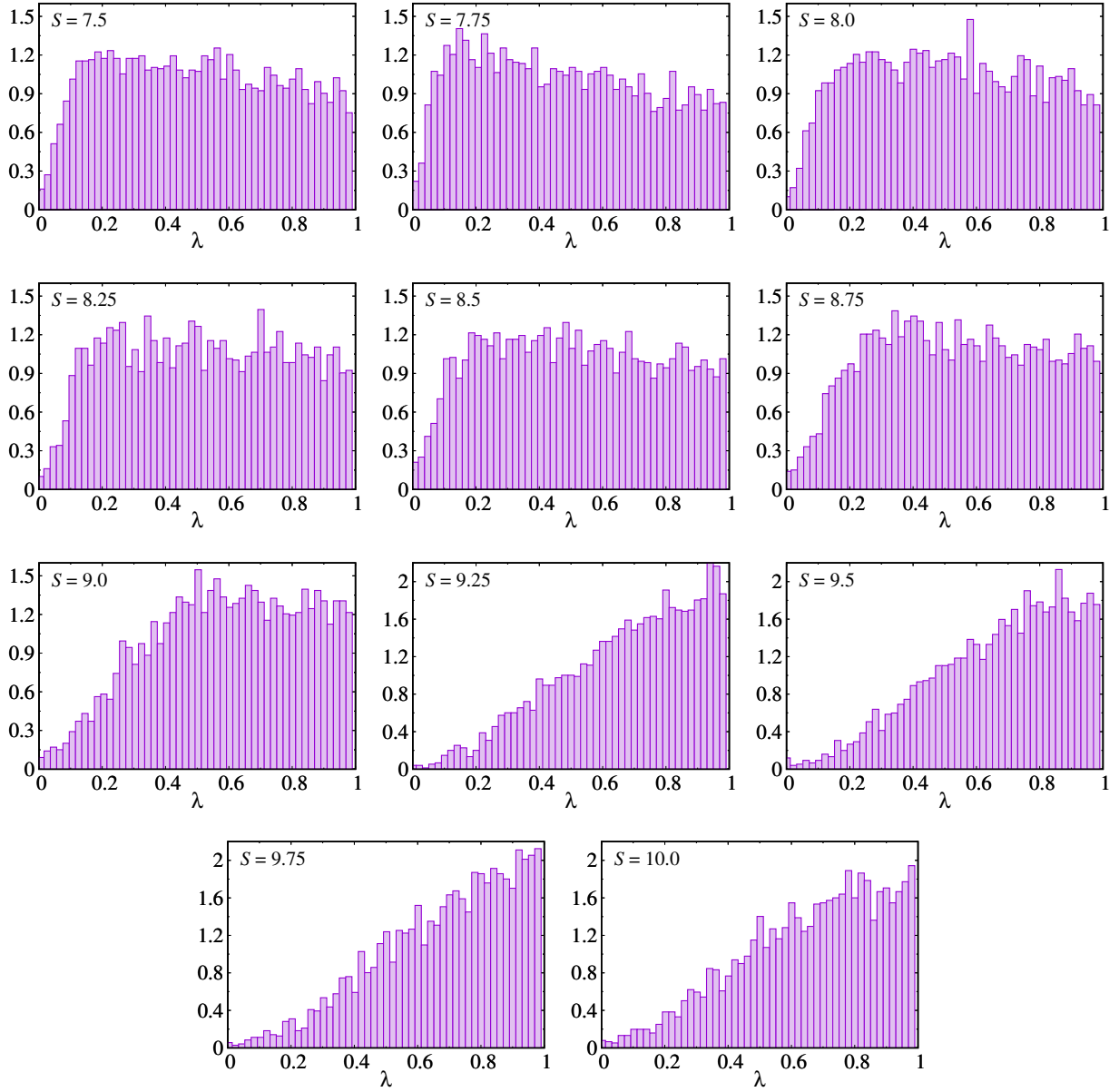


Figure 5.7: Normalized distribution of the positive eigenvalues of the Dirac operator, ρ_λ , in the near-zero region.

a feature that was also verified in instanton liquid model simulations [145, 146].

For $S \geq 8.75$, the shape of the spectral density is observed to start changing until, above $S = 9.25$, the almost vanishing of ρ_λ as $\lambda \rightarrow 0$ is no longer a finite size effect, but likely a signal that chiral symmetry is being restored. In Fig. 5.8, we plot the full range of eigenvalues generated with the purpose of showing, in a qualitative way and without clear volume effects, the overall change in the spectral density pointing towards a possible restoration of the chiral symmetry.

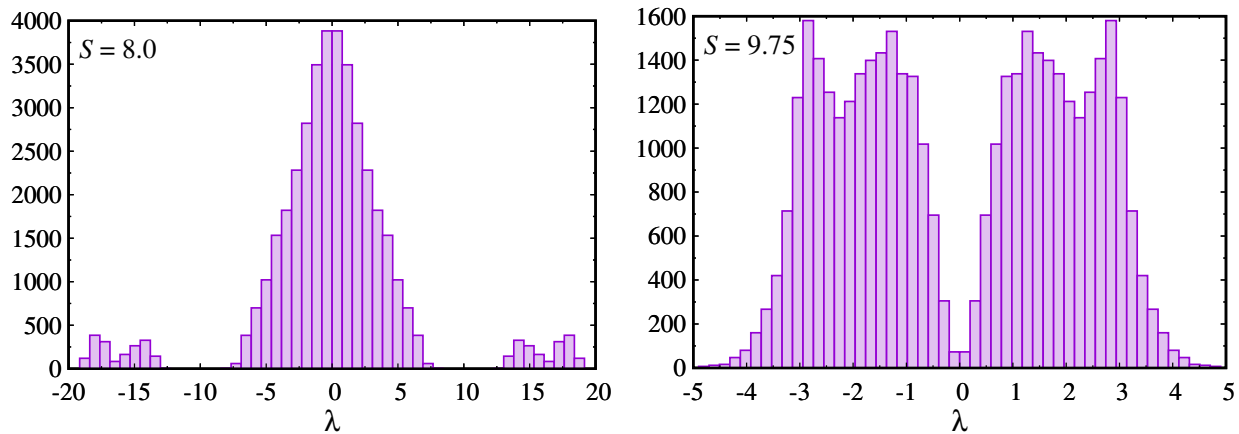


Figure 5.8: Full range of the eigenvalue distribution of the Dirac operator.

5.4 SUMMARY AND DISCUSSION

In this chapter we have presented a qualitative analysis of the instanton-dyon ensemble with $N_f = 1$ quarks. As observed by the calculated holonomy, there is no longer a deconfinement phase transition; rather a smooth crossover. It is quite interesting that, at the available precision, the dyon density plot showed a similar inflection point around the crossover action $S_c = 8.689$ extracted from the holonomy. Moreover, the qualitative behavior of the spectral density also has a clear change at $S = 8.75$ where $\rho_\lambda \rightarrow 0$ as $\lambda \rightarrow 0$. All this suggests that deconfinement and chiral restoration crossovers, happen around the same temperature. The crossover behavior has also been encountered in analytical approximations of instanton models such as in [147].

Finally, one should notice that for $N_f = 1$ there is no spontaneous symmetry breaking, the only chiral symmetry left is the axial $U_A(1)$ which is always broken by the anomaly and there are no Nambu-Goldstone bosons in the theory. In spite of not seeing a clear vanishing of the quark condensate, i.e., there is no gap in the eigenvalue spectrum near $\lambda = 0$, our results may point to a slow restoration of the axial symmetry at high enough temperature, a phenomenon which has recently spiked some interest in lattice studies of QCD with $N_f \geq 2$ [148, 149].

CHAPTER 6

CONCLUSIONS

The understanding of the confining mechanism in non-Abelian gauge theories has been a difficult challenge through out history due to its non-perturbative nature. For a while, it has been suggested that topological non-trivial gauge configurations are responsible for such phenomenon but none of the available configurations at the time had the required mathematical properties to back that statement. The discovery of the KvBLL caloron solution with non-trivial holonomy, whose unique feature of having instanton-dyons as constituent fields, have provided a concrete and promising path of study. In what constitutes the first part of this work, we have constructed a statistical ensemble of the aforementioned instanton-dyons and performed a series of sophisticated numerical simulations to study a wide range of properties of $SU(2)$ Yang-Mills theory at finite temperature. The overall conclusion is that various characteristic features of the confinement dynamics can be reproduced with such an ensemble, namely, the temperature evolution of the holonomy potential, the critical behavior of the order parameter (expectation value of the Polyakov loop) characterizing the second order nature of the deconfinement phase transition, the linear rising quark-antiquark potential at large separations, and the area law of spatial Wilson Loops. Finite volume effects and the influence of the free parameters of the ensemble were thoroughly investigated with the Debye screening mass and the short-range interaction playing a crucial role for the accurate description of physical observables. The optimization of such parameters have allowed the model to quantitatively describe, for the first time, lattice data with satisfactory accuracy, such as the temperature dependance of the order parameter and the total chromo-magnetic charge density.

In the second part, the ensemble was modified to include one-flavor quarks. The fermionic interaction was introduced via the matrix elements T_{IJ} , which were fully computed without approximations. The conclusion here is that the deconfinement second order phase transition becomes

a smooth crossover in the presence of quarks, having a non-vanishing holonomy even at the lowest temperatures explored. We also computed the spectral density of the Dirac operator, since it is intimately related to the order parameter of the chiral phase transition. In a qualitative fashion, we were able to appreciate a chiral crossover, which is in agreement with instanton model results, happening around the same temperature as the deconfinement one.

The success in reproducing the confinement features of pure gauge $SU(2)$, naturally suggests to extend this work to $SU(3)$ and verify the validity of the ensemble by comparing them once again with the available lattice data. The fermion study, must be explored in depth, by first investigating the flavor number dependence, which arguably defines the critical properties of the chiral phase transition, and then move on to higher rank gauge groups. An interesting property that this framework might allow to examine is the phenomena related to magnetic catalysis, namely, how the chiral phase transition changes in the presence of strong magnetic fields. This is just an example of how this approach may be extended to study further phenomenological properties of QCD and perhaps provide more satisfying answers to the remaining unsolved questions.

APPENDIX A

TOPOLOGICAL CHARGE

In this appendix, we will show that the topological charge Q_T of a Yang-Mills field $A_\mu(x)$ is defined as

$$Q_T = \frac{1}{16\pi^2} \int d^4x \operatorname{Tr} F_{\mu\nu} \tilde{F}_{\mu\nu}. \quad (\text{A.1})$$

We begin by examining the integrand and rewriting it using the fact that the dual strength tensor satisfies the equation of motion $D_\mu \tilde{F}_{\mu\nu} = \partial_\mu \tilde{F}_{\mu\nu} - i[A_\mu, \tilde{F}_{\mu\nu}] = 0$, therefore

$$\begin{aligned} \operatorname{Tr} F_{\mu\nu} \tilde{F}_{\mu\nu} &= \operatorname{Tr} \left\{ (\partial_\mu A_\nu - \partial_\nu A_\mu) \tilde{F}_{\mu\nu} - i(A_\mu A_\nu - A_\nu A_\mu) \tilde{F}_{\mu\nu} \right\} \\ &= \operatorname{Tr} \left\{ (\partial_\mu A_\nu - \partial_\nu A_\mu) \tilde{F}_{\mu\nu} - iA_\mu [A_\nu, \tilde{F}_{\mu\nu}] \right\} \\ &= \operatorname{Tr} \left\{ (\partial_\mu A_\nu - \partial_\nu A_\mu) \tilde{F}_{\mu\nu} - A_\mu \partial_\nu \tilde{F}_{\mu\nu} \right\} \\ &= \operatorname{Tr} \left\{ (\partial_\mu A_\nu) \tilde{F}_{\mu\nu} - \partial_\nu (A_\mu \tilde{F}_{\mu\nu}) \right\}. \end{aligned} \quad (\text{A.2})$$

Making use of the antisymmetry of $\varepsilon_{\mu\nu\alpha\beta}$ and the cyclic property of the trace, it is straight forward to obtain the following identities

$$\tilde{F}_{\mu\nu} \equiv \frac{1}{2} \varepsilon_{\mu\nu\alpha\beta} F_{\alpha\beta} = \varepsilon_{\mu\nu\alpha\beta} (\partial_\alpha A_\beta - iA_\alpha A_\beta), \quad (\text{A.3})$$

and

$$\begin{aligned} \operatorname{Tr} \{ \varepsilon_{\mu\nu\alpha\beta} \partial_\mu (A_\nu A_\alpha A_\beta) \} &= \operatorname{Tr} \{ \varepsilon_{\mu\nu\alpha\beta} [(\partial_\mu A_\nu) A_\alpha A_\beta + (\partial_\mu A_\alpha) A_\beta A_\nu + (\partial_\mu A_\beta) A_\nu A_\alpha] \} \\ &= 3 \operatorname{Tr} \{ \varepsilon_{\mu\nu\alpha\beta} (\partial_\mu A_\nu) A_\alpha A_\beta \}, \end{aligned} \quad (\text{A.4})$$

which allow to write the integrand as a total derivative of the form

$$\begin{aligned}
\text{Tr } F_{\mu\nu} \tilde{F}_{\mu\nu} &= \text{Tr} \{ \varepsilon_{\mu\nu\alpha\beta} [(\partial_\mu A_\nu)(\partial_\alpha A_\beta - i A_\alpha A_\beta) - \partial_\nu(A_\mu \partial_\alpha A_\beta - i A_\mu A_\alpha A_\beta)] \} \\
&= \text{Tr} \{ \varepsilon_{\mu\nu\alpha\beta} [\partial_\mu(A_\nu \partial_\alpha A_\beta) - i(\partial_\mu A_\nu) A_\alpha A_\beta + \partial_\mu(A_\nu \partial_\alpha A_\beta - i A_\nu A_\alpha A_\beta)] \} \\
&= \text{Tr} \left\{ \varepsilon_{\mu\nu\alpha\beta} \left[\partial_\mu(A_\nu \partial_\alpha A_\beta) - \frac{i}{3} \partial_\mu(A_\nu A_\alpha A_\beta) + \partial_\mu(A_\nu \partial_\alpha A_\beta - i A_\nu A_\alpha A_\beta) \right] \right\} \\
&= \partial_\mu \text{Tr} \left\{ 2\varepsilon_{\mu\nu\alpha\beta} \left(A_\nu \partial_\alpha A_\beta - \frac{2}{3} i A_\nu A_\alpha A_\beta \right) \right\}. \tag{A.5}
\end{aligned}$$

The definition of Q_T is thus rewritten as

$$Q_T = \frac{1}{16\pi^2} \int d^4x \text{Tr } F_{\mu\nu} \tilde{F}_{\mu\nu} = \int d^4x \partial_\mu K_\mu, \tag{A.6}$$

where

$$K_\mu \equiv \frac{1}{8\pi^2} \varepsilon_{\mu\nu\alpha\beta} \text{Tr} \left\{ A_\nu \partial_\alpha A_\beta - \frac{2}{3} i A_\nu A_\alpha A_\beta \right\} \tag{A.7}$$

is called the *Chern-Simmons current*¹. According to Gauss' Theorem, the volume integral over the 4-dimensional Euclidean space is equal to the surface integral of the K_μ current over the boundary surface S_E^3 , that is

$$Q_T = \oint_{S_E^3} ds_\mu K_\mu. \tag{A.8}$$

As it is mentioned on Section 3.1, the boundary condition on the gauge field A_μ , demands it to behave as a pure gauge configuration along the surface S_E^3 , leading to a vanishing $F_{\mu\nu}$, thereby,

¹Just for the sake of completeness, we notice that using $\text{Tr } t^a t^b = \delta^{ab}/2$ and $\text{Tr } t^a t^b t^c = i\varepsilon^{abc}/4$, K_μ can be easily expressed in terms of color components as

$$K_\mu = \frac{1}{16\pi^2} \varepsilon_{\mu\nu\alpha\beta} \left(A_\nu^a \partial_\alpha A_\beta^a + \frac{1}{3} \varepsilon^{abc} A_\nu^a A_\alpha^b A_\beta^c \right).$$

from Eq. (A.3) we have that $\varepsilon_{\mu\nu\alpha\beta}\partial_\alpha A_\beta = i\varepsilon_{\mu\nu\alpha\beta}A_\alpha A_\beta$ and so

$$\begin{aligned}
Q_T &= \frac{i}{24\pi^2} \oint_{S_E^3} ds_\mu \varepsilon_{\mu\nu\alpha\beta} \text{Tr} \{A_\nu A_\alpha A_\beta\} \\
&= \frac{1}{24\pi^2} \oint_{S_E^3} ds_\mu \varepsilon_{\mu\nu\alpha\beta} \text{Tr} \left\{ \left(U \partial_\nu U^\dagger \right) \left(U \partial_\alpha U^\dagger \right) \left(U \partial_\beta U^\dagger \right) \right\} \\
&= -\frac{1}{24\pi^2} \oint_{S_E^3} ds_\mu \varepsilon_{\mu\nu\alpha\beta} \text{Tr} \left\{ U^\dagger (\partial_\nu U) U^\dagger (\partial_\alpha U) U^\dagger (\partial_\beta U) \right\}. \tag{A.9}
\end{aligned}$$

The topological charge Q_T thus only depends on the gauge group element U evaluated on S_E^3 . This suggests that the integration above can be carried out over group space, so we must find the measure of the group; formally speaking, the measure for the manifold of the group, known as *Haar Measure* (see [80, 150]).

In general, the measure is denoted by $d\mu(U)$. Since U can be expressed in terms of a set of parameters $\{\xi_i\}$, then $d\mu(U)$ will be an integration over the ξ_i 's multiplied by a weighting function $\rho(\xi_i)$ which leaves the measure invariant under the group algebra, in the sense that for V also an element of the group, then for $U' = VU$

$$d\mu(U) \equiv \rho(\xi_1, \dots, \xi_m) d\xi_1 \dots d\xi_m = d\mu(U') = \rho(\xi'_1, \dots, \xi'_m) d\xi'_1 \dots d\xi'_m. \tag{A.10}$$

In the specific case of $SU(2)$; let us notice that another way of parametrizing $S_{SU(2)}^3$ is by using a set of three Euler angles, which by obvious reasons will be denoted as (ξ_1, ξ_2, ξ_3) . And propose as weighting function for the Haar measure

$$\rho(\xi_1, \xi_2, \xi_3) = \varepsilon_{ijk} \text{Tr} \left\{ U^\dagger \frac{\partial U}{\partial \xi_i} U^\dagger \frac{\partial U}{\partial \xi_j} U^\dagger \frac{\partial U}{\partial \xi_k} \right\}, \tag{A.11}$$

which we can see it satisfies Eq. (A.10) by taking once again V as a fixed group element, such that

$$U(\xi_1, \xi_2, \xi_3) \rightarrow U'(\xi'_1, \xi'_2, \xi'_3) = VU(\xi_1, \xi_2, \xi_3) \implies \begin{aligned} U &= V^\dagger U', \\ U^\dagger &= U'^\dagger V. \end{aligned} \tag{A.12}$$

Substituting these into Eq. (A.11) yields

$$\begin{aligned}\rho(\xi_1, \xi_2, \xi_3) &= \varepsilon_{ijk} \text{Tr} \left\{ U'^{\dagger} V V^{\dagger} \frac{\partial U'}{\partial \xi'_l} \frac{\partial \xi'_l}{\partial \xi_i} U'^{\dagger} V V^{\dagger} \frac{\partial U'}{\partial \xi'_m} \frac{\partial \xi'_m}{\partial \xi_j} U'^{\dagger} V V^{\dagger} \frac{\partial U'}{\partial \xi'_n} \frac{\partial \xi'_n}{\partial \xi_k} \right\} \\ &= \varepsilon_{ijk} \frac{\partial \xi'_l}{\partial \xi_i} \frac{\partial \xi'_m}{\partial \xi_j} \frac{\partial \xi'_n}{\partial \xi_k} \text{Tr} \left\{ U'^{\dagger} \frac{\partial U'}{\partial \xi'_l} U'^{\dagger} \frac{\partial U'}{\partial \xi'_m} U'^{\dagger} \frac{\partial U'}{\partial \xi'_n} \right\}.\end{aligned}\quad (\text{A.13})$$

However, since the Jacobian determinant of the transformation $\vec{\xi}' \rightarrow \vec{\xi}$ is given by

$$\det \left| \frac{\partial \vec{\xi}'}{\partial \vec{\xi}} \right| \equiv \frac{1}{6} \varepsilon_{ijk} \varepsilon_{lmn} \frac{\partial \xi'_l}{\partial \xi_i} \frac{\partial \xi'_m}{\partial \xi_j} \frac{\partial \xi'_n}{\partial \xi_k} \implies \varepsilon_{lmn} \det \left| \frac{\partial \vec{\xi}'}{\partial \vec{\xi}} \right| = \varepsilon_{ijk} \frac{\partial \xi'_l}{\partial \xi_i} \frac{\partial \xi'_m}{\partial \xi_j} \frac{\partial \xi'_n}{\partial \xi_k}.\quad (\text{A.14})$$

And since

$$d\xi_1 d\xi_2 d\xi_3 = \det \left| \frac{\partial \vec{\xi}'}{\partial \vec{\xi}} \right| d\xi'_1 d\xi'_2 d\xi'_3,\quad (\text{A.15})$$

the weighting function takes the form

$$\begin{aligned}\rho(\xi_1, \xi_2, \xi_3) &= \varepsilon_{lmn} \text{Tr} \left\{ U'^{\dagger} \frac{\partial U'}{\partial \xi'_l} U'^{\dagger} \frac{\partial U'}{\partial \xi'_m} U'^{\dagger} \frac{\partial U'}{\partial \xi'_n} \right\} \det \left| \frac{\partial \vec{\xi}'}{\partial \vec{\xi}} \right| \\ &= \rho(\xi'_1, \xi'_2, \xi'_3) \det \left| \frac{\partial \vec{\xi}'}{\partial \vec{\xi}} \right|.\end{aligned}\quad (\text{A.16})$$

Therefore,

$$\rho(\xi_1, \xi_2, \xi_3) d\xi_1 d\xi_2 d\xi_3 = \rho(\xi'_1, \xi'_2, \xi'_3) d\xi'_1 d\xi'_2 d\xi'_3.\quad (\text{A.17})$$

Once the group measure has been defined, we want to express Q_{T} as an integral over group space. This is achieved by transferring the spatial dependence of $U(x)$ to the set of parameters ξ_i , such that $U(x) = U(\xi_1(x), \xi_2(x), \xi_3(x))$. Eq. (A.9) thus takes the form

$$Q_{\text{T}} = -\frac{1}{24\pi^2} \oint_{S_E^3} ds_{\mu} \varepsilon_{\mu\nu\alpha\beta} \text{Tr} \left\{ U'^{\dagger} \frac{\partial U}{\partial \xi_i} U'^{\dagger} \frac{\partial U}{\partial \xi_j} U'^{\dagger} \frac{\partial U}{\partial \xi_k} \right\} \frac{\partial \xi_i}{\partial x_{\nu}} \frac{\partial \xi_j}{\partial x_{\alpha}} \frac{\partial \xi_k}{\partial x_{\beta}}.\quad (\text{A.18})$$

The integral is easier to calculate by taking the Gaussian surface S_E^3 as an infinite hypercube, since it is written in Cartesian coordinates x_{μ} . The integral will split into 8, corresponding to the integration on the surface of each one of the 8 sides of the hypercube. Let us take, the side located

at $x_4 = \infty$. Its contribution to Q_T is given by

$$\begin{aligned}
& -\frac{1}{24\pi^2} \int dx_1 dx_2 dx_3 \varepsilon_{lmn} \text{Tr} \left\{ U^\dagger \frac{\partial U}{\partial \xi_i} U^\dagger \frac{\partial U}{\partial \xi_j} U^\dagger \frac{\partial U}{\partial \xi_k} \right\} \frac{\partial \xi_i}{\partial x_l} \frac{\partial \xi_j}{\partial x_m} \frac{\partial \xi_k}{\partial x_n} \\
& = -\frac{1}{24\pi^2} \int d\xi_1 d\xi_2 d\xi_3 \varepsilon_{ijk} \text{Tr} \left\{ U^\dagger \frac{\partial U}{\partial \xi_i} U^\dagger \frac{\partial U}{\partial \xi_j} U^\dagger \frac{\partial U}{\partial \xi_k} \right\} \\
& = -\frac{1}{24\pi^2} \int d\xi_1 d\xi_2 d\xi_3 \rho(\xi_1, \xi_2, \xi_3) \\
& = -\frac{1}{24\pi^2} \int d\mu(U), \tag{A.19}
\end{aligned}$$

where Eq. (A.14) and Eq. (A.15) have been used.

Since the contributions from all sides of the hypercube are equal, we conclude that the topological charge is

$$Q_T \propto \int d\mu(U), \tag{A.20}$$

i.e. is the integral of the group measure over the group space. This means, as pointed out by Rajaraman in [80], that Q_T is proportional to the volume of group space spanned by U as it varies on S_E^3 . Homotopy theory tells us that when we integrate over S_E^3 once, the group manifold $S_{\text{SU}(2)}^3$ may be spanned some integer number of times and that number is Q_T . The proportionality constant, is chosen such that $Q_T \in \mathbb{Z}$.

It is important to mention that since the quantity $\text{Tr} F_{\mu\nu} \tilde{F}_{\mu\nu}$ is gauge invariant, therefore Q_T must be as well.

APPENDIX B

PROPERTIES OF 'T HOOFT SYMBOLS.

$$\eta_{\mu\nu}^a = \begin{cases} \varepsilon_{\mu\nu}^a & \mu, \nu = 1, 2, 3, \\ -\delta_\nu^a & \mu = 4, \\ \delta_\mu^a & \nu = 4, \\ 0 & \mu = \nu = 4. \end{cases} \quad (\text{B.1})$$

$$\eta_{\mu\nu}^a \eta_{\mu\nu}^b = 4\delta^{ab} \quad (\text{B.2})$$

$$\eta_{\mu\nu}^a \eta_{\mu\alpha}^a = 3\delta_{\nu\alpha} \quad (\text{B.3})$$

$$\eta_{\mu\nu}^a \eta_{\mu\nu}^a = 12 \quad (\text{B.4})$$

$$\eta_{\mu\nu}^a \eta_{\alpha\beta}^a = \delta_{\mu\alpha} \delta_{\nu\beta} - \delta_{\mu\beta} \delta_{\nu\alpha} + \varepsilon_{\mu\nu\alpha\beta} \quad (\text{B.5})$$

$$\eta_{\mu\nu}^a \eta_{\mu\alpha}^b = \delta^{ab} \delta_{\nu\alpha} + \varepsilon^{abc} \eta_{\nu\alpha}^c \quad (\text{B.6})$$

$$\varepsilon_{\mu\nu\alpha\gamma} \eta_{\beta\gamma}^a = \delta_{\beta\mu} \eta_{\nu\alpha}^a - \delta_{\beta\nu} \eta_{\mu\alpha}^a + \delta_{\alpha\beta} \eta_{\mu\nu}^a \quad (\text{B.7})$$

$$\varepsilon^{abc} \eta_{\mu\nu}^b \eta_{\alpha\beta}^c = \delta_{\mu\alpha} \eta_{\nu\beta}^a - \delta_{\mu\beta} \eta_{\nu\alpha}^a - \delta_{\nu\alpha} \eta_{\mu\beta}^a + \delta_{\nu\beta} \eta_{\mu\alpha}^a \quad (\text{B.8})$$

$$\eta_{\mu\nu}^a \bar{\eta}_{\mu\beta}^b = \eta_{\mu\beta}^a \bar{\eta}_{\mu\alpha}^b \quad (\text{B.9})$$

$$\eta_{\mu\nu}^a \bar{\eta}_{\mu\nu}^b = 0 \quad (\text{B.10})$$

The dual tensor $\bar{\eta}_{\mu\nu}^a$ satisfies the same relations with the only exception that the substitution $\varepsilon_{\mu\nu\rho\sigma} \rightarrow -\varepsilon_{\mu\nu\rho\sigma}$ has to be made when applicable.

APPENDIX C

FERMION ZERO MODES

The fermion zero modes are defined as the solutions to the differential equation

$$i\mathcal{D}\psi = 0, \tag{C.1}$$

with $i\mathcal{D} = \gamma_\mu (\partial_\mu - iA_\mu)$ the Dirac operator defined in the background of the gauge field A_μ .

Our goal here is to derive the zero modes in the background of the instanton-dyon fields, which in the *hedgehog gauge* are given by (see Sections 3.4 and 3.5)

$$\begin{aligned} A_4^{M,\bar{M}} &= H(r)n_a \frac{\tau^a}{2}, & H(r) &\equiv \pm \left(\frac{1}{r} - v \coth(vr) \right) \\ A_i^{M,\bar{M}} &= \mathcal{A}(r)\varepsilon_{aij}n_j \frac{\tau^a}{2}, & \mathcal{A}(r) &\equiv \frac{1}{r} - \frac{v}{\sinh(vr)} \end{aligned} \tag{C.2}$$

where $n_a = x_a/r$ and the (lower)upper sign corresponds to the (anti)self-dual solution. We take the Euclidean Dirac matrices in the chiral representation as

$$\gamma_\mu = \begin{pmatrix} 0 & -i\sigma_\mu^- \\ i\sigma_\mu^+ & 0 \end{pmatrix}, \quad \text{with} \quad \sigma_\mu^\pm = (\vec{\sigma}, \mp i), \tag{C.3}$$

such that, in the chiral basis, we may write the time dependent spinor field in terms of its left and right-handed components as $\psi(\vec{r}, x_4) = (\chi_L, \chi_R)^T \exp(-i\omega x_4)$. The antiperiodic boundary condition for physical fermions, constraints the Matsubara frequencies to $\omega = (2N + 1)\pi T$, for $N \in \mathbb{N}$. Consequently, Eq. (C.1) splits into two independent set of equations, namely Weyl equations,

corresponding to the right and left-handed components

$$\begin{aligned}
i\sigma_\mu^- D_\mu \chi_R = 0 &\Rightarrow [(\partial_4 - iA_4) \mathbb{1} - i\sigma_i (\partial_i - iA_i)] \chi_R = 0 \\
i\sigma_\mu^+ D_\mu \chi_L = 0 &\Rightarrow [(\partial_4 - iA_4) \mathbb{1} + i\sigma_i (\partial_i - iA_i)] \chi_L = 0.
\end{aligned} \tag{C.4}$$

In a basis rooted in the algebra of angular momentum addition¹, both the left and right-handed solutions are commonly assumed to follow the radial ansatz

$$\chi_\alpha^A = [(\xi(r) \mathbb{1} + \eta(r) n_i \tau^i) \epsilon]_{\alpha A} e^{-i\omega x_4}, \tag{C.5}$$

where χ_α^A is clearly a 2×2 matrix with color ($A = 1, 2$) and spinor ($\alpha = 1, 2$) indices entangled; and where $\epsilon = i\tau^2$ satisfies the relations

$$\epsilon \vec{\sigma} \epsilon = \vec{\sigma}^T, \quad \epsilon \vec{\sigma}^T \epsilon = \vec{\sigma}. \tag{C.6}$$

Writing explicitly the background dyonic fields from Eq. (C.2), the Weyl equations take the form

$$\begin{aligned}
(i\sigma_\mu^\pm D_\mu)_{AB}^{\alpha\beta} (\chi_{L/R})_\beta^B &= \left\{ \delta^{\alpha\beta} (\delta^{AB} \partial_4 - i\frac{H}{2} (n_a \tau^a)^{AB}) \pm i(\sigma^i)^{\alpha\beta} \left[\delta^{AB} \partial_i - i\frac{\mathcal{A}}{2} (\varepsilon_{aij} n_j \tau^a)^{AB} \right] \right\} \\
&\times \left[\epsilon^{B\beta} \xi + (\tau_m \epsilon)^{B\beta} n_m \eta \right] \\
&= \left[-i\omega \eta n_i - i \left(\frac{H}{2} \pm \mathcal{A} \right) n_i \xi + \frac{H}{2} \varepsilon_{ikm} n_k n_m \eta \mp i \partial_i \xi \mp \varepsilon_{ikm} \partial_k (n_m \eta) \right] \\
&\times (\sigma^i \epsilon)^{A\alpha} + \left[-i\omega \xi - i \left(\frac{H}{2} \mp \mathcal{A} \right) \eta \mp i \partial_i (n_i \eta) \right] \epsilon^{A\alpha} \\
&= 0,
\end{aligned} \tag{C.7}$$

where upper and lower signs correspond to the left and right-handed components, respectively. Since η and ξ are only functions of r , it is easy to see that the right-handed fermions satisfy the

¹See [81, 96] for a thorough discussion on this topic.

equations

$$\begin{aligned}\omega\xi + \left(\frac{H}{2} + \mathcal{A} - \frac{2}{r}\right)\eta - \partial_r\eta &= 0, \\ \omega\eta + \left(\frac{H}{2} - \mathcal{A}\right)\xi - \partial_r\xi &= 0\end{aligned}\tag{C.8}$$

while the left-handed

$$\begin{aligned}\omega\xi + \left(\frac{H}{2} - \mathcal{A} + \frac{2}{r}\right)\eta + \partial_r\eta &= 0, \\ \omega\eta + \left(\frac{H}{2} + \mathcal{A}\right)\xi + \partial_r\xi &= 0.\end{aligned}\tag{C.9}$$

C.1 RIGHT-HANDED SOLUTION

To simplify our notation, let us define $\partial_r\eta = \eta'$ and $\partial_r\xi = \xi'$ and notice that Eq. (C.8) can be expressed in matrix form as

$$\begin{pmatrix} \eta' \\ \xi' \end{pmatrix} = \begin{pmatrix} \frac{H}{2} + \mathcal{A} - \frac{2}{r} & \omega \\ \omega & \frac{H}{2} - \mathcal{A} \end{pmatrix} \begin{pmatrix} \eta \\ \xi \end{pmatrix}.\tag{C.10}$$

Following [151], we see that the coefficient matrix $M(r)$, can be split into a diagonal matrix $M_0(r)$ plus a non-diagonal $M_1(r)$, i.e. $M(r) = M_0(r) + M_1(r)$, where

$$M_0(r) = \begin{pmatrix} \frac{H}{2} - \frac{1}{r} & 0 \\ 0 & \frac{H}{2} - \frac{1}{r} \end{pmatrix}, \quad M_1(r) = \begin{pmatrix} \mathcal{A} - \frac{1}{r} & \omega \\ \omega & \frac{1}{r} - \mathcal{A} \end{pmatrix}.\tag{C.11}$$

Therefore, the general solutions to Eq. (C.10) are

$$\begin{pmatrix} \eta(r) \\ \xi(r) \end{pmatrix} = \exp\left[\int_0^r dr' M_0(r')\right] \begin{pmatrix} u_1(r) \\ u_2(r) \end{pmatrix},\tag{C.12}$$

where u_1 and u_2 are the solutions to the system $\vec{u}' = M_1(r)\vec{u}$, which will turn out to be easier to solve. Before that, let us examine the exponential factor. When the background field is a self-dual

M -type dyon, $H(r) = 1/r - v \coth(vr)$ and

$$\exp \left[\int_0^r dr' M_0(r') \right] = \exp \left[-\frac{1}{2} \int_0^r dr' \left(\frac{1}{r'} + v \coth(vr') \right) \right] = \frac{1}{\sqrt{r \sinh(rv)}}. \quad (\text{C.13})$$

On the other hand, for an anti-self-dual field, namely an \bar{M} antidyon, $H(r) = v \coth(vr) - 1/r$ and

$$\exp \left[\int_0^r dr' M_0(r') \right] = \exp \left[\frac{1}{2} \int_0^r dr' \left(v \coth(vr') - \frac{3}{r'} \right) \right] = \sqrt{\frac{\sinh(rv)}{r^3}}. \quad (\text{C.14})$$

Once the exponential factors have been determined, let us look at the functions u_1 and u_2 , which satisfy the equations

$$\begin{aligned} u_1' &= \left(\mathcal{A} - \frac{1}{r} \right) u_1 + \omega u_2 = -\frac{v}{\sinh vr} u_1 + \omega u_2 \\ u_2' &= \omega u_1 + \left(\frac{1}{r} - \mathcal{A} \right) u_2 = \omega u_1 + \frac{v}{\sinh vr} u_2, \end{aligned} \quad (\text{C.15})$$

where we have used Eq. (C.2). To solve the coupled system of equations, we can decouple one equation by obtaining a second order differential equation of u_2 , for example.

$$\begin{aligned} u_2'' &= -\frac{\cosh(\tilde{r})}{\sinh^2(\tilde{r})} u_2 + \frac{1}{\sinh(\tilde{r})} u_2' + \tilde{\omega} u_1' \\ &= \frac{1 - \cosh(\tilde{r})}{\sinh^2(\tilde{r})} u_2 + \tilde{\omega}^2 u_2, \end{aligned} \quad (\text{C.16})$$

with $\tilde{r} = rv$ and $\tilde{\omega} = \omega/v$ defined for simplicity. After some basic manipulation, the equation is reduced to

$$-\frac{d^2 u_2}{d\tilde{r}^2} - \frac{1}{2 \cosh^2\left(\frac{\tilde{r}}{2}\right)} u_2 = -\tilde{\omega}^2 u_2, \quad (\text{C.17})$$

and can be identified as the 1D Schrödinger equation of a particle in the modified Pöschl-Teller potential

$$\frac{d^2 \Psi}{dx^2} + \left(k^2 + \frac{\lambda(\lambda+1)}{a^2 \cosh^2\left(\frac{x}{a}\right)} \right) \Psi = 0, \quad (\text{C.18})$$

whose two (odd and even) independent solutions [152–154], expressed in terms of the hypergeomet-

ric function $F(a, b; c; z)$, are given by

$$\begin{aligned}\Psi^E(x) &= \left[\cosh\left(\frac{x}{2}\right) \right]^{\lambda+1} F\left(\alpha, \beta; \frac{1}{2}; -\sinh^2\left(\frac{x}{2}\right)\right), \\ \Psi^O(x) &= \left[\cosh\left(\frac{x}{2}\right) \right]^{\lambda+1} \sinh\left(\frac{x}{2}\right) F\left(\alpha + \frac{1}{2}, \beta + \frac{1}{2}; \frac{3}{2}; -\sinh^2\left(\frac{x}{2}\right)\right),\end{aligned}\quad (\text{C.19})$$

where $\alpha = (\lambda + 1 + ika)$ and $\beta = (\lambda + 1 - ika)$. It is straight forward to see that Eq. (C.18) is reduced to Eq. (C.17) when $k^2 = -\tilde{\omega}^2$, $a = 2$ and $\lambda = 1$; therefore, making use of the symmetric property $F(a, b; c; z) = F(b, a; c; z)$, the solutions to Eq. (C.17) are simply

$$\begin{aligned}u_2^E(r) &= \left[\cosh(\omega r) - \frac{v}{2\omega} \tanh\left(\frac{vr}{2}\right) \sinh(\omega r) \right], \\ u_2^O(r) &= \left(1 - \frac{4\omega^2}{v^2}\right)^{-1} \left[-\frac{2\omega}{v} \sinh(\omega r) + \tanh\left(\frac{vr}{2}\right) \cosh(\omega r) \right].\end{aligned}\quad (\text{C.20})$$

Combining Eqs. (C.13), (C.14) and (C.20), we have that

$$\xi(r) = \begin{cases} \frac{1}{\sqrt{r \sinh(rv)}} (C_E u_2^E(r) + C_O u_2^O(r)), & \text{for } M\text{-dyon} \\ \sqrt{\frac{\sinh(rv)}{r^3}} (C_E u_2^E(r) + C_O u_2^O(r)), & \text{for } \bar{M}\text{-antidyon},\end{cases}\quad (\text{C.21})$$

where C_E and C_O are constants to be determined. It can be shown that the \bar{M} solution diverges in the limit $r \rightarrow 0$, hence we must have $C_E = C_O = 0$. As for the M dyon, $[r \sinh(rv)]^{-1/2} C_O u_2$ is the only non-divergent term at the origin and thus $C_E = 0$, resulting in

$$\xi(r) = \begin{cases} \frac{C}{\sqrt{r \sinh(rv)}} \left(1 - \frac{4\omega^2}{v^2}\right)^{-1} \left[-\frac{2\omega}{v} \sinh(\omega r) \right. \\ \left. + \tanh\left(\frac{vr}{2}\right) \cosh(\omega r) \right], & \text{for } M\text{-dyon} \\ 0, & \text{for } \bar{M}\text{-antidyon.}\end{cases}\quad (\text{C.22})$$

As for u_1 , we can use the general solution $u_2 = C_E u_2^E(r) + C_O u_2^O(r)$ and plug it into the second line of Eq. (C.15), obtaining

$$\begin{aligned}u_1(r) &= C_E \left[\sinh(\omega r) - \frac{v \cosh(\omega r) (2 \operatorname{csch}(vr) + \omega^2 \tanh\left(\frac{vr}{2}\right))}{2\omega} \right] \\ &+ C_O \left[-\frac{2\omega}{v} \cosh(\omega r) + \coth\left(\frac{vr}{2}\right) \sinh(\omega r) \right].\end{aligned}\quad (\text{C.23})$$

When multiplied by Eq. (C.14), we see that the first and second terms in brackets are divergent in the limits $r \rightarrow 0$ and $r \rightarrow \infty$; therefore, $C_E = C_O = 0$ for the \bar{M} solution, consistently with the result previously obtained. When multiplied by Eq. (C.13), namely, the corresponding factor to the M -dyon, both limits approach zero and the $\eta(r)$ is normalizable.

$$\eta(r) = \begin{cases} \frac{C}{\sqrt{r \sinh(rv)}} \left(1 - \frac{4\omega^2}{v^2}\right)^{-1} \left[-\frac{2\omega}{v} \cosh(\omega r) + \coth\left(\frac{vr}{2}\right) \sinh(\omega r)\right], & \text{for } M\text{-dyon} \\ 0, & \text{for } \bar{M}\text{-antidyon.} \end{cases} \quad (\text{C.24})$$

The normalization constant C is easily obtained by noticing that

$$[\chi_\alpha^A]^\dagger \chi_\alpha^A = 2(\eta^2 + \chi^2), \quad (\text{C.25})$$

where χ_α^A is of course given by Eq. (C.5). Therefore

$$\int d^3x [\chi_\alpha^A]^\dagger \chi_\alpha^A = \frac{8\pi C^2}{v^2} \left(1 - \frac{4\omega^2}{v^2}\right)^{-2} \Rightarrow C = \frac{v}{\sqrt{8\pi}} \left(1 - \frac{4\omega^2}{v^2}\right). \quad (\text{C.26})$$

A simple look into the asymptotic behavior of the solutions will give us some insight on the constraints on the Matsubara frequencies. From Eq. (C.8), in the large distance limit, the differential equations are reduced to

$$\begin{aligned} \eta' &= \left(\frac{H}{2} + \mathcal{A} - \frac{2}{r}\right) \eta + \omega \xi, & \xrightarrow{r \rightarrow \infty} & \eta' = \mp \frac{v}{2} \eta + \omega \xi \\ \xi' &= \left(\frac{H}{2} - \mathcal{A}\right) \xi + \omega \eta & & \xi' = \mp \frac{v}{2} \xi + \omega \eta \end{aligned} \quad (\text{C.27})$$

where the upper and lower signs correspond to the M and \bar{M} dyon equations, respectively. The solution is found by plugging in the function $\rho_\pm \equiv \eta \pm \xi$, thus obtaining

$$\begin{aligned} \eta(r) &= C_+ e^{(\mp \frac{v}{2} + \omega)r} + C_- e^{(\mp \frac{v}{2} - \omega)r} \\ \xi(r) &= C_+ e^{(\mp \frac{v}{2} + \omega)r} - C_- e^{(\mp \frac{v}{2} - \omega)r}, \end{aligned} \quad (\text{C.28})$$

with C_\pm some normalization constants. In the case of the \bar{M} dyons (lower sign), the term in the exponential becomes $v/2 \pm \omega$, meaning that in order to have finite η and ξ at $r \rightarrow \infty$, the frequency

must simultaneously satisfy $\omega > v/2$ and $\omega < -v/2$, thus ruling out the existence of a right-handed zero mode for the anti-self-dual dyon \bar{M} , as previously observed.

Analogously, for the self-dual M dyon, the normalizability requirement constraints the frequency to $-v/2 < \omega < v/2$. Since $v = 2\pi\nu T$ with $\nu \in [0, 1]$, the antiperiodic boundary condition implies that $-\nu < 2N + 1 < \nu$ for $N \in \mathbb{N}$, which clearly cannot be satisfied; therefore, the M dyon must not have an antiperiodic right-handed zero mode.

From the index theorem, it is known that the KvBLL caloron has one zero mode; moreover, as it has been discussed extensively in the literature [87, 155–157], its location depends on the imposed boundary conditions, being that a periodic zero mode will only exist for a background M -dyon field while an antiperiodic one for an L -dyon. Since this work focuses on physical fermions, i.e. with antiperiodic boundary conditions, we must look at the zero mode of the latter background field. For this, we must recall that the A_μ^L field can be obtained from A_μ^M by first replacing $v \rightarrow \bar{v} = 2\pi T - v$ and then apply the time dependent gauge transformation $U = \exp(-i\pi T x_4 n_i \tau^i)$ (see Appendix C of [47] and references within). The asymptotic zero mode is then obtained from Eq. (C.28) simply by replacing $v \rightarrow \bar{v}$ and $\omega \rightarrow \omega - \pi T$

$$\begin{aligned}\eta(r) &= C_+ e^{[\mp(\pi T - \frac{v}{2}) + \omega - \pi T]r} + C_- e^{[\mp(\pi T - \frac{v}{2}) - \omega + \pi T]r} \\ \xi(r) &= C_+ e^{[\mp(\pi T - \frac{v}{2}) + \omega - \pi T]r} - C_- e^{[\mp(\pi T - \frac{v}{2}) - \omega + \pi T]r}.\end{aligned}\tag{C.29}$$

Now the frequency is constrained to $\omega \in (v/2, 2\pi T - v/2)$ and the antiperiodicity of the zero mode can only be satisfied when $\omega = \pi T$.

Finally, recalling that the right-handed spinor associated to the M -dyon $\chi_R^{(M)}$ is given by the radial ansatz Eq. (C.5) with $\xi(r)$ and $\eta(r)$ shown in Eqs. (C.22), (C.24) and (C.26). To obtain the full zero mode solution corresponding to the L dyon, we then make the replacement $v \rightarrow \bar{v}$ and multiply by U from the right to obtain

$$\begin{aligned}\chi_R^L &= U \chi_R^M(v \rightarrow \bar{v}) \\ &= \exp(-i\pi T x_4 n_i \tau^i) (\xi \mathbf{1} + \eta n_i \tau^i) \epsilon e^{-i\omega x_4} \\ &= \frac{1}{2} e^{-ix_4(\omega - \pi T)} (\xi - \eta) (\mathbf{1} - n_i \tau^i) \epsilon + \frac{1}{2} e^{-ix_4(\omega + \pi T)} (\xi + \eta) (\mathbf{1} + n_i \tau^i) \epsilon.\end{aligned}\tag{C.30}$$

It should be clear that in order to satisfy the antiperiodicity and finiteness at large distances, taking $\omega = 0$ in the above equation is completely analogous to $\omega = \pi T$ in Eq. (C.29); therefore, the shift in the frequency $\omega \rightarrow \omega - \pi T$ is simply a consequence of the gauge transformation U . Given that

$$\begin{aligned}\xi(r; \omega = 0) &= \frac{\bar{v} \tanh\left(\frac{\bar{v}r}{2}\right)}{\sqrt{8\pi r} \sinh(\bar{v}r)}, \\ \eta(r; \omega = 0) &= 0,\end{aligned}\tag{C.31}$$

the L -dyon zero mode (in the hedgehog gauge) reduces to

$$\begin{aligned}\chi_R^{(L)} &= \frac{\bar{v} \tanh\left(\frac{\bar{v}r}{2}\right)}{2\sqrt{8\pi r} \sinh(\bar{v}r)} \left[e^{i\pi T x_4} (\mathbf{1} - n_i \tau^i) + e^{-i\pi T x_4} (\mathbf{1} + n_i \tau^i) \right] \epsilon. \\ &= \frac{\bar{v} \tanh\left(\frac{\bar{v}r}{2}\right)}{\sqrt{8\pi r} \sinh(\bar{v}r)} e^{-i\pi T x_4 n_i \tau^i} \epsilon\end{aligned}\tag{C.32}$$

C.2 LEFT-HANDED SOLUTION

Let us now first begin by looking into the asymptotics of the left-handed equations portrayed in Eq. (C.9)

$$\begin{aligned}\eta' &= -\left(\frac{H}{2} - \mathcal{A} - \frac{2}{r}\right) \eta - \omega \xi, & \xrightarrow{r \rightarrow \infty} & \eta' = \pm \frac{v}{2} \eta - \omega \xi \\ \xi' &= -\left(\frac{H}{2} + \mathcal{A}\right) \xi - \omega \eta, & & \xi' = \pm \frac{v}{2} \xi - \omega \eta.\end{aligned}\tag{C.33}$$

Once again, by rewriting the equation for $\rho_{\pm} = \xi \pm \eta$, the equations are easily solvable and one obtains

$$\begin{aligned}\eta(r) &= C_+ e^{(\pm \frac{v}{2} - \omega)r} + C_- e^{(\pm \frac{v}{2} + \omega)r} \\ \xi(r) &= C_+ e^{(\pm \frac{v}{2} - \omega)r} - C_- e^{(\pm \frac{v}{2} + \omega)r}.\end{aligned}\tag{C.34}$$

For the M dyon case (upper sign), the condition of finiteness at large distances, imposes the simultaneous restriction $\omega > v/2$ and $\omega < -v/2$, now ruling out the existence of a left-handed zero mode for the self-dual field. On the other hand, for the \bar{M} antidyon, the frequency restriction is given by $-v/2 < \omega < v/2$; therefore, completely analogous to what was done in the previous

section, we find that the only antiperiodic left-handed zero mode corresponds to the anti-self-dual field \bar{L} , where $\omega \in (v/2, 2\pi T - v/2)$.

To find the general solution of the left-handed zero mode, let us look at the full differential equations (Eq. (C.9)), which in matrix form are

$$\begin{pmatrix} \eta' \\ \xi' \end{pmatrix} = \begin{pmatrix} -\frac{H}{2} + \mathcal{A} - \frac{2}{r} & -\omega \\ -\omega & -\frac{H}{2} - \mathcal{A} \end{pmatrix} \begin{pmatrix} \eta \\ \xi \end{pmatrix}. \quad (\text{C.35})$$

Since we are only interested in the \bar{M} case, to later be transform into the \bar{L} one, the general solutions are given by

$$\begin{pmatrix} \eta \\ \xi \end{pmatrix} = \frac{1}{\sqrt{r \sinh(rv)}} \begin{pmatrix} w_1 \\ w_2 \end{pmatrix}, \quad (\text{C.36})$$

where $w_{1,2}$ satisfy the equations

$$\begin{aligned} w_1' &= -\frac{v}{\sinh vr} w_1 - \omega w_2 \\ w_2' &= -\omega w_1 + \frac{v}{\sinh vr} w_2. \end{aligned} \quad (\text{C.37})$$

As with the asymptotic case, it is clear that Eq. (C.37) is the same system as Eq. (C.15) with the substitution $\omega \rightarrow -\omega$; consequently, $w_{1,2}(r; \omega) = u_{1,2}(r; -\omega)$ and so

$$\begin{aligned} \xi(r) &= \frac{v}{\sqrt{8\pi r \sinh(rv)}} \left[-\frac{2\omega}{v} \sinh(\omega r) + \tanh\left(\frac{vr}{2}\right) \cosh(\omega r) \right], \\ \eta(r) &= \frac{v}{\sqrt{8\pi r \sinh(rv)}} \left[\frac{2\omega}{v} \cosh(\omega r) - \coth\left(\frac{vr}{2}\right) \sinh(\omega r) \right]. \end{aligned} \quad (\text{C.38})$$

Once again, similarly to what was done in the preceding section, the zero mode associated to the \bar{L} antidyon is obtained by the substitution $v \rightarrow \bar{v}$, followed by the gauge transformation $U^\dagger = \exp(i\pi T x_4 n_i \tau^i)$, resulting in

$$\begin{aligned} \chi_L^{(\bar{L})} &= \frac{\bar{v} \tanh\left(\frac{\bar{v}r}{2}\right)}{2\sqrt{8\pi r \sinh(\bar{v}r)}} \left[e^{i\pi T x_4} (\mathbf{1} + n_i \tau^i) + e^{-i\pi T x_4} (\mathbf{1} - n_i \tau^i) \right] \epsilon \\ &= \frac{\bar{v} \tanh\left(\frac{\bar{v}r}{2}\right)}{\sqrt{8\pi r \sinh(\bar{v}r)}} e^{i\pi T x_4 n_i \tau^i} \epsilon \end{aligned} \quad (\text{C.39})$$

where we have used $\omega = 0$ to preserve the antiperiodic boundary conditions.

REFERENCES

- [1] H. D. Politzer, “Reliable Perturbative Results for Strong Interactions?”, *Phys. Rev. Lett.* **30**, [,274(1973)], 1346–1349 (1973).
- [2] D. J. Gross and F. Wilczek, “Ultraviolet Behavior of Nonabelian Gauge Theories”, *Phys. Rev. Lett.* **30**, [,271(1973)], 1343–1346 (1973).
- [3] A. A. Belavin, A. M. Polyakov, A. S. Schwartz, and Yu. S. Tyupkin, “Pseudoparticle Solutions of the Yang-Mills Equations”, *Phys. Lett.* **B59**, 85–87 (1975).
- [4] C. G. Callan Jr., R. F. Dashen, and D. J. Gross, “Toward a Theory of the Strong Interactions”, *Phys. Rev.* **D17**, [,36(1977)], 2717 (1978).
- [5] E. V. Shuryak, “The Role of Instantons in Quantum Chromodynamics. 1. Physical Vacuum”, *Nucl. Phys.* **B203**, 93 (1982).
- [6] E. V. Shuryak, “The Role of Instantons in Quantum Chromodynamics. 2. Hadronic Structure”, *Nucl. Phys.* **B203**, 116–139 (1982).
- [7] E. V. Shuryak, “The Role of Instantons in Quantum Chromodynamics. 3. Quark - Gluon Plasma”, *Nucl. Phys.* **B203**, 140–156 (1982).
- [8] D. Diakonov and V. Yu. Petrov, “Instanton Based Vacuum from Feynman Variational Principle”, *Nucl. Phys.* **B245**, 259–292 (1984).
- [9] M. A. Shifman, A. I. Vainshtein, and V. I. Zakharov, “QCD and Resonance Physics. Theoretical Foundations”, *Nucl. Phys.* **B147**, 385–447 (1979).
- [10] D. Diakonov and V. Yu. Petrov, “Chiral Condensate in the Instanton Vacuum”, *Phys. Lett.* **147B**, 351–356 (1984).
- [11] D. Diakonov and V. Yu. Petrov, “A Theory of Light Quarks in the Instanton Vacuum”, *Nucl. Phys.* **B272**, 457–489 (1986).

- [12] P. V. Pobylitsa, “The Quark Propagator and Correlation Functions in the Instanton Vacuum”, Phys. Lett. **B226**, 387–392 (1989).
- [13] G. 't Hooft, “Symmetry Breaking Through Bell-Jackiw Anomalies”, Phys. Rev. Lett. **37**, 8–11 (1976).
- [14] E. V. Shuryak, “Toward the Quantitative Theory of the Topological Effects in Gauge Field Theories. 1. Phenomenology and the Method of Collective Coordinates”, Nucl. Phys. **B302**, 559–573 (1988).
- [15] E. V. Shuryak, “Toward the Quantitative Theory of the Topological Effects in Gauge Field Theories. 2. The SU(2) Gluodynamics”, Nucl. Phys. **B302**, 574–598 (1988).
- [16] E. V. Shuryak, “Toward the Quantitative Theory of the Topological Phenomena in Gauge Theories. 3. Instantons and Light Fermions”, Nucl. Phys. **B302**, 599–620 (1988).
- [17] E. V. Shuryak and J. J. M. Verbaarschot, “Chiral Symmetry Breaking and Correlations in the Instanton Liquid”, Nucl. Phys. **B341**, 1–26 (1990).
- [18] T. Schäfer and E. V. Shuryak, “The Interacting instanton liquid in QCD at zero and finite temperature”, Phys. Rev. **D53**, 6522–6542 (1996).
- [19] M. A. Nowak, J. J. M. Verbaarschot, and I. Zahed, “Flavor Mixing in the Instanton Vacuum”, Nucl. Phys. **B324**, 1–33 (1989).
- [20] E.-M. Ilgenfritz and M. Muller-Preussker, “Statistical Mechanics of the Interacting Yang-Mills Instanton Gas”, Nucl. Phys. **B184**, 443–460 (1981).
- [21] T. Schäfer and E. V. Shuryak, “Instantons in QCD”, Rev. Mod. Phys. **70**, 323–426 (1998).
- [22] D. Diakonov, “Instantons at work”, Prog. Part. Nucl. Phys. **51**, 173–222 (2003).
- [23] T. C. Kraan and P. van Baal, “Periodic instantons with nontrivial holonomy”, Nucl. Phys. **B533**, 627–659 (1998).
- [24] T. C. Kraan and P. van Baal, “Monopole constituents inside SU(N) calorons”, Phys. Lett. **B435**, 389–395 (1998).
- [25] K. M. Lee and C. h. Lu, “SU(2) calorons and magnetic monopoles”, Phys. Rev. **D58**, 025011 (1998).

- [26] G. Ripka, “Dual superconductor models of color confinement”, *Lect. Notes Phys.* **639**, pp.1–135 (2004).
- [27] K.-I. Kondo, S. Kato, A. Shibata, and T. Shinohara, “Quark confinement: Dual superconductor picture based on a non-Abelian Stokes theorem and reformulations of YangMills theory”, *Phys. Rept.* **579**, 1–226 (2015).
- [28] D. Diakonov and V. Petrov, “Confining ensemble of dyons”, *Phys. Rev.* **D76**, 056001 (2007).
- [29] D. Diakonov, “Topology and confinement”, *Nucl. Phys. Proc. Suppl.* **195**, 5–45 (2009).
- [30] P. Gerhold, E. M. Ilgenfritz, and M. Muller-Preussker, “An SU(2) KvBLL caloron gas model and confinement”, *Nucl. Phys.* **B760**, 1–37 (2007).
- [31] E. Shuryak and T. Sulejmanpasic, “Holonomy potential and confinement from a simple model of the gauge topology”, *Phys. Lett.* **B726**, 257–261 (2013).
- [32] R. Larsen and E. Shuryak, “Classical interactions of the instanton-dyons with antidyons”, *Nucl. Phys.* **A950**, 110–128 (2016).
- [33] R. Larsen and E. Shuryak, “Interacting ensemble of the instanton-dyons and the deconfinement phase transition in the SU(2) gauge theory”, *Phys. Rev.* **D92**, 094022 (2015).
- [34] Y. Liu, E. Shuryak, and I. Zahed, “Confining dyon-antidyon Coulomb liquid model. I.”, *Phys. Rev.* **D92**, 085006 (2015).
- [35] Y. Liu, E. Shuryak, and I. Zahed, “Dense Instanton-Dyon Liquid Model: Diagrammatics”, *Phys. Rev.* **D98**, 014023 (2018).
- [36] A. R. Zhitnitsky, “Confinement- deconfinement phase transition and fractional instanton quarks in dense matter”, in *Continuous advances in QCD. Proceedings, 7th Workshop, QCD 2006, Minneapolis, USA, May 11-14, 2006*, [,207(2006)] (2006), pp. 207–213.
- [37] E. Poppitz, T. Schfer, and M. Unsal, “Continuity, Deconfinement, and (Super) Yang-Mills Theory”, *JHEP* **10**, 115 (2012).
- [38] E. Poppitz and M. Unsal, “Seiberg-Witten and ‘Polyakov-like’ magnetic bion confinements are continuously connected”, *JHEP* **07**, 082 (2011).

- [39] K.-I. Kondo, “Gauge-invariant description of Higgs phenomenon and quark confinement”, *Phys. Lett.* **B762**, 219–224 (2016).
- [40] P. Faccioli and E. Shuryak, “QCD topology at finite temperature: Statistical mechanics of self-dual dyons”, *Phys. Rev.* **D87**, 074009 (2013).
- [41] R. Larsen and E. Shuryak, “Instanton-dyon Ensemble with two Dynamical Quarks: the Chiral Symmetry Breaking”, *Phys. Rev.* **D93**, 054029 (2016).
- [42] R. Larsen and E. Shuryak, “Instanton-dyon ensembles with quarks with modified boundary conditions”, *Phys. Rev.* **D94**, 094009 (2016).
- [43] Y. Liu, E. Shuryak, and I. Zahed, “Light quarks in the screened dyon-antidyon Coulomb liquid model. II.”, *Phys. Rev.* **D92**, 085007 (2015).
- [44] Y. Liu, E. Shuryak, and I. Zahed, “The Instanton-Dyon Liquid Model III: Finite Chemical Potential”, *Phys. Rev.* **D94**, 105011 (2016).
- [45] Y. Liu, E. Shuryak, and I. Zahed, “Light Adjoint Quarks in the Instanton-Dyon Liquid Model IV”, *Phys. Rev.* **D94**, 105012 (2016).
- [46] Y. Liu, E. Shuryak, and I. Zahed, “The Instanton-Dyon Liquid Model V: Twisted Light Quarks”, *Phys. Rev.* **D94**, 105013 (2016).
- [47] M. A. Lopez-Ruiz, Y. Jiang, and J. Liao, “Confinement, Holonomy and Correlated Instanton-Dyon Ensemble I: SU(2) Yang-Mills Theory”, *Phys. Rev.* **D97**, 054026 (2018).
- [48] M. A. Lopez-Ruiz, Y. Jiang, and J. Liao, “Confinement from Correlated Instanton-Dyon Ensemble in SU(2) Yang-Mills Theory”, *Preprint* arXiv:1903.02684 [hep-ph] (2019).
- [49] J. I. Kapusta and C. Gale, *Finite-Temperature Field Theory: Principles and Applications*, Cambridge Monographs on Mathematical Physics (Cambridge University Press, New York, 2011).
- [50] M. L. Bellac, *Thermal Field Theory*, Cambridge Monographs on Mathematical Physics (Cambridge University Press, New York, 2011).
- [51] M. Laine and A. Vuorinen, “Basics of Thermal Field Theory”, *Lect. Notes Phys.* **925**, 1–281 (2016).

- [52] B. M. McCoy, “The Connection between statistical mechanics and quantum field theory”, in *Statistical mechanics and field theory. Proceedings, 7th Physics Summer School (1994)*, pp. 26–128.
- [53] M. Shifman, *Advanced Topics in Quantum Field Theory*. (Cambridge University Press, Cambridge, 2012).
- [54] M. A. Nowak, M. Rho, and I. Zahed, *Chiral nuclear dynamics* (World Scientific, Singapore, 1996).
- [55] A. M. Polyakov, “Thermal Properties of Gauge Fields and Quark Liberation”, *Phys. Lett.* **72B**, 477–480 (1978).
- [56] L. Susskind, “Lattice Models of Quark Confinement at High Temperature”, *Phys. Rev.* **D20**, 2610–2618 (1979).
- [57] L. D. McLerran and B. Svetitsky, “Quark Liberation at High Temperature: A Monte Carlo Study of SU(2) Gauge Theory”, *Phys. Rev.* **D24**, 450 (1981).
- [58] H. J. Rothe, “Lattice gauge theories: An Introduction”, *World Sci. Lect. Notes Phys.* **43**, 1–381 (1992).
- [59] J. Greensite, “An Introduction to the Confinement Problem”, *Lect. Notes Phys.* **821**, 1–211 (2011).
- [60] K. Holland and U.-J. Wiese, “The Center symmetry and its spontaneous breakdown at high temperatures”, 1909–1944 (2000).
- [61] B. Svetitsky and L. G. Yaffe, “Critical Behavior at Finite Temperature Confinement Transitions”, *Nucl. Phys.* **B210**, 423–447 (1982).
- [62] B. Svetitsky, “Symmetry Aspects of Finite Temperature Confinement Transitions”, *Phys. Rept.* **132**, 1–53 (1986).
- [63] R. Fiore, F. Gliozzi, and P. Provero, “Critical behavior of 3-D SU(2) gauge theory at finite temperature: Exact results from universality”, *Phys. Rev.* **D58**, 114502 (1998).
- [64] J. Engels, J. Fingberg, and M. Weber, “Finite Size Scaling Analysis of SU(2) Lattice Gauge Theory in (3+1)-dimensions”, *Nucl. Phys.* **B332**, 737–759 (1990).

- [65] J. Engels, S. Mashkevich, T. Scheideler, and G. Zinovev, “Critical behavior of SU(2) lattice gauge theory: A Complete analysis with the χ^2 method”, *Phys. Lett.* **B365**, 219–224 (1996).
- [66] J. Engels, J. Fingberg, and D. E. Miller, “Phenomenological renormalization and scaling behavior of SU(2) lattice gauge theory”, *Nucl. Phys.* **B387**, 501–519 (1992).
- [67] M. Teper, “The Finite temperature phase transition of SU(2) gauge fields in (2+1)-dimensions”, *Phys. Lett.* **B313**, 417–424 (1993).
- [68] M. Caselle and M. Hasenbusch, “Deconfinement transition and dimensional crossover in the 3-D gauge Ising model”, *Nucl. Phys.* **B470**, 435–453 (1996).
- [69] T. Celik, J. Engels, and H. Satz, “The Order of the Deconfinement Transition in SU(3) Yang-Mills Theory”, *Phys. Lett.* **125B**, 411–414 (1983).
- [70] J. B. Kogut, M. Stone, H. W. Wyld, W. R. Gibbs, J. Shigemitsu, S. H. Shenker, and D. K. Sinclair, “Deconfinement and Chiral Symmetry Restoration at Finite Temperatures in SU(2) and SU(3) Gauge Theories”, *Phys. Rev. Lett.* **50**, 393 (1983).
- [71] J. Goldstone, “Field Theories with Superconductor Solutions”, *Nuovo Cim.* **19**, 154–164 (1961).
- [72] J. Goldstone, A. Salam, and S. Weinberg, “Broken Symmetries”, *Phys. Rev.* **127**, 965–970 (1962).
- [73] Y. Nambu, “Quasiparticles and Gauge Invariance in the Theory of Superconductivity”, *Phys. Rev.* **117**, [132(1960)], 648–663 (1960).
- [74] T. Banks and A. Casher, “Chiral Symmetry Breaking in Confining Theories”, *Nucl. Phys.* **B169**, 103–125 (1980).
- [75] E. V. Shuryak, “The QCD vacuum, hadrons and the superdense matter”, *World Sci. Lect. Notes Phys.* **71**, [World Sci. Lect. Notes Phys.8,1(1988)], 1–618 (2004).
- [76] R. D. Pisarski and F. Wilczek, “Remarks on the Chiral Phase Transition in Chromodynamics”, *Phys. Rev.* **D29**, 338–341 (1984).
- [77] D. J. Gross, R. D. Pisarski, and L. G. Yaffe, “QCD and Instantons at Finite Temperature”, *Rev. Mod. Phys.* **53**, 43 (1981).

- [78] S. Coleman, *Aspects of Symmetry* (Cambridge University Press, Cambridge, 1985).
- [79] A. I. Vainshtein, V. I. Zakharov, V. A. Novikov, and M. A. Shifman, “ABC’s of Instantons”, *Sov. Phys. Usp.* **25**, 195 (1982).
- [80] R. Rajaraman, *Solitons and Instantons. An Introduction to Solitons and Instantons in Quantum Field Theory* (North-Holland, Amsterdam, Netherlands, 1982).
- [81] V. A. Rubakov, *Classical theory of gauge fields* (Princeton University Press, Princeton, NJ, 2002).
- [82] E. B. Bogomolny, “Stability of Classical Solutions”, *Sov. J. Nucl. Phys.* **24**, 449 (1976).
- [83] R. Jackiw, C. Nohl, and C. Rebbi, “Conformal Properties of Pseudoparticle Configurations”, *Phys. Rev.* **D15**, 1642 (1977).
- [84] G. ’t Hooft, “Computation of the Quantum Effects Due to a Four-Dimensional Pseudoparticle”, *Phys. Rev.* **D14**, 3432–3450 (1976).
- [85] B. J. Harrington and H. K. Shepard, “Euclidean Solutions and Finite Temperature Gauge Theory”, *Nucl. Phys.* **B124**, 409–412 (1977).
- [86] B. J. Harrington and H. K. Shepard, “Periodic Euclidean Solutions and the Finite Temperature Yang-Mills Gas”, *Phys. Rev.* **D17**, 2122 (1978).
- [87] F. Bruckmann, “Topological objects in QCD”, *Eur. Phys. J. ST* **152**, 61–88 (2007).
- [88] L. B. W. Jolley, *Summation of Series* (Dover Publications, New York, USA, 1961).
- [89] R. Hofmann, *The Thermodynamics of Quantum Yang-Mills Theory* (World Scientific, Singapore, 2012).
- [90] A. M. Polyakov, “Particle Spectrum in the Quantum Field Theory”, *JETP Lett.* **20**, 194–195 (1974).
- [91] G. ’t Hooft, “Magnetic Monopoles in Unified Gauge Theories”, *Nucl. Phys.* **B79**, 276–284 (1974).
- [92] H. Georgi and S. L. Glashow, “Unified weak and electromagnetic interactions without neutral currents”, *Phys. Rev. Lett.* **28**, 1494 (1972).

- [93] M. K. Prasad and C. M. Sommerfield, “An Exact Classical Solution for the ’t Hooft Monopole and the Julia-Zee Dyon”, *Phys. Rev. Lett.* **35**, 760–762 (1975).
- [94] N. S. Manton, “Complex Structure of Monopoles”, *Nucl. Phys.* **B135**, 319–332 (1978).
- [95] M. A. Lohe, “Two-Dimensional and Three-Dimensional Instantons”, *Phys. Lett.* **70B**, 325–328 (1977).
- [96] Ya. M. Shnir, *Magnetic monopoles* (Springer, Berlin, Germany, 2005).
- [97] K.-M. Lee and P. Yi, “Monopoles and instantons on partially compactified D-branes”, *Phys. Rev.* **D56**, 3711–3717 (1997).
- [98] K.-M. Lee, “Instantons and magnetic monopoles on $R^{*3} \times S^{*1}$ with arbitrary simple gauge groups”, *Phys. Lett.* **B426**, 323–328 (1998).
- [99] W. Nahm, “A Simple Formalism for the BPS Monopole”, *Phys. Lett.* **90B**, 413–414 (1980).
- [100] P. J. Braam and P. van Baal, “Nahm’s Transformation for Instantons”, *Commun. Math. Phys.* **122**, 267 (1989).
- [101] M. F. Atiyah, N. J. Hitchin, V. G. Drinfeld, and Yu. I. Manin, “Construction of Instantons”, *Phys. Lett.* **A65**, 185–187 (1978).
- [102] E. Corrigan, D. B. Fairlie, S. Templeton, and P. Goddard, “A Green’s Function for the General Selfdual Gauge Field”, *Nucl. Phys.* **B140**, 31–44 (1978).
- [103] E. Corrigan and P. Goddard, “Construction of Instanton and Monopole Solutions and Reciprocity”, *Annals Phys.* **154**, 253 (1984).
- [104] H. Osborn, “Calculation of Multi - Instanton Determinants”, *Nucl. Phys.* **B159**, 497–511 (1979).
- [105] D. Diakonov, N. Gromov, V. Petrov, and S. Slizovskiy, “Quantum weights of dyons and of instantons with nontrivial holonomy”, *Phys. Rev.* **D70**, 036003 (2004).
- [106] N. Weiss, “The Effective Potential for the Order Parameter of Gauge Theories at Finite Temperature”, *Phys. Rev.* **D24**, 475 (1981).
- [107] D. Diakonov and N. Gromov, “SU(N) Caloron Measure and its Relation to Instantons”, *Phys. Rev.* **D72**, 025003 (2005).

- [108] G. W. Gibbons and C. N. Pope, “The Positive Action Conjecture and Asymptotically Euclidean Metrics in Quantum Gravity”, *Commun. Math. Phys.* **66**, 267–290 (1979).
- [109] N. Metropolis, A. W. Rosenbluth, M. N. Rosenbluth, A. H. Teller, and E. Teller, “Equation of state calculations by fast computing machines”, *J. Chem. Phys.* **21**, 1087–1092 (1953).
- [110] W. K. Hastings, “Monte Carlo Sampling Methods Using Markov Chains and Their Applications”, *Biometrika* **57**, 97–109 (1970).
- [111] F. Bruckmann, S. Dinter, E.-M. Ilgenfritz, M. Muller-Preussker, and M. Wagner, “Cautionary remarks on the moduli space metric for multi-dyon simulations”, *Phys. Rev.* **D79**, 116007 (2009).
- [112] A. Dumitru, Y. Guo, Y. Hidaka, C. P. K. Altes, and R. D. Pisarski, “Effective Matrix Model for Deconfinement in Pure Gauge Theories”, *Phys. Rev.* **D86**, 105017 (2012).
- [113] S. Lin, R. D. Pisarski, and V. V. Skokov, “Zero interface tension at the deconfining phase transition for a matrix model of a $SU(\infty)$ gauge theory”, *Phys. Rev.* **D87**, 105002 (2013).
- [114] D. Smith, A. Dumitru, R. Pisarski, and L. von Smekal, “Effective potential for $SU(2)$ Polyakov loops and Wilson loop eigenvalues”, *Phys. Rev.* **D88**, 054020 (2013).
- [115] R. D. Pisarski and V. V. Skokov, “Chiral matrix model of the semi-QGP in QCD”, *Phys. Rev.* **D94**, 034015 (2016).
- [116] A. Pelissetto and E. Vicari, “Critical phenomena and renormalization group theory”, *Phys. Rept.* **368**, 549–727 (2002).
- [117] S. Digal, S. Fortunato, and P. Petreczky, “Heavy quark free energies and screening in $SU(2)$ gauge theory”, *Phys. Rev.* **D68**, 034008 (2003).
- [118] K. Huebner and C. Pica, “Renormalized Polyakov loops in various representations in finite temperature $SU(2)$ gauge theory”, *PoS LATTICE2008*, 197 (2008).
- [119] S. Nadkarni, “Nonabelian Debye Screening. 2. The Singlet Potential”, *Phys. Rev.* **D34**, 3904 (1986).
- [120] C. Borgs, “Area Law for Spatial Wilson Loops in High Temperature Lattice Gauge Theories”, *Nucl. Phys.* **B261**, 455–460 (1985).

- [121] E. Manousakis and J. Polonyi, “Nonperturbative Length Scale in High Temperature QCD”, Phys. Rev. Lett. **58**, 847 (1987).
- [122] G. S. Bali, J. Fingberg, U. M. Heller, F. Karsch, and K. Schilling, “The Spatial string tension in the deconfined phase of the (3+1)-dimensional SU(2) gauge theory”, Phys. Rev. Lett. **71**, 3059–3062 (1993).
- [123] L. Karkkainen, P. Lacock, D. E. Miller, B. Petersson, and T. Reisz, “Space - like Wilson loops at finite temperature”, Phys. Lett. **B312**, 173–178 (1993).
- [124] J. Greensite and R. Hllwieser, “Double-winding Wilson loops and monopole confinement mechanisms”, Phys. Rev. **D91**, 054509 (2015).
- [125] A. D’Alessandro and M. D’Elia, “Magnetic monopoles in the high temperature phase of Yang-Mills theories”, Nucl. Phys. **B799**, 241–254 (2008).
- [126] J. Liao and E. Shuryak, “Strongly coupled plasma with electric and magnetic charges”, Phys. Rev. **C75**, 054907 (2007).
- [127] J. Liao and E. Shuryak, “Angular Dependence of Jet Quenching Indicates Its Strong Enhancement Near the QCD Phase Transition”, Phys. Rev. Lett. **102**, 202302 (2009).
- [128] J. Xu, J. Liao, and M. Gyulassy, “Consistency of Perfect Fluidity and Jet Quenching in semi-Quark-Gluon Monopole Plasmas”, Chin. Phys. Lett. **32**, 092501 (2015).
- [129] S. K. Das, F. Scardina, S. Plumari, and V. Greco, “Toward a solution to the R_{AA} and v_2 puzzle for heavy quarks”, Phys. Lett. **B747**, 260–264 (2015).
- [130] A. Ramamurti and E. Shuryak, “Role of QCD monopoles in jet quenching”, Phys. Rev. **D97**, 016010 (2018).
- [131] S. Shi, J. Liao, and M. Gyulassy, “Probing the Color Structure of the Perfect QCD Fluids via Soft-Hard-Event-by-Event Azimuthal Correlations”, Chin. Phys. **C42**, 104104 (2018).
- [132] E. V. Shuryak, “What RHIC experiments and theory tell us about properties of quark-gluon plasma?”, Nucl. Phys. **A750**, 64–83 (2005).
- [133] M. Gyulassy and L. McLerran, “New forms of QCD matter discovered at RHIC”, Nucl. Phys. **A750**, 30–63 (2005).

- [134] B. Muller, J. Schukraft, and B. Wyslouch, “First Results from Pb+Pb collisions at the LHC”, *Ann. Rev. Nucl. Part. Sci.* **62**, 361–386 (2012).
- [135] E. Shuryak, “Strongly coupled quark-gluon plasma in heavy ion collisions”, *Rev. Mod. Phys.* **89**, 035001 (2017).
- [136] J. Liao and E. Shuryak, “Magnetic Component of Quark-Gluon Plasma is also a Liquid!”, *Phys. Rev. Lett.* **101**, 162302 (2008).
- [137] C. Ratti and E. Shuryak, “The Role of monopoles in a Gluon Plasma”, *Phys. Rev.* **D80**, 034004 (2009).
- [138] D. Diakonov and V. Yu. Petrov, “Quark Propagator and Chiral Condensate in an Instanton Vacuum”, *Sov. Phys. JETP* **62**, 204–214 (1985).
- [139] N. Weiss, “The Wilson Line in Finite Temperature Gauge Theories”, *Phys. Rev.* **D25**, 2667 (1982).
- [140] D. Diakonov and M. Oswald, “Covariant derivative expansion of fermionic effective action at high temperatures”, *Phys. Rev.* **D70**, 016006 (2004).
- [141] K. Fukushima and V. Skokov, “Polyakov loop modeling for hot QCD”, *Prog. Part. Nucl. Phys.* **96**, 154–199 (2017).
- [142] P. Scior, S. R. Edwards, and L. von Smekal, “Fractional Charge and Confinement of Quarks”, *PoS LATTICE2013*, 361 (2014).
- [143] A. V. Smilga and J. Stern, “On the spectral density of Euclidean Dirac operator in QCD”, *Phys. Lett.* **B318**, 531–536 (1993).
- [144] A. V. Smilga, *Lectures on quantum chromodynamics* (World Scientific, Singapore, 2001).
- [145] J. J. M. Verbaarschot, “Chiral random matrix theory and the spectrum of the Dirac operator zero virtuality”, *Acta Phys. Polon.* **B25**, 133–149 (1994).
- [146] J. J. M. Verbaarschot, “Spectrum of the Dirac operator in a QCD instanton liquid: Two versus three colors”, *Nucl. Phys.* **B427**, 534–544 (1994).
- [147] M. A. Nowak, J. J. M. Verbaarschot, and I. Zahed, “Chiral Fermions in the Instanton Vacuum at Finite Temperature”, *Nucl. Phys.* **B325**, 581–592 (1989).

- [148] G. Cossu, S. Aoki, H. Fukaya, S. Hashimoto, T. Kaneko, H. Matsufuru, and J.-I. Noaki, “Finite temperature study of the axial $U(1)$ symmetry on the lattice with overlap fermion formulation”, *Phys. Rev.* **D87**, [Erratum: *Phys. Rev.*D88,no.1,019901(2013)], 114514 (2013).
- [149] V. Dick, F. Karsch, E. Laermann, S. Mukherjee, and S. Sharma, “Microscopic origin of $U_A(1)$ symmetry violation in the high temperature phase of QCD”, *Phys. Rev.* **D91**, 094504 (2015).
- [150] M. S. Swanson, *Path Integrals and Quantum Processes* (Academic Press, Boston, USA).
- [151] E. Shuryak and T. Sulejmanpasic, “The Chiral Symmetry Breaking/Restoration in Dyonic Vacuum”, *Phys. Rev.* **D86**, 036001 (2012).
- [152] G. Poschl and E. Teller, “Bemerkungen zur Quantenmechanik des anharmonischen Oszillators”, *Z. Phys.* **83**, 143–151 (1933).
- [153] J. Lekner, “Reflectionless eigenstates of the sech² potential”, *Am. J. Phys.* **75**, 1151–1157 (2007).
- [154] S. Flugge, *Practical Quantum Mechanics* (Springer, Berlin, Germany, 1974).
- [155] M. Garcia Perez, A. Gonzalez-Arroyo, C. Pena, and P. van Baal, “Weyl-Dirac zero mode for calorons”, *Phys. Rev.* **D60**, 031901 (1999).
- [156] F. Bruckmann, D. Negradi, and P. van Baal, “Constituent monopoles through the eyes of fermion zero modes”, *Nucl. Phys.* **B666**, 197–229 (2003).
- [157] F. Bruckmann, “On the zero of the fermion zero mode”, *Phys. Rev.* **D71**, 101701 (2005).

Miguel Ángel López Ruiz

CONTACT INFORMATION	Center for Exploration of Energy and Matter Indiana University, 2401 N. Milo B. Sampson Lane Bloomington, IN 47408, USA	malopezr@iu.edu
EDUCATION	Indiana University Ph.D. Physics • Advisor: Jinfeng Liao, Ph.D. • Thesis Topic: <i>Confinement and Chiral Phase Transitions in $SU(2)$ Gauge Theory via Topological Objects.</i> Indiana University M.S. Physics Universidad Nacional Autónoma de México B.S. Physics • Advisor; Roelof Bijker, Ph.D. • Thesis Topic: <i>The flavor and spin of light baryons: A comparison between three effective models.</i>	Bloomington, IN 47405, USA May 2019 Bloomington, IN 47405, USA Aug. 2013 Mexico City, Mexico Jun. 2012
RESEARCH EXPERIENCE	Research Assistant Center for Exploration of Energy and Matter, Nuclear Theory Center, Indiana University. Supervisor: Jinfeng Liao, Ph.D. Summer Undergraduate Research Thomas Jefferson National Accelerator Facility, Newport News, VA. Supervisor: José Goity, Ph.D.	Jan. 2013– May 2019 Jun. 7–Jul. 31, 2010
PUBLICATIONS	<ol style="list-style-type: none">1. M. A. Lopez-Ruiz, Y. Jiang and J. Liao, “<i>Confinement from Correlated Instanton-Dyon Ensemble in $SU(2)$ Yang-Mills Theory</i>,” arXiv:1903.02684 [hep-ph].2. M. A. Lopez-Ruiz, Y. Jiang, and J. Liao, “<i>Confinement, Holonomy, and Correlated Instanton-Dyon Ensemble: $SU(2)$ Yang-Mills Theory</i>,” Phys. Rev. D 97, 054026 (2018) [arXiv:1611.02539 [nucl-th]].3. M. A. Lopez-Ruiz, T. Yenez-Martinez, A. P. Szczepaniak and J. Liao, “<i>Emergent Kink Statistics at Finite Temperature</i>,” Nucl. Phys. A 966, 324 (2017) [arXiv:1605.08017 [nucl-th]].4. M. A. Lopez-Ruiz, Y. Jiang and J. Liao, “<i>Confinement in a correlated Instanton-Dyon Ensemble</i>,” J. Phys. Conf. Ser. 876, no. 1, 012014 (2017).5. R. Bijker, S. Díaz-Gómez, M. A. Lopez-Ruiz and E. Santopinto, “<i>Baryons in the unquenched quark model</i>,” AIP Conf. Proc. 1753, 050003 (2016) doi:10.1063/1.4955361 [arXiv:1608.07629 [hep-ph]].	
AWARDS	Student Awards • “Becas CONACYT al Extranjero” Doctoral scholarship awarded by the Mexican National Council for Science and Technology (CONACYT).	Sep. 2015–Jul. 2018

PRESENTATIONS

Talks at Physics Meetings

- **M. A. Lopez-Ruiz**, “*Confinement in a correlated ensemble of dyons*”, XL Symposium on Nuclear Physics, Cocoyoc, Morelos, Mexico (January 7, 2017).
- **M. A. Lopez-Ruiz**, “*Confinement from instanton-dyons in $SU(2)$ Gauge Theory at finite temperature*”, Workshop on Gauge topology: from lattice to colliders, Trento, Italy (November 9, 2016).
- **M. A. Lopez-Ruiz**, “*Comparison of the predictions of flavor and spin content in effective models of baryons*” (in Spanish), XXVI Annual Reunion of the SMF Division of Particles and Fields, Mexico City, Mexico (May 21, 2012).
- **M. A. Lopez-Ruiz**, “*The Flavor and Spin of Baryons*”, III Mexican Mini-Workshop on Flavour Physics, Mexico City, Mexico (Dec 9, 2011).

Poster presentations

- **M. A. Lopez-Ruiz**, Y. Jiang, and J. Liao, “*Confinement in $SU(2)$ Yang-Mills Theory from Correlated Instanton-Dyon Ensemble*”, Quark Matter 2017, Chicago, IL, USA (Feb 6, 2017).
- **M. A. Lopez-Ruiz** and R. Bijker, “*The Flavor of the Nucleon*”, LIV National Congress of Physics, Merida, Yucatan, Mexico (October 13, 2011).
- **M. A. Lopez-Ruiz** and M. Zumaya-Hernandez, “*Simulation and visualization of Brownian motion*”, LIV National Congress of Physics, Merida, Yucatan, Mexico (October 10, 2011).
- **M. A. Lopez-Ruiz** and R. Bijker, “*The Flavor and Spin of the Nucleon*”, European Summer Campus 2011 - Between two infinities: Particle Physics, Astroparticle Physics and Cosmology, Strasbourg, France (July 6, 2011).

Colloquia and Seminars

- **M. A. Lopez-Ruiz**, “*Confinement: Topology Vs. Lattice*”, CEEM-NTC Lunch Seminar, Indiana University, Bloomington, IN (April 12, 2018).
- **M. A. Lopez-Ruiz**, “*Confinement from instanton-dyon ensemble in $SU(2)$ pure gauge theory*”, CEEM-NTC Lunch Seminar, Indiana University, Bloomington, IN (October 28, 2016).
- **M. A. Lopez-Ruiz**, “*Confinement/Deconfinement transition in the $SU(2)$ dyon ensemble*”, CEEM-NTC Lunch Seminar, Indiana University, Bloomington, IN (March 24, 2016).
- **M. A. Lopez-Ruiz**, “*Emergent Kink Statistics at Finite Temperature*”, CEEM-NTC Lunch Seminar, Indiana University, Bloomington, IN (March 10, 2016).

TEACHING
EXPERIENCE**Assistant Instructor**

- M211 - Calculus I Spring 2018
Department of Mathematics,
Indiana University,
Bloomington, IN, USA.
- P201 & P202 - General Physics I & II Spring/Fall 2017
Department of Physics,
Indiana University,
Bloomington, IN, USA.

Lab Instructor

- P201 - General Physics I Laboratory Fall 2012
Department of Physics,
Indiana University,
Bloomington, IN, USA.

Teaching Assistant

- Introduction to Elementary Particles I Spring 2011
Instructor: Alexis Armando Aguilar Arevalo, Ph.D
Facultad de Ciencias,

Universidad Nacional Autonoma de Mexico,
Mexico City, Mexico.

SERVICE

Student volunteer

- IU Science Fest
Department of Physics,
Indiana University,
Bloomington, IN, USA.

Oct. 2012, 2015 & 2017